UNIVERSIDADE FEDERAL DE MINAS GERAIS
PROGRAMA DE PÓS-GRADUAÇÃO EM SANEAMENTO, MEIO AMBIENTE E RECURSOS HÍDRICOS

Ana Flávia Souza Foureaux

A SUSTAINABLE SOLUTION FOR FRESH-WATER DEMAND IN MINING SECTORS: PROCESS WATER RECLAMATION AND METALS RECOVERY FROM POX EFFLUENT BY MEMBRANE DISTILLATION FOLLOWED BY ION EXCHANGE RESINS

Belo Horizonte
2021

Ana Flávia Souza Foureaux

A SUSTAINABLE SOLUTION FOR FRESH-WATER DEMAND IN MINING SECTORS: PROCESS WATER RECLAMATION AND METALS RECOVERY FROM POX EFFLUENT BY MEMBRANE DISTILLATION FOLLOWED BY ION EXCHANGE RESINS

Versão final

Tese apresentada ao Programa de Pós-Graduação em Saneamento, Meio Ambiente e Recursos Hídricos na Universidade Federal de Minas Gerais como requisito parcial para obtenção do título de doutora

Orientadora: Profa. Dra. Míriam C. S. Amaral Moravia

Coorientadora: Dra. Lucilaine V. S. Santos

Belo Horizonte
2021

F774s

Foureaux, Ana Flávia Souza.
A sustainable solution for fresh-water demand in mining sectors [recurso eletrônico]: process water reclamation and metals recovery from pox effluent by membrane distillation followed by ion exchange resins / Ana Flávia Souza Foureaux.- 2021.
1 recurso online (xvii, 193 f. : il., color.) : pdf.

Orientadora: Míriam Cristina Santos Amaral Moravia.
Coorientadora: Lucilaine Valéria de Souza Santos.

Tese (doutorado) - Universidade Federal de Minas Gerais, Escola de Engenharia. .

Bibliografia: f. 162-193.
Exigências do sistema: Adobe Acrobat Reader.

1. Engenharia sanitária - Teses. 2. Meio ambiente - Teses. 3. Água - Reutilização - Teses. 4. Efluente - Qualidade - Teses. 5. Recuperação de metais - Teses. 6. Adsorção - Teses. I. Moravia, Míriam Cristina Santos Amaral. II. Santos, Lucilaine Valéria de Souza. III. Universidade Federal de Minas Gerais. Escola de Engenharia. IV. Título.

CDU: 628(043)

Ficha catalográfica elaborada pela bibliotecária Roseli Alves de Oliveira CRB/6 2121
Biblioteca Prof. Mário Werneck, Escola de Engenharia da UFMG

UNIVERSIDADE FEDERAL DE MINAS GERAIS
[ESCOLA DE ENGENHARIA]
COLEGIADO DO CURSO DE GRADUAÇÃO / PÓS-GRADUAÇÃO EM [SANEAMENTO, MEIO AMBIENTE E RECURSOS HÍDRICOS]

FOLHA DE APROVAÇÃO

["A Sustainable Solution for Fresh-Water Demand in Mining Sectors: Process Water Reclamation and Metals Recovery from Pox Effluente by Membrane Distillation Followed by Ions Exchange Resins"]

[ANA FLÁVIA SOUZA FOUREAUX]

Tese de Doutorado] defendida e aprovada, no dia **[** 19 de abril de 2021**]**, pela Banca Examinadora designada pelo [Colegiado do Programa de Pós-Graduação **EM SANEAMENTO, MEIO AMBIENTE E RECURSOS HÍDRICOS**] da Universidade Federal de Minas Gerais constituída pelos seguintes professores:

[Prof. Dr. Frederico de Araujo Kronemberger**] - Membro Externo]**

[UFRJ]

[Profª. Drª. Isabel Cristina Tessaro**] - Membro Externo]**

[UFRGS]

[Prof. Dr. Julio Cézar Balarini**] - Membro Interno]**

[UFMG]

[Prof. Dr. Ruben Dario Sinisterra Millán - **Membro Interno]**

[UFMG]

[Profª. Drª. Lucilaine Valéria de Souza Santos - **coorientadora]**

[PUC-MINAS]

[Profª. Drª. Miriam Cristina Santos Amaral Moravia - **Orientadora]**

[UFMG]

APROVADA PELO COLEGIADO DO PPG SMARH

Sonaly Cristina Rezende Borges de Lima - Coordenadora

Belo Horizonte, 19 de abril de 2021.

Documento assinado eletronicamente por **Lucilaine Valéria de Souza Santos**, **Usuário Externo**, em 19/04/2021, às 19:53, conforme horário oficial de Brasília, com fundamento no art. 5º do Decreto nº 10.543, de 13 de novembro de 2020.

Documento assinado eletronicamente por **Miriam Cristina Santos Amaral Moravia**, **Professora do Magistério Superior**, em 17/08/2021, às 08:05, conforme horário oficial de Brasília, com fundamento no art. 5º do Decreto nº 10.543, de 13 de novembro de 2020.

Documento assinado eletronicamente por **Frederico de Araujo Kronemberger**, **Usuário Externo**, em 23/08/2021, às 13:04, conforme horário oficial de Brasília, com fundamento no art. 5º do Decreto nº 10.543, de 13 de novembro de 2020.

Documento assinado eletronicamente por **Julio Cezar Balarini**, **Professor do Magistério Superior**, em 24/08/2021, às 17:20, conforme horário oficial de Brasília, com fundamento no art. 5º do Decreto nº 10.543, de 13 de novembro de 2020.

Documento assinado eletronicamente por **Ruben Dario Sinisterra Millan**, **Professor do Magistério Superior**, em 30/08/2021, às 13:28, conforme horário oficial de Brasília, com fundamento no art. 5º do Decreto nº 10.543, de 13 de novembro de 2020.

Documento assinado eletronicamente por **Isabel Cristina Tessaro**, **Usuário Externo**, em 31/08/2021, às 18:20, conforme horário oficial de Brasília, com fundamento no art. 5º do Decreto nº 10.543, de 13 de novembro de 2020.

A autenticidade deste documento pode ser conferida no site https://sei.ufmg.br/sei/controlador_externo.php?acao=documento_conferir&id_orgao_acesso_externo=0, informando o código verificador **0682067** e o código CRC **12BE2D89**.

Referência: Processo nº 23072.220106/2021-12 SEI nº 0682067

AGRADECIMENTOS

Agradeço aos meus pais, Vera e Carlos, que são os meus exemplos, pelo amor incondicional e por se dedicarem tanto a mim. Sou muito grata pelos sacrifícios que fizeram para eu chegar até aqui. Agradeço pelo colo nas situações difíceis, pelos conselhos nos momentos de dúvida, pelos ensinamentos ao longo da vida e pelo incentivo, bem como pelo carinho em todos os instantes. Obrigada por torcerem e estarem sempre ao meu lado me incentivando. Amo vocês.

Agradeço ao Henrique pelo companheirismo, carinho e motivação que foram fundamentais para eu seguir firme nessa realização. Agradeço pela torcida e por me ajudar a concretizar os meus e os nossos objetivos adicionando leveza, amor e felicidade em meus dias.

Agradeço ao Victor e ao Yuri, pela amizade e pelo comprometimento. Sou muito grata a vocês por toda a ajuda, parceria e por terem enfrentado os desafios desse projeto comigo. Vocês foram essenciais para o desenvolvimento de todo o trabalho. Agradeço à minha família pelo carinho, torcida e pensamentos positivos. Agradeço às minhas amigas Ana Paula, Cintia e Duda que, mesmo estando distantes, fisicamente, estão sempre presentes na minha vida, bem como aos amigos queridos que tive o privilégio de conhecer e conviver na pós graduação. Ao Geaps, grupo, que agregou muito à minha formação. Além disso, agradeço a todas as alunas de iniciação científica que contribuíram para a realização desse projeto: Leidiane, Aline e Débora, obrigada pelo comprometimento de vocês.

Agradeço à minha orientadora, professora Míriam Amaral, e à minha coorientadora, Lucilaine, pelo apoio, atenção e ensinamentos ao longo do desenvolvimento deste projeto. Agradeço à banca examinadora por ter aceitado prontamente o convite e pela disponibilidade em avaliar o meu trabalho. Agradeço aos professores do SMARH e do CEFET pelos ensinamentos, contribuição e incentivo para a minha formação. Também agradeço aos funcionários do DESA por sempre estarem dispostos a me auxiliar.

Agradeço às agências de fomento, CNPq, CAPES e FAPEMIG, pelo apoio financeiro para a realização do projeto e à empresa Dupont pela doação das resinas.

RESUMO

Entre os processos de beneficiamento do ouro, a oxidação sob pressão (OSP) é aplicada visando à maior taxa de recuperação desse metal. No entanto, OSP gera elevado volume de efluente, que contém altas concentrações de ácido (H_2SO_4) e metais. Nesse sentido, é necessário adotar métodos de tratamento eficazes para atender às legislações ambientais, e permitir a recuperação desses subprodutos. Nesse cenário, a destilação por membrana de contato direto (DMCD) foi avaliada em substituição aos tratamentos convencionais e comparada, em termos de viabilidade operacional e aspectos econômicos, com a nanofiltração (NF) para o tratamento/ beneficiamento desse tipo de efluente. Também se avaliou a aplicação da DMCD em diferentes temperaturas de alimentação (55 – 65 °C) e taxas de recirculação (0,3 - 1,5 L/min). Duas membranas comerciais, de poli (tetrafluoroetileno) e poli (vinilidenefluoreto), foram comparadas, bem como a contribuição de um espaçador, em termos de taxa de recuperação do permeado e a eficiência de retenção. As menores taxas de molhamento foram obtidas em temperaturas de alimentação e vazão de recirculação reduzidas (60 ºC e 0,30 L/s, respectivamente), o que permitiu maior grau de recuperação do permeado. Porém, o aumento na temperatura e na vazão de alimentação levou a resistências mais baixas. Nessa perspectiva, a resistência da membrana teve a maior contribuição para a transferência de massa, enquanto a resistência associada à incrustação teve efeitos desprezíveis. Nas melhores condições (PTFE com espaçador, temperatura de alimentação de 60 °C e 0,3 L/min) o processo teve um fluxo médio de 6,82 L/m^2.h de permeado e grau de recuperação de 33,9%. Sob essas condições operacionais, obteve-se elevada retenção de metais e ácidos, >99,2% e >99,9%, respectivamente, gerando um permeado que pode ser utilizado diretamente como água de reúso na mineração. O concentrado gerado pela DMCD apresenta altas concentrações de metais e com o objetivo de recuperar os elementos de maior interesse econômico (Ni^{2+}, Cu^{2+} e Co^{2+}) as resinas de troca iônica Amberlyst A26, Dowex M 4195 e Amberlite IRC747 foram utilizadas. Nessa perspectiva, a Dowex M 4195 foi a resina mais eficaz, que apresentou a seguinte ordem de seletividade iônica Cu^{2+}> Ni^{2+}> Co^{2+} com 98, 57 e 23 %, respectivamente, de adsorção. Os resultados também indicaram que a elevação da concentração de resina aumentou a porcentagem de remoção desses metais. Logo, a DMCD seguida da troca iônica foi considerada uma alternativa promissora para a reutilização de água de processo, recuperação de metais e, consequentemente, beneficiamento do efluente da OSP.

Palavras-chave: Destilação por membrana, água de reúso, efluente da OSP, recuperação de metais, adsorção.

ABSTRACT

Among the gold beneficiation process, oxidation under pressure (POX) is applied to aim higher recovery grades. However, the POX generates a large amount of effluent, which contains high acid concentrations (H_2SO_4) and metals. In this sense, it is necessary to adopt effective treatment methods to meet increasingly restrictive environmental legislation and, moreover, allow these by-products recoveries. In this scenario, the direct contact membrane distillation (DCMD) was evaluated in substitution of conventional treatments and compared in terms of operational viability and economic aspects with nanofiltration (NF) for the POX effluent treatment/beneficiation. The application of DCMD at different temperatures was also evaluated at different feed temperatures (55 – 65 °C) and recirculation flowrates (0.3 – 1.5 L/min). Two different commercial membranes, poly(tetrafluoroethylene) and poly(vinylidenefluoride), were compared, including the contribution of an additional spacer, in terms of distillate recovery grade and retention efficiency. Lower wetting rates were obtained for lower feed temperatures and recirculation flowrate (60 ºC and 0.30 L/s, respectively), which allowed for a greater permeate recovery grade. In contrast, an increase in both feed temperature and recirculation flowrate led to lower resistances. Among them, the resistance imposed by the membrane had the highest contribution to mass transfer, whereas fouling resistance had negligible effects. Under the best conditions (PTFE with spacer, feed temperature of 60 °C and 0.3 L/min) the process had an average distillate flux of 6.82 $L/m^2.h$ and a permeate recovery grade of 33.9%, without compromising the permeate physicochemical quality. Under these operational conditions high values of metals and acidy retention were achieved, >99.2% and >99.9 %, respectively, generating a permeate that can be used directly as reuse water in the mining plant. The DCMD's concentrate generated by this process presents high metals concentrations and in order to recover the greatest economic interest elements (Ni^{2+}, Cu^{2+} and Co^{2+}) the Amberlyst A26, Dowex M 4195 and Amberlite IRC747 resins were applied. In this context, Dowex M 4195 was the most effective resin, presenting an ion selectivity order $Cu^{2+} > Ni^{2+} > Co^{2+}$ with 98, 57 and 23 % of this resin adsorption, respectively. The results also indicated that increasing resin concentration increased the percent removal of these metals. Overall, DCMD followed by ion exchange resins was considered as a promising alternative for process water reclamation, metals recovery and, consequently, POX effluent beneficiation.

Keywords: Membrane distillation, reuse water, POX effluent, metals recovery, adsorption.

LIST OF FIGURES

LIST OF TABLES

LIST OF ABBREVIATIONS AND SYMBOLS

a_m – Membrane area filtration

A_m – The amortization factor

A_t – The isotherm equilibrium binding constant

C_c – The solute content in the concentrate

Ce – Equilibrium concentration

C_{cap} – Capital cost

C_f – The solute content in the feed

C_p – The solute content in the permeation

D_H – The hydraulic module diameter

h_f – The convective heat transfer coefficient of the feed

h_m – The convective heat transfer coefficient of the membrane

h_p – The convective heat transfer coefficient of the permeate

i_r – Brazilian investment rate

J_{pc} – The water flux after physical cleaning

J_{cc} – The water flux after chemical cleaning

J_p – Permeate flux

J_w – The pure water permeate flux through the membrane before effluent filtration

k_1 – The pseudo-first order rate constant

K_d –The distribution coefficient

K_{DR} – The Dubinin-Radushkevich isotherm constant

k_l – The Langmuir equilibrium constant

m_i – The permeate mass corresponding at t_i

P_1 – Vapor pressure at feed membrane surface

P_2 – Vapor pressure at permeate membrane surface

P_f – Vapor pressure at the feed bulk

P_p – Vapor pressure at the permeate bulk

P_w –The water vapor pressure

q_e –The ion exchange capacity

q_s – The theoretical isotherm saturation capacity

Q_f – Feed flow rate

R^2 – Coefficient of determination

$R_{fouling}$ – Fouling resistance in DCMD

R_L – The separation factor

R_{total} – Total resistance in DCMD

RR_{MD} – Water recovery grade using destillation membrane

S_b – Calcium sulfate supersaturation index on the bulk solution

S_m – Calcium sulfate supersaturation index on the membrane surface

T_f – Temperature at the DCMD bulk feed

t_i – Initial time (h)

T_p – Temperature at the DCMD bulk permeate

$T_{w,f}$ – Temperature at the DCMD membrane surface facing the feed

$T_{w,p}$ – Temperature at the DCMD membrane surface facing the permeate

v_{Pt} – Permeate volume in t_i (L)

α_f – The feed water activity coefficient.

$\Delta\pi$ – The osmotic pressure difference

$\Delta G°$ – Gibbs free energy change

$\Delta H°$ – The enthalpy change

ΔHv – The water vaporization heat

Δp – Vapor pressure difference

ΔP – Transmembrane pressure

$\Delta S°$ – The entropy change

Δt –The permeate's collection time in hours

ΔV – The permeate's collected volume

μ – Water dynamic viscosity

ν – The kinematic viscosity of liquid water

τ – DCMD temperature polarization effect

A – The pipe's cross-sectional area

AEM – Anion exchange membranes

AGMD – Air gap membrane distillation

AMD – Acid mine drainage

ARD – Acid rock drainage

b – The Temkin's isotherm constant related to the adsorption heat

BES– Bioelectrochemical system

CAPEX – Capital expense

CEM – Cation exchange membrane

CP – Concentration polarization

DCMD – Direct contact membrane distillation

E – The average energy of adsorption

ED – Electrodialysis

FC – Feed controller

FD – The total flux decline

FO – Flux decline due to fouling

h – Convective heat transfer coefficient

HE – Heat exchanger.

IEP – Isoelectric point

IX – Ion-exchange

J(T) – The permeate flux obtained at a temperature

LEP – Liquid entry pressure

m – Resin’s mass (g)

MD – Membrane distillation

MWCO – Membrane molecular weight cut-off

NF – Nanofiltration

Nu – Nusselt number

Nuf – Nusselt number in the feed

OPEX – Operational expense

P – Pressure (Pa)

PL – Design plant life (years)

POX – Pressure oxidation process

PP – Polypropylene

Pr – Prandtl number

PTFE – Polytetrafluoroethylene

PVDF – Polyvinylidene fluoride

r – Membranes' modules radius

R – The ideal gas constant

R (%) – Recovery grade

Re – Reynolds number

RO – Reverse osmosis

SC – Speed controller

SEC – The specific energy consumption

SEM – Scanning Electron Microscopy

SGMD – Sweep gas membrane distillation

T – Temperature

TP – Temperature polarization

TPC – Temperature polarization coefficient

UF – Ultrafiltration

V – Volume

W – The rate of work done by the pump

TABLE OF CONTENTS

1 CHAPTER 1

INTRODUCTION

1.1 BACKGROUND AND JUSTIFICATION

Mining is a relevant activity for the world's economy, and it is characterized by the interest of profit in minerals exploration and exploitation in the soil or subsoil (GONÇALVES., 2013; LUFIN and ATIENZA., 2011). This activity contributes directly to technological advancement, and providing raw materials necessary to fabricate different products, which act to maintain the population's life quality (SHENVI *et al.*, 2015). According to the "Brazilian Mineral Yearbook: Principal Metals Substances", developed by the National Department of Mineral Production (BRASIL., 2018) (DNPM), there are 37 metallic substances in Brazil which corresponded to about 80% of the total ore production value in the country in 2018. Among these elements, aluminum, copper, iron, manganese, niobium, nickel and gold are the main contributors, with 8870 mines distributed in the country (IBRAM., 2015). Considering 2018, the country raised about US$ 103 billion for the exploitation of mineral resources, exporting part of its production to countries such as China, Japan, Canada and United States (WGC., 2018).

Among these minerals, gold mining stands out since it is considered one of the oldest financial assets, in addition, it presents a high economic value in the market. Moreover, due to its physical and chemical properties, such as corrosion resistance, high malleability, ductility and good electrical conductivity, this ore consumption is not only linked to the jewels manufacture, which demand about 50% of this metal production, but also it is used in technological applications (HER, JAFFRAY and ALLEN., 2017; QIN *et al.*, 2018; QIN *et al.*, 2019).

Although gold mining is relevant in the world's economic scenario and in technological development, the auriferous ores processing generates negative impacts on the environment. Gold and most ores are not used in the direct form as it is mined. Thus, for its beneficiation it is necessary to change the particle size, shape and concentration of the interest species without provoking chemical alteration in these compounds (LUZ *et al.*, 2004). This process is necessary when a large part of ores, that contain gold, present this element in a sulphide occluded matrix, mainly in Pyrite (FeS_2), Arsenopyrite (FeAsS) and Pyrrhotite (FeS), reducing gold recovery by direct leaching with cyanide, which is not able to achieve desired gold recovery levels (> 80%) (GUZMAN and PAPANGELAKIS., 2018; FRASER, WALTON and WELLS., 1991). The gold's ore that presents this characteristic is called as refractory and it requires a prior treatment to achieve, by the oxidization reagents action, the crystalline sulfides structures disruption, therefore making gold more accessible (IVANNIKOV *et al.*, 2018; KEFENI *et al.*, 2017).

Among the gold's beneficiation step, stands out the pre-treatment called pressure oxidation (POX). This technology has been widely used since the 1980s, takes place in autoclaves at high pressure (~21 atm) and at temperatures between 200 °C and 220 °C. This condition promotes the oxidation of the sulfides into sulfates, metals solubilization and sulfuric acid generation. After the POX, the gold, previously occluded in the mineral matrix, is released, and reaches prominent recovery values in the next stages (RICCI *et al*., 2015; IVANNIKOV *et al*., 2018). In this sense, Yu *et al*. (2019) reported that for sulfide-rich matrices, gold recovery by the conventional leaching process varies between 55 - 70% and after POX, recoveries up to 86% could be achieved.

According to Guzman, Thorpe and Papangelakis (2018) and Kaur *et al*. (2018) the main reactions for pyrite oxidation can be seen in Eq. 1.1 to Eq.1.4:

$$FeS_2 + \frac{7}{2}O_{2(aq)} + H_2O \rightarrow Fe^{2+} + 2SO_4^{2-} + 2H^+ \quad (1.1)$$

According to Akcil and Koldas. (2006), a significant portion of ferrous iron (Fe^{2+}) that is found in acid environment will oxidize to ferric iron (Fe^{3+}), according to the following reaction Eq. 1.2:

$$Fe^{2+} + \frac{1}{4}O_{2(aq)} + H^+ \rightarrow Fe^{3+} + \frac{1}{2}H_2O \quad (1.2)$$

The ferrous iron oxidation in ferric iron involves chemical and biological mechanisms and depends on O_2 concentration available in the environment as well the pH and bacterial activity (AKCIL and KOLDAS., 2006; SIERRA, ÁLVAREZ, SAIZ and GALLEGO., 2003; KEFENI and MSAGATI., 2017).

If the pH of the solution, where the ferric iron is present, is in the range of 2.3 to 3.5, this element will precipitate as $Fe(OH)_3$ and jarosite, as can be seen in Eq. 1.3, that represents a complete Fe hydrolysis reaction (AKCIL and KOLDAS., 2006; KEFENI and MSAGATI., 2017; SKOUSEN *et al.*, 2017).

$$Fe^{3+} + 3H_2O \rightarrow Fe(OH)_3 + 3H^+ \quad (1.3)$$

Any Fe^{3+} from Eq. (1.2) that does not precipitate from solution through Eq. (1.3) may be used to oxidize additional pyrite, according to the following in Eq. 1.4 (ALKCIL and KOLDAS., 2006; KEFENI, MSAGATI and MAMBA., 2017).

$$FeS_2 + 14Fe^{3+} + 8H_2O \rightarrow 15Fe^{2+} + 2SO_4^{2-} + 16H^+ \quad (1.4)$$

Although the POX technique is necessary for gold mining, it is responsible for high water consumption and, consequently, a large volume of liquid effluent is generated, which is composed of significant sulphate, metals and high acidity concentrations at an elevated outlet temperature (JOHNSON., 2014; KAUR *et al.*, 2018; LÓPEZ *et al.*, 2018; SKOUSEN *et al.*, 2017). The gold processing effluents composition varies according to the location, but, in general, high sulfate contents and metal ions concentrations are reported in several studies, as presented in Table 1.1.

Table 1.1 – The gold processing effluents composition considering different locations

Mine	pH	Electrical conductivity	SO_4^{2-}	Al^{3+}	Ca^{2+}	Co^{2+}	Cr^{2+}	Cu^{2+}	Fe^{2+}	K^{+}	Mg^{2+}	Mn^{2+}	Na^{+}	Ni^{2+}	Zn^{2+}	Location	Ref.
Gold	3.1	5.2	n.a.	224.4	498.4	1.4	0.7	0.2	2135.0	n.a.	428.2	30.2	84.0	3.7	6.9	South Africa	KEFENI, MSAGATI and MAMBA., 2015
Gold[1]	1.3	18.7	18.2	445.0	347.0	20.0	n.a.	95.7	467.0	6.4	n.a.	2575.0	18.6	102.0	82.0	Brazil	AMARAL *et al.*, 2018
Gold	1.8	12.4	5501.0	n.a.	444.0	n.a.	n.a.	n.a.	n.a.	n.a.	288.0	n.a.	n.a.	n.a.	n.a.	Brazil	REIS *et al*., 2018
Gold	2.4	n.a.	n.a.	n.a.	561.0	0.8	n.a.	n.a.	835.0	n.a.	358.0	30.0	192.0	1.8	0.9	South Africa	KEFENI *et al.*, 2018
Gold	2.4	n.a.	n.a.	0.9	561.0	0.8	n.a.	n.a.	835.0	n.a.	385.0	30.0	192.0	1.8	0.9	South Africa	KEFENI, MSAGATI and NKAMBULE., 2017

Except for pH and electrical conductivity (mS/cm) all the other units correspond to mg/L. n.a.: not available. [1]Example of POX effluent composition.

Due to the high acidity of POX's effluent, it contributes to the metals solubilization increasing their toxicity in the environment. Moreover, these compounds are considered persistent and may continue even after mining has ceased its activity, potentially harming the ecosystem and human health (MIGASZEWSKI, GAŁUSZKA and DOŁĘGOWSKA., 2018; RYU *et al.*, 2019; KESIEME., 2015). Once this effluent meets water, this resource becomes contaminated compromising the biodiversity balance. In contact with the soil, it makes it structurally unstable and highly prone to erosion (ROYCHOWDHURY, SARKAR and DATTA., 2015). Due to these negative impacts, Migaszewski, Gałuszka and Dołęgowska (2018) and RoyChowdhury, Sarkar and Datta (2015) consider this type of effluent as the worst environmental concern related to mining activity.

In this context, the high demand for water and the management of acidic effluents from gold mining are the greatest challenges faced by this sector to meet increasingly restrictive environmental legislation. On the other hand, this effluent type can be considered a source of valuable metals and a source of process water (VECINO *et al*., 2021).

The progressive water recycling increases have met part of the industrial water demand. This substitution promotes an economic advantage to the industry, that the costs related to the freshwater acquisition are increasing due to its scarcity (GHERNAOUT, ELBOUGHDIRI and AL ARNI., 2019; LACKEY *et al*., 2020). However, the decentralized treatment for industrial effluent is more effective because it can be applied in the same place where the effluent is produced, reducing the cost associated with the water recycling transportation (RICCI *et al*., 2016).

In this sense, the application of a direct contact membrane distillation (DCMD) stands out. DCMD consists of a thermal process that presents a theoretical rejection of 100% of non-volatile compounds, thus generating the permeate with high physical-chemical quality, which can be used as an industrial reuse water (RAHIMPOUR, KAZEROONI and PARHOUDEH., 2019). In addition, DCMD is an example of decentralized and modular treatment, that increases its flexibility in relation to the effluent volume to be treated and allows its application in the same location in which the effluent is produced. Another factor that contributes to the DCMD expansion on an industrial scale is the possibility of using the residual heat from the effluents to generate the process driving force (KHAYET and MATSUURA., 2011; ULLAH *et al*., 2018).

Although, it is necessary to treat the concentrate stream generated during the DCMD operation, since it presents higher contaminants concentrations than the raw POX effluent that fed this process. In this concentrate, the presence of high value-added metals, due to their growing price and wide industrial applications, makes their recovery from this stream attractive (ULLOA *et al*., 2020). Among these metals, nickel (Ni^{2+}), copper (Cu^{2+}) and cobalt (Co^{2+}) can be highlighted.

Nickel, for example, stands out for its magnetism, melting point at approximately 1,453 °C, in addition to its high resistance to oxidation and corrosion. Due to these characteristics, this metal is widely used in diverses industries. It is estimated that this metal is used in approximately 300,000 different products for consumption, industry, catalysts, military equipment, currencies,

transport and in civil construction applications, with more than half of its production related to manufacturing of stainless steel (KIM *et al.*, 2013; KIM *et al.*, 2018). The current value of nickel tone is US$17,790.00 according to the London Metal Exchange (LME) (LME, 2021).

Cobalt presents high hardness and melting point (1,480 ºC), properties that influence its wide application as raw material in the steel industry. Also, this metal is widely used in the military industry for making engines, cutting and milling tools and in the hospital industry in making prostheses (SOFIA and MONTERIO., 2016). Cobalt commercial price per ton is around US$ 45,225.00; however, this value varies significantly due to the limited reserves and its increased demand (LME., 2021; WANG *et al*., 2017). In March 2018, cobalt prices per ton achieved US$ 95,000.00 due to the electric cars' batteries and other electricals, such as smartphones, manufacture growth (LME., 2019).

Another metal found in POX effluent that has an aggregate economic value is copper, which has a melting point of 1,358 °C and is recognized for its high ductility and malleability, as well as being very resistant to corrosion, especially when tin is added to form bronze. Moreover, to being an excellent conductor of heat and electricity, copper is the most widely used metal in electrical equipment and systems (RODRIGUES, SILVA and GUERRA., 2012). According to the LME (LME., 2021), copper current value per ton is US$ 7,865.00.

Due to the economic value attributed to these metals, it is advantageous to recover them. In this context, neutralization followed by chemical precipitation is the most conventional treatment applied to the POX effluent. However, this method does not allow the recovery of the acid solution and produces a large sludge volume as a residue process. The most popular alkaline industrial chemicals that are used for neutralization include calcium hydroxide ($Ca(OH)_2$), soda ash ($NaCO_3$), calcium oxide (CaO), limestone ($CaCO_3$), caustic soda (NaOH), ammonium hydroxide (NH_4OH) and magnesium hydroxide ($Mg(OH)_2$) (INAP., 2003). The amount of alkaline material required for the neutralization process, as well as the neutralization efficiency of each substance, can be seen in Table 1.2.

Table 1.2 - Alkali materials commonly considered for POX effluent neutralization – Alkali requirement and neutralization efficiency

Alkali Materials	Alkali Requirement (ton/ton of acidity)[a]	Neutralization Efficiency (%)
Limestone ($CaCO_3$)	1.00	30 - 50
Calcium hydroxide ($Ca(OH)_2$)	0.74	90
Un-hydrated (quick) lime (CaO)	0.56	90
Soda ash (Na_2CO_3)	1.06	60 - 80
Caustic soda (NaOH)	0.80	100

[a]Quantity of alkalizing material expressed in relation to $CaCO_3$ per unit of acidity

Evaluating Table 1.2, each reagent achieves distinct neutralization efficiency. Among these reagents, sodium hydroxide stands out because it can provoke a considerably pH increment, which allows the complete dissociation favoring the metals insoluble formation. However, the NaOH is the most expensive reagent than other alkaline compounds (KEFENI, MSAGATI and MAMBA., 2017). It is also worth noting that the demand for alkaline agents is high given the effluent's acidity, which makes the neutralization process even more costly for the mining company.

In addition to the multiple efficiencies that can be obtained using the precipitation, according to the various alkalizing types application, it is necessary to consider other factors that may also influence this process results. Thus, metal concentration, oxygen availability, and the pH range in the POX effluent are relevant factors that determine this technique's success. Therefore, to obtain significant metals recovery results by precipitation, it is necessary constant operational control. Moreover, it is indispensable to consider that after the alkalization and, consequently, insoluble metals sedimentation, the sludge formed by these elements must be treated and placed correctly, which increases this application method costs. In this context, it is necessary to highlight the relevant factor that refers to the storage of these residues in dams, since this practice should be avoided according to recent ruptures of these structures in Minas Gerais, as occurred

in 2015 at the Fundão dam in Bento Rodrigues city and in 2019 at the Mina do Córrego do Feijão dam, in Brumadinho city.

In this perspective, the ion-exchange technique is used aiming for the separation and concentration of inorganic ions since ions from the solution (adsorvate) exchanging different ions, that present the same charge, in the solid phase (adsorbent). According to KOŁODYŃSKA *et al*. (2014), tion-exchange resins has been growing in recent years to remove metal ions from effluents from hydrometallurgical processes, mainly in acidic solutions. As the increased adsorbate concentration favors the adsorption, the application of DCMD followed by ion-exchange aiming the metals recovery becomes an attractive option.

Thus, this study aims to contribute to scientific advances in the POX effluent beneficiation and another effluent with similar physicochemical characteristics. It also intends to corroborate to its valuation through the generation of industrial reuse water, in an increasing water stress scenario, and metals recovery applying advanced treatments, which reduces the gold mining sector waste generation. Consequently, it can promote an increase in the gold mining economic advantages and, equally, help to reconcile these advantages with the environmental disadvantages, that are generated by this sector. In addition, this research will contribute to reduce the deficit of studies related to the DCMD's concentrate treatment using a real acid mining effluent.

1.2 HYPOTHESES

The present study presents the following hypotheses:

- the residual heat of the POX effluent will be sufficient for the DCMD application eliminating the necessity of the feed heating stages;

- the DCMD's permeate will present adequate physical-chemical quality for use as an industrial reuse water;

- it will not be necessary to promote additional cooling to the DCMD's concentrate for the metals recovery by ion-exchange since the higher temperature may contribute to the recovery of the elements of interest.

1.3 OBJECTIVES

1.3.1 General objective

Propose a treatment and beneficiation route to reduce the negative environmental impacts caused during the gold beneficiation by the POX process, enabling the generation of water for industrial reuse and metals recovery by integrating membrane distillation with ion-exchange techniques.

1.3.2 Specific objectives

1. Evaluate the DCMD application as an alternative to the conventional methods for value-added compounds recovery from acidic effluents;

2. Compare the technical feasibility and economic aspects to generating industrial reuse water from the POX effluent applying UF-NF and DCMD;

3. Analyze the effect of temperature, feed flow rate and the inclusion of an additional spacer can influence the permeate quality, as well as the membrane wetting during the DCMD process;

4. Compare the efficiency of PTFE and PVDF DCMD's membranes to achieve greater permeate flux, higher recovery grade and greater chemical resistance;

5. Analyze the recovery of Ni^{2+}, Co^{2+} and Cu^{2+} from the DCMD's concentrated stream using resins evaluating the balance, kinetics and thermodynamics of the tests.

1.4 DOCUMENT STRUCTURE

This Ph.D. thesis is divided into 8 chapters: Chapter 1 is an introduction and contains a theme presentation, hypotheses, objectives and the document structure; Chapter 2 addresses objective 1; Chapter 3 addresses the objective 2; Chapter 4 contemplates objectives 3 and 4; Chapter 5 refers to the recovery of the metals of interest, which are concentrated in the DCMD process in chapter 4, applying ion-exchange resins. Finally, Chapters 6 and 7 contain the final considerations and the published articles referring to this study, respectively.

2 CHAPTER 2

DIRECT CONTACT MEMBRANE DISTILLATION AS AN ALTERNATIVE TO THE CONVENTIONAL METHODS FOR VALUE ADDED COMPOUNDS RECOVERY FROM ACIDIC EFFLUENTS: REVIEW

2.1 ACID MINE DRAINAGE (AMD)

Acid effluents deserve special attention given that they are associated with numerous environmental negative impacts such as the increase in soils and water sources acidity, in addition to the dissolved salts content. They are also responsible for various humans and animals' health problems if disposed without proper treatment in water bodies intended for consumption (ENVIRONMENTAL., 2003; BORMA and SOARES., 2002). Due to these factors, it is essential to apply a treatment before these effluents' disposal, generating a lower socio-environmental impact. Among the industrial segments responsible for the largest acid effluents generation, highlights the mining and metallurgical industry.

Mining is an activity that has been explored for thousands of years and is responsible for generating a great source of economic wealth. Due to the intense mining activity in Brazilian territory, there must be a constant national policy update and studies development aiming to reduce the environmental impact generated by this sector. As a result of mining activities, there are innumerable physical landscape changes, a significant contribution in the greenhouse gases emission and solid waste generation. Moreover, there is a significant interaction with surface and underground water resources, which the use is not limited to the mining process, but also the ore processing, hydrometallurgy, pyrometallurgy and transport activities, as well as mine closure (IBRAM., 2012)

Therefore, despite its significant contribution to economic growth, this activity causes social and environmental damages (TOST *et al*., 2018; VIVODA, and KEMP., 2019; GOYAL, ROUTROY and SHAH., 2018), especially due to the effluent generated as the acid mine drainage (AMD). This is due to AMD composition, which is constituted by high sulfuric acid concentration and different metals specially iron, that in contact with water and oxygen promote the pyrite oxidation. This chemical reaction makes this effluent more acid which contributes to the metals solubilization and, therefore, its toxicity. In this context, it is perceived that environmental norms and regulations are becoming more rigorous, thus requiring more effective treatments for these effluents discharge. Nevertheless, analyzing the AMD by products it is also worth mentioning that the efficiency of this treatment with the recovery of these compounds allows the generation of industrial reuse water, thus contributing to the water demands reduction, which is increasingly scarce (ROYCHOWDHURY, SARKAR and DATTA., 2015; DOW *et al*., 2012; RAHIMPOUR, KAZEROONI and PARHOUDEH., 2019).

Table 2.1- Acid mine drainage composition for different mining activities and countries. Except for pH and electrical conductivity (mS/cm) all the other units correspond to mg/L. n.a.: not available; [a] abandoned mine

Mine	pH	Electrical conductivity	SO_4^{2-}	Al^{3+}	Ca^{2+}	Co^{2+}	Cr^{2+}	Cu^{2+}	Fe^{2+}	K^{+}	Mg^{2+}	Mn^{2+}	Na^{+}	Ni^{2+}	Zn^{2+}	Location	Ref.
Coal	2.4	3.6	n.a.	0.9	561.2	0.8	0.3	0.2	835.0	n.a.	384.8	29.7	192.0	1.8	0.9	South Africa	Kefeni *et al.*2015
Coal [a]	3.3	n.a.	1950.0	40.0	1070.0	n.a.	n.a.	n.a.	186.0	9	272	13.0	14.0	n.a.	n.a.	South Korea	Seo *et al*., 2017
Coal	3.0	n.a.	300.0	10.0	n.a.	n.a.	n.a.	0.5	40.0	n.a.	n.a.	6.0	n.a.	2.0	3.0	United States	Ryan *et al*., 2017
Coal	2.6	7.1	7337.0	n.a.	311.0	n.a.	n.a.	n.a.	n.a.	1241.0	n.a.	23.0	454.0	n.a.	5.0	Brazil	Buzzi *et al*., 2013
Coal	2.5	8.1	7862.0	n.a.	258.0	n.a.	n.a.	n.a.	n.a.	385.0	155.0	33.0	385.0	n.a.	3.0	Brazil	Buzzi *et al*., 2013
Coal	2.9	9.9	6300.0	n.a.	232.0	n.a.	n.a.	n.a.	2822.0	414.0	199.0	50.0	414.0	n.a.	25.0	Brazil	Buzzi *et al*., 2013
Coal	2.8	4.5	1570.0	n.a.	230.0	n.a.	n.a.	n.a.	n.a.	296.0	71.0	9.0	296.0	n.a.	2.0	Brazil	Buzzi *et al*., 2013
Coal	2.9	4.2	3522.0	n.a.	239.0	n.a.	n.a.	n.a.	40.0	221.0	67.0	n.a.	221.0	n.a.	1.0	Brazil	Buzzi *et al*., 2013
Coal	2.8	1.2	518.0	n.a.	143.0	n.a.	n.a.	n.a.	n.a.	1059.0	19.0	1.0	1059.0	n.a.	1.0	Brazil	Buzzi *et al*., 2013
Coal	4.5	1.8	7399.0	n.a.	n.a.	n.a.	n.a.	n.a.	n.a.	1792.0	47.0	30.0	1792.0	n.a.	10.0	Brazil	Buzzi *et al*., 2013
Coal	3.1	n.a.	n.a.	n.a.	498.0	1.4	n.a.	n.a.	2135.0	n.a.	428.0	30.0	84.0	3.7	6.9	South Africa	Kefeni *et al*., 2018
Coal	3.5	n.a.	1375.0	19.9	296.6	0.2	n.a.	n.a.	53.3	n.a.	130.1	6.2	n.a.	0.2	0.4	Czech Republic	Heviánková *et al*., 2014
Coal	3.1	n.a.	n.a.	245.0	498.0	1.4	n.a.	n.a.	2135.0	n.a.	428.0	30.0	84.0	3.7	6.9	South Africa	Kefeni *et al*., 2017
Coal [a]	2.5	n.a.	n.a.	174.6	n.a.	n.a.	n.a.	0.4	315.9	n.a.	n.a.	36.9	n.a.	1.6	4.2	United States	Peiravi *et al*., 2017
Coal [a]	n.a.	n.a.	n.a.	34.8	94.2	n.a.	n.a.	25.1	226.4	n.a.	18	n.a.	n.a.	n.a.	18.3	Republic of Korea	Park *et al*., 2015
Copper	2.4	n.a.	n.a.	63.4	n.a.	0.4	0.1	14.7	331.2	5.3	67.0	66.3	3.4	0.3	80.4	China	Chen *et al*., 2014
Copper	2.9	n.a.	3602.0	n.a.	n.a.	n.a.	n.a.	1400.0	27.9	n.a.	n.a.	n.a.	n.a.	0.6	20.4	Chile	Hurtado *et al*., 2018
Copper-Gold-Silver [a]	3.7	14.8	17430.0	1233.0	534.3	4.1	0.1	77.3	16.7	6.2	2265.0	161.5	647.8	1.5	48.9	Australia	Kaur *et al*., 2018

Copper-Zinc	2.6	n.a.	n.a.	260.0	500.0	0.5	n.a.	35.3	443.0	n.a.	771	29.3	158.0	1.3	410.0	Finland	Tolonen *et al*., 2014
Gold	3.1	5.2	n.a.	224.4	498.4	1.4	0.7	0.2	2135.0	n.a.	428.2	30.2	84.0	3.7	6.9	South Africa	Kefeni *et al*.2015
Gold	1.3	18.7	18.2	445.0	347.0	20.0	n.a.	95.7	467.0	6.4	n.a.	2575.0	18.6	102.0	82.0	Brazil	Amaral *et al*., 2018
Gold	1.8	12.4	5501.0	n.a.	444.0	n.a.	n.a.	n.a.	n.a.	n.a.	288.0	n.a.	n.a.	n.a.	n.a.	Brazil	Reis *et al*., 2018
Gold	2.4	n.a.	n.a.	n.a.	561.0	0.8	n.a.	n.a.	835.0	n.a.	358.0	30.0	192.0	1.8	0.9	South Africa	Kefeni *et al*., 2018
Gold	2.4	n.a.	n.a.	0.9	561.0	0.8	n.a.	n.a.	835.0	n.a.	385.0	30.0	192.0	1.8	0.9	South Africa	Kefeni *et al*., 2017
Pb-Zn	1.9	n.a.	6690.0	53.0	n.a.	n.a.	0.4	4.4	1240.0	n.a.	n.a.	13.7	n.a.	n.a.	144.5	China	Chen *et al*., 2015
Polymetallic	2.7	n.a.	6966.0	168.0	n.a.	n.a.	0.1	60.4	520.0	n.a.	n.a.	116.7	n.a.	n.a.	80.1	China	Chen *et al*., 2015
Pyrite	2.7	n.a.	6883.0	117.0	n.a.	n.a.	0.2	n.a.	3150.0	n.a.	n.a.	27.7	n.a.	n.a.	4.9	China	Chen *et al*., 2015
Pyrite	2.5	n.a.	7931.0	1878.0	n.a.	n.a.	0.2	n.a.	3580.0	n.a.	n.a.	145.7	n.a.	n.a.	80.9	China	Chen *et al*., 2015
Silver [a]	2.9	7.5	2194.0	234.0	500.0	1.9	0.2	n.a.	115.0	29.0	408.0	44.0	1154.0	2.8	77.0	Australia	Pozo *et al*., 2017
Silver [a]	2.7	10.0	3499.0	472.0	547.0	2.7	0.4	5.8	564.0	41.0	590.0	58.0	1451.0	4.3	145.0	Australia	Pozo *et al*., 2017
Silver [a]	2.8	9.0	3200.0	403.0	533.0	2.5	0.4	n.a.	399.0	33.0	461.0	50.0	1422.0	3.9	50.0	Australia	Pozo *et al*., 2017

2.2 AMD ENVIRONMENT IMPACT

The number of environmentally impacted areas from mining activity has become increasingly higher due to the emergence of recently abandoned mines. Due to the high corrosivity, elevated metal concentrations and low pH, these acidic effluents are listed as hazardous waste in several countries (LAN *et al*., 2009), and their impact on soil, ground and surface water biota has been pointed out in several studies (ROYCHOWDHURY, SARKAR and DATTA.,2015; VIERS *et al.*, 2019; DENICOLA and STAPLETON., 2002; NIYOGI, MCKNIGHT and LEWIS., 1999; GRAY., 1997; MCCARTHY., 2011; GRANDE *et al*., 2018; ARSÈNE-PLOETZE *et al*., 2018; ZHANG *et al.*, 2019; LIAO *et al*., 2016; DENICOLA and STAPLETON., 2016; KIMBALL, CALLENDER and AXTMANN., 1995; HERLIHY *et al*., 1990). Liao *et al.* (2016) showed the distribution and migration of Cd^{2+}, Cu^{2+}, Zn^{2+}, As^{3+} and Pb^{2+} derived from AMD and their associated health implications to local inhabitants. In total, 74 crop and their corresponding soil samples were analyzed applying carcinogenic and non-carcinogenic risk for hazard evaluation. Results showed that the local soils were heavily polluted with Cd^{2+}, Cu^{2+} and As^{3+} and the estimated total cancer risk exceeded the United States Environmental Protection Agency (USEPA) accepted value of 1×10^{-4}, indicating unsuitability of the soil for cultivating food crops (LIAO *et al*., 2016). When Chamorro *et al.* (2018) assessed the toxicity of an acid effluent by means of water quality and land bioassays, several lethal and sub lethal results was reported by different effluent proportions. The effluent studied presented a pH of 4.01, in addition to high concentrations of sulfate (2,300.0 mg/L), copper (372.2 mg/L), manganese (124.5 mg/L) and zinc (77.8 mg/L), and three different vegetables were considered for the toxicity assessment. *Lactuca sativa* (lettuce), *Raphanus sativus* (radish), and *Triticum aestivum* (wheat) began to present inhibition in their germination process from the proportions of 12.5, 6.5 and 6.25 (v/v %), respectively. Among them, wheat was the most tolerant when comparing the results of 50% lethality (LC50) after 144 h, corresponding to LC50 = 62 v/v %, followed by LC50 = 21 v/v % for lettuce and LC50 = 17 v/v % for radish.

Considering the number of studies reporting environment contamination and impact by acidic effluents over the past years, it is important to propose effective remediation methods as well as the contaminated areas recovery. Mocq and Hare (2018) when evaluating Lake Arnoux (Quebec, Canada) physicochemical properties and benthic invertebrate communities after its restoration process, observed that the pH increased by about one unit and the concentrations of many trace metals declined substantially. Over the years of restoration, between 2008 and 2010, it was

observed that communities in highly contaminated stations tended to be dominated by burrowing taxa such as larvae of *Chironomus* (Chironomidae) and Oligochaeta, whereas less contaminated stations had taxonomic and functional communities that were more diverse (MOCQ and HARE., 2018).

It is a fact that these metal compounds present high toxicity as demonstrated by Chamorro *et al.* (2018) and Shao *et al.*(2018). For this reason, several regulatory agencies have stablished legislation regulating these effluents discharge into the environment. In Table 2.1 are presented the water quality standard established by the Environmental Protection Agency (EPA), its comparison with the standards established by the National Council of the Environment (CONAMA – Brazil), and the effects caused by continuous ingestion and in high concentrations of these metallic compounds. Although some of these compounds are considered nutrients, such as iron and copper, they are also associated with human health impacts in high concentrations (KARIM., 2018; PLUMLEE, MORMAN and ZIEGLER., 2006).

Although the AMD composition varies according to the location and mining activity, in general high sulfate contents derived from the oxidation process are reported in different studies, as can be seen in Table 2.1.

Table 2.2 - Established limits by the agencies EPA and CONAMA regarding the water quality standard and the observed effects associated with these compounds' ingestion

Water Quality Standard	EPA USEPA., 2002	CONAMA BRASIL., 2005	Health effects	Ref.
pH	5-9	5-9		
Al^{3+} (mg/L)	0.01	-	Behavioral and morphological changes associated with Alzheimer's disease and age-related neurodegeneration	OLIVER and GREGORY., 2015; BONDY., 2016.
As^{3+} (mg/L)	0.01	0.50	A variety of complications in body organ systems: integumentary, nervous, respiratory, cardiovascular, hematopoietic, immune, endocrine, hepatic, renal, reproductive system and development	MOHAMMED *et al.*, 2015.
Cd^{2+} (mg/L)	0.05	0.20	Few human studies have shown associations between cadmium exposure and diabetes, hypercholesterolemia, hypertriglyceridemia, kidney and liver disease	OLIVER and GREGORY., 2015; SWADDIWUDHIPONG *et al.*,2015.
Co^{2+} (mg/L)	0.1	-	Cardiomyopathy, nerve deafness and goiter, lung disease, pneumoconiosis, fibrosis	ZADNIPRYANY *et al.*, 2017; CARSON, ELLIS and MCCANN., 2018.
Cr^{2+} (mg/L)	0.1	1.0	Carcinogen associated with lung, nasal, and sinus cancers	MISHRA and BHARAGAVA., 2016.

Cu^{2+} (mg/L)	1.3	1.0	Acute irritation to upper respiratory tract, changes in the nervous system, gastrointestinal irritation, depression and lung cancer	GARRAWAY.,1983; MOREIRA *et al.*, 2019.
Fe^{2+} (mg./L)	0.3	15.0	Pneumoconiosis, vomiting, gastrointestinal bleeding, lethargy, restlessness, and perhaps gray cyanosis.	CARSON, ELLIS and MCCANN., 2018.
Hg^{1+} (mg/L)	-	0.01	Neurological disturbances including ataxia, sensory loss and constriction of visual field. Kidney and liver damage. Fetus development issues	GARRAWAY., 1983.
Mn^{2+} (mg/L)	0.05	1.00	Dyspnoea, alveolar inflammation	GARRAWAY., 1983.
Ni^{2+} (mg/L)	0.10	0.01	Dyspnoea, interstitial pneumonitis	GARRAWAY., 1983.
Pb^{2+} (mg/L)	0.015	0.500	Neurological damage, behavior and haematological effects	OLIVER and GREGORY., 2015; GARRAWAY., 1983.
Zn^{2+} (mg/L)	5	5	Reproductive effects	OLIVER and GREGORY., 2015.

2.3 AMD TREATMENT OPTIONS

According to Kefeni *et al.* (2017), some methods and processes can be used to treat AMD, although, these treatments are considered to be complex and costly. The traditional neutralization and the metals precipitation procedure, followed by discharge, generates large wastes volume, causes high consumption of alkalizing agents and generates large amounts of unstable sludge, which need to be disposed correctly in order to avoid secondary pollution (LAN *et al*., 2009, TANG *et al*., 2009). Different treatments techniques have been studied for AMD. In this context, among these methods used for recycling hydrochloric acids and salts include ion-exchange (CSICSOVSZKI, KÉKESI and TÖRÖK., 2005); selective precipitation (HERAS *et al*., 2004; JANDOVA, MAIXNER and GRYGAR., 2002); anion exchange and membrane electrowinning (CSICSOVSZKI, KÉKESI and TÖRÖK., 2005); microwave-hydrothermal process (CIMINELLI, DIAS and BRAGA., 2006); electrodialysis (URANO, ASE and NAITO., 1984; PAQUAY *et al*., 2000); solvent extraction (AGRAWAL *et al*., 2007); membrane distillation (TOMASZEWSKA., 2001; TOMASZEWSKA, GRYTA and MORAWSKI., 1998) or combination of these methods (CSICSOVSZKI, KÉKESI and TÖRÖK., 2005; WIŚNIEWSKI and WIŚNIEWSKA., 1999). Table 2.2 presents a detailed report about the previous studies quoted and others.

Table 2.3 - Summary of studies that aimed the selective recovery of value-added compounds in acidic effluent

Method	Method description	Objective	Effluent characteristics	Results	Ref.
AMD Treatments					
Membrane Separation Process	Electrodialysis (ED) tests were conducted in a laboratory cell with five compartments, using HDX 100 and HDX 200 as a cation and anion exchange membranes, respectively.	Acid mine drainage treatment by ED for water recovery.	Real: AMD from a coal mine.	ED is suitable for recovering water from acid mine drainage, with contaminant removal efficiencies greater than 97%.	BUZZI *et al*., 2013.
	UF process worked as a pretreatment stage. The metals were retained in the NF stage while its permeate was subjected to the RO for high-quality water obtainment and acid concentration.	UF–NF–RO integrated system for metals concentration, and recovery of acid and water.	Real: ADM from gold mine.	Recovery of a purified acid stream was possible, besides the production of a metal enriched stream and the generation of high-quality reuse water.	AMARAL *et al*., 2018.
Precipitation and Neutralization	Sodium hydroxide, calcium hydroxide and sodium carbonate were used. For precipitation tests, the pH was increased by adding a small amount of neutralizing agent, at 200 rpm.	Proper conditions that can selectively precipitate and recover the dissolved Fe^{2+}, Al^{3+} and Mn^{2+}.	Real: AMD from an abandoned coal mine.	Recovery ratios of dissolved Fe^{2+} and Al^{3+} reached 99.2 – 99.3% at pH 4.5. Recovery of Mn^{2+} reached 37.8 – 87.5% at pH 8.5.	SEO *et al*., 2017.

Wood ash and calcium hydroxide was dosed at different amounts. A 20 min reaction time was considered, at 150 rpm.	Compare the removal efficiency of wood ash and calcium hydroxide.	Real: AMD from a coal mine.	Removal efficiency was 100% for almost all metals (Fe^{2+}, As^{3+}, Co^{2+}, Cu^{2+}, and Al^{3+}) except for Mn^{2+} (30%), Ni^{2+} (20%), and Zn^{2+} (53%).	HEVIÁNKOVÁ, BESTOVÁ and KYNCL., 2014.
Ferrous ions were first oxidized by 0.15 mL/L 30% H_2O_2, and then a four-step fractional precipitation was applied with the selective addition of Ca $(OH)_2$ and Na_2S solutions.	Recycling of Fe^{2+}, Cu^{2+}, Zn^{2+} and Mn^{2+} from acid mine drainage.	Real: AMD from copper mine.	Recovery efficiencies were > 79.7% for Fe^{2+}, Cu^{2+}, Zn^{2+} and Mn^{2+} after the precipitation process.	CHEN *et al*., 2014.
Different amounts of lime, bayer hydrotalcite, bayer liquor, sodium carbonate and sodium hydroxide were added to 25 mL of AMD. The mixture was agitated for 24 h.	Comparison of bayer liquor and precipitates performance with commercially available alkali used in the treatment process.	Real: AMD from a copper-gold-silver mine.	Lime and Bayer precipitates were more effective in removing the metals. Their removal capacity was approximately the same for Al^{3+}, Cu^{2+}, Fe^{2+}, Zn^{2+} and Ni^{2+}, achieving acceptable discharge limits.	KAUR *et al*., 2018.
The sample had its pH raised to 9.5, being further agitated (150 rpm/1 min), followed by slow mixing (50 rpm/5 min) and then left to settle for 30 min.	Comparison of by-products from quicklime with commercial quicklime and hydrated lime.	Real: AMD of a copper-zinc.	Remover capacities over 99% of Al^{+3}, As^{2+}, Cd^{2+}, Co^{2+}, Cu^{2+}, Fe^{2+}, Mn^{2+}, Ni^{2+}, Zn^{2+} and approximately 60% of sulphate were obtained for the by-products.	TOLONEN *et al*., 2014.

Adsorption	The sample had its pH adjusted to 5 - 6 and aerated for partial oxidation of Fe^{2+}. Thereafter, 102 mg nanoparticles were added, and the samples were stirred for 1 h at 60 °C.	Synthesis of high purity α-Fe_2O_3 nanoparticles and its removal capacity evaluation of potentially toxic metal ions.	Real: AMD from a gold and coal mine.	Treatment resulted in complete removal of Al^{3+}, Mg^{2+}, Mn^{2+} and Fe^{2+} while for Zn^{2+} and Ni^{2+} over 80% and Ca and Na in between 47 and 72% removals.	KEFENI *et al*., 2018.
	The sample had its pH adjusted to 5 - 6 and then aerated. 40 ml of fresh AMD and 80 mL oxidized AMD were mixed, followed by the addition of 100–102 mg of nanoparticles, being further stirred and heated to 60 °C, for 1 h.	Insights into the relative efficiency magnetic nanoparticles for metal removal either via incorporation or adsorption route from AMD.	Real: AMD from a gold and coal mine.	Results have shown complete removal of Al^{3+}, Mg^{2+}, and Mn^{2+}, while for Fe^{2+}, Ni^{2+} and Zn^{2+} over 90% removals were recorded.	KEFENI, MAMBA and MSAGATI., 2017.
Electrochemical	Direct and indirect oxidation test were considered. For the direct oxidation reactor, Fe^{2+} was used for the anolyte while $NaHCO_3$ was used as catholyte. In the indirect oxidation reactor, $NaHCO_3$ was used as the electrolyte.	Neutralizing agent generation via electrochemical reactions.	Real: AMD from an abandoned coal mine.	The neutralizing agent produced by electrochemical methods showed potential in selective recovery of dissolved metals in AMD.	PARK *et al*., 2015.

The biocathode was operated during 28 days after inoculation with planktonic microorganisms (*Desulfovibrio* and *Desulfomicrobium*). 2.2 g/L Na_2SO_4 and 0.5 g/L $NaHCO_3$ were added as the only sulfate and carbon source. The medium was prepared under anaerobic conditions.	BES for metals Separation into a concentrated sludge.	Real: AMD from an abandoned silver mine.	Removal and recovery of the main cations Al^{3+}, Fe^{2+}, Mg^{2+}, Zn^{2+} into a concentrate stream, in addition to 85 ± 2% sulfate removal and also reducing salinity.	POZO *et al*., 2017.
Activated sludge with 5 times dilution (6.5% *Serratia* spp) from a local wastewater treatment plant was placed in the anode chamber (deoxygenated). No external nutrients were added. The AMD was treated in the cathode chamber.	Efficiency comparison for AMD treatment.	Real: AMD from an abandoned coal mine.	More than 99% of Al^{3+}, Fe^{2+} and Pb^{2+} were removed, and removal rates of 93%, 91%, 89% and 69% were achieved for Cd^{2+}, Zn^{2+}, Mn^{2+} and Co^{2+} respectively.	PEIRAVI *et al*., 2017.

Among these different treatment's techniques, the direct contact membrane distillation associated with the ion-exchange will be discussed to obtain a water reuse and to promote a metal recover.

2.4 PRESSURE DRIVEN MEMBRANE SEPARATION PROCESS

The membrane separation processes (MSP), that combine operation ability with the excellent treatment quality, has become a promising technology for acid mining effluent treatment (URTIAGA *et al*., 2013, PINO *et al*., 2018). Among the classical MSP stand out the microfiltration (MF), ultrafiltration (UF), nanofiltration (NF) and reverse osmosis (RO) techniques, which use the pressure gradient as the driving force and these membranes differ mainly by pores size and, consequently, what it is able to reject. The effluent characteristics that will be treated (feed) and the water quality, which will be obtained after membrane separation (permeate), define which membrane type is most applicable according to its selectivity.

RO and NF are physical separation technologies that use a semipermeable membrane acting as a selective barrier, on which an external pressure is applied, provoking a water passage through the membrane retaining part of the constituents present in the feed (SHENVI *et al*., 2015; MALAEB and AYOUB., 2011; MILLER, SHEMER and SEMIAT., 2014). Some studies indicate that NF membranes provide higher permeability since they present larger molecular weight cut-off (MWCO) than RO, and, consequently, need a lower pressure application to generate the same permeate volume, considering the same effective filtration area when compared to the RO (GEISE and FREEMAN., 2014; YING ZHAO *et al*., 2017) . Nevertheless, NF also presents a lower monovalent ions rejection (<70%) than RO processes, but they offer a reasonable multivalent ions rejections (> 99%) and organic matter (> 90%), while RO membrane presents high efficiency (> 99%) in all of these elements retention (TANG, CHONG and FANE., 2011; AL MAMUN *et al.,* 2017;BAKER., 2000). Thus, both methods show high potential for acid mining effluent treatment aimed metal and acid solution recovery and reuse water production (AGUIAR *et al*., 2016).

According to López *et al.* (2018), NF application for POX treatment has been studied and they achieved a metal rejection >85 % and high acid permeation through the membrane, since sulphuric acid is found as a monovalent ion (HSO_4^-), which is easier to permeate the NF than

the divalent ion (SO_4^{2-}). According to Fu and Wang (2011), RO membranes are capable of rejecting more than 95% of metal in solution, being that copper and nickel rejection efficiency by RO is higher than 99.5%. In order to achieve better efficiencies in the metals, and, mainly, acid solution retention as well reuse water generation, it is possible to notice the increase about the treatment route that integrates NF and then RO (RICCI *et al*., 2017; AGUIAR *et al*., 2016; AMARAL *et al*., 2018; RICCI *et al*., 2015; ANDRADE *et al*., 2017) . For example, Ricci *et al.* (2015) observed a 99% increase in acid concentration in the retentate compared to the feed. On the other hand, if only consider the NF application, this concentration achieved was 82%.

However, one of the major obstacles in the driven-pressure membranes use is the fouling phenomenon. The fouling results in several detrimental effects on the process efficiency. Among these effects, it is worth noting the decrease in water production due to the flux decline. Because of this flux drop-in, it is necessary to increase the pressure, applied as the driving force, to obtain the same water rate production. In addition, fouling also contributes to the gradual membrane degradation thereby decreasing the permeate quality and the membrane lifespan (NG and ELIMELECH., 2004). Moreover, the application of NF and RO is restricted to effluents with temperatures below 40 ºC since this is the maximum operating value of most of these membranes. The POX effluent reaches around 200 ºC and then is cooled, in the mining plant, to 50-80 ºC. This effluent to be treated by NF and/or RO still needs to be subjected to further cooling, which adds an operational cost to these techniques (REIS *et al*., 2018).

With this additional cooling cost to apply the NF or RO in order to treat a POX effluent the membrane distillation (MD) process has been emphasizing since the latter uses as a driving force the vapor pressure gradient. This gradient is obtained by the current's temperature difference as the feed (POX effluent) can present a 45-85 ºC and permeate (treated effluent) can stays at a room temperature (25 ºC) (ZARE and KARGARI., 2018). Thus, the MD, which will be detailed afterwards, can utilize the residual heat from the POX effluent to be operated, dispensing the cooling step and thereby lowering operating costs.

2.5 MEMBRANE DISTILLATION

Membrane distillation (MD) is an emerging process with great potential to treat concentrated effluents. The MD is commonly employed in the non-volatile compound's separation. This

method driving force is a vapor pressure difference between the two sides of hydrophobic membrane surfaces, that is constituted by a non-wetted micropores, which allows mass transfer of volatiles molecules through the microporous of hydrophobic membrane (CAMACHO *et al*., 2013; KIM *et al*., 2013; KIM *et al*., 2018; BINIAZ *et al*., 2019; LAQBAQBI *et al*., 2019; SOUHAIMI and MATSUURA., 2011; SALLS *et al*., 2018; TAI *et al*., 2019).

This technology has been shown to be effective in water and wastewater treatment and it is widely used to concentrate aqueous solutions simultaneously generating a distillate with high physical chemical quality without requiring a pre-treatment as in others pressure-driven membrane separation processes (MSP). In addition, MD operates at relatively low temperatures. Generally, in this process, gradients temperatures between 10 to 20 °C may be sufficient to produce distilled water. Therefore, the residual heat associated with the effluent could be used to drive the MD system, which can still be achieved by taking advantage of waste heat or by integrating with some renewable energy, such as the solar one (RYU *et al*., 2019; BINIAZ *et al*., 2019; JOHN *et al*., 2004; ZHANG *et al*., 2019). Besides, since mass transfer occurs in the vapor phase, MD is not limited by the osmotic pressure difference between the feed and permeate, being capable of concentrating non-volatiles solutions until their saturation without significant decline of the permeate flux and quality (LAQBAQBI *et al*., 2019).

In this context, MD has been shown as a promising treatment in order to recover acid and metal species since only vapors from volatile molecules can be transported through the pores, that composes the membrane surface. Moreover, other fact that contributes to the MD's application refers to the development of increasingly chemically resistant membranes for tolerating extreme pH conditions (SCHÄFER, *et al*., 2000).

Among the MD process advantages, stands out: (i) the ability of 100% (theoretical) rejection of non-volatile compounds and inorganic ions; (ii) the possibility of operating at a relatively low temperature when compared to the conventional distillation process; (iii) lower operating pressures when compared to the classical MSP that have the pressure gradient as the driving force and, (iv) less influence of the fouling phenomenon due to less chemical interaction between process solution and membrane surface (BINIAZ *et al*., 2019; WANG and CHUNG., 2015; MANNA and PAL., 2016). Moreover, MD could be operated without pre-treatment since it is able to treat a high concentrated feed stream, being less sensitive to concentration polarization effect than other classical membrane separation process (MSP) (BINIAZ *et al*., 2019;

ALKHUDHIRI and HILAL., 2018). However, large-scale MD applications are still challenging, hampered by the lower energy efficiency associated, and a lack of MD modules manufactured for large-scale applications (BINIAZ *et al*., 2019).

Thus, MD has been highlighted by the distillate quality generated in its process, which can be used as industrial reuse water, yielding a lower demand for this non-renewable resource. In addition, MD application allows acid and metals concentration, elements which have an aggregate economic value, as mentioned before, allowing a greater operational costs reduction.

2.5.1 MD configuration and modules

Unlike the other membrane separation process (MSP), which the permeate is directly collected on the lower pressure side, the vapor transported through the membrane can be condensed via different methods, classifying the process in four major configurations. These configurations are: direct contact membrane distillation (DCMD), air gap membrane distillation (AGMD), sweep gas membrane distillation (SGMD) and vacuum membrane distillation (VMD), all of which represented in Figure 2.1.

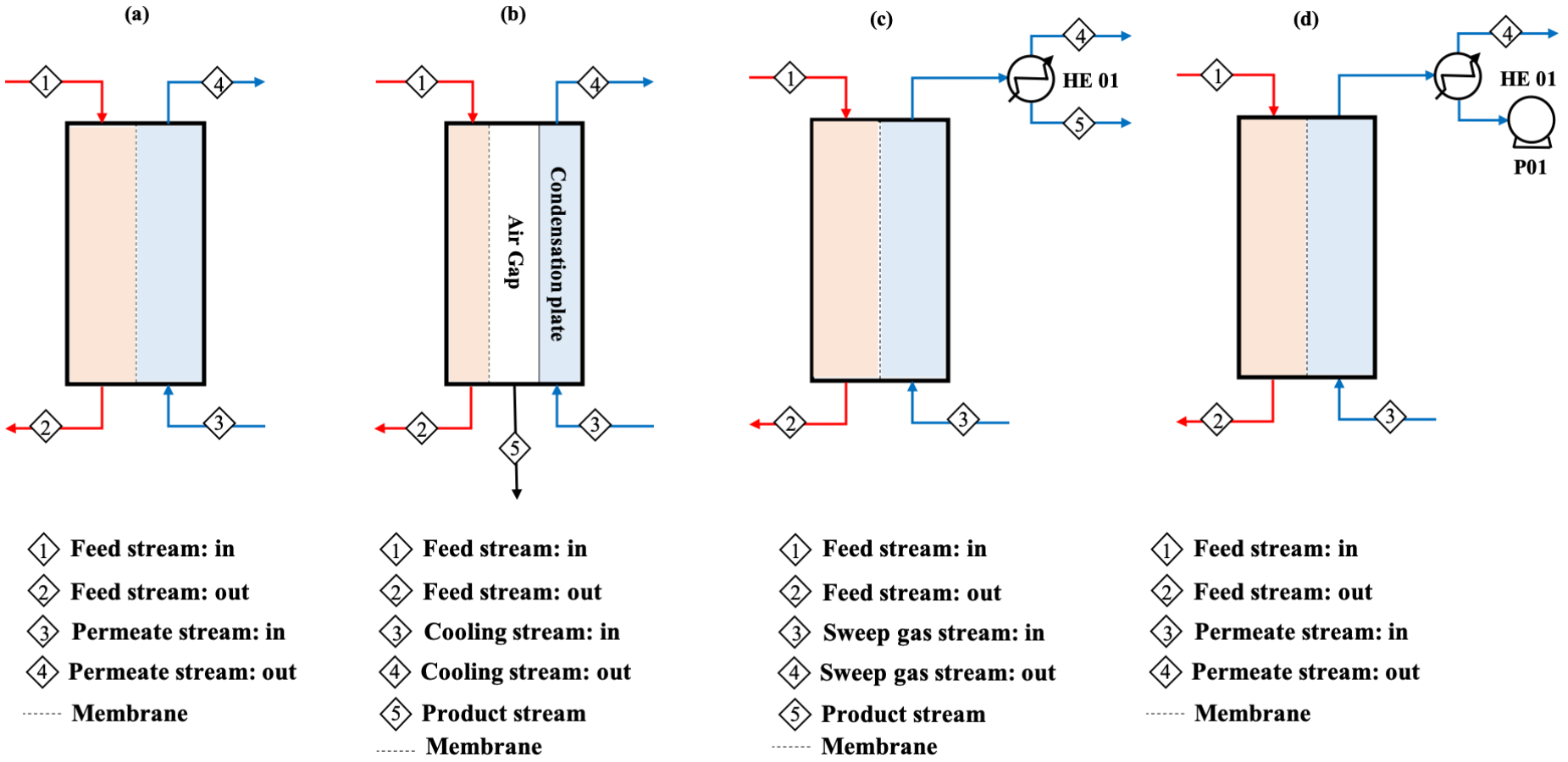

Figure 2.1 - Different membrane distillation configuration. (a): Direct contact membrane distillation (DCMD); (b): Air gap membrane distillation (AGMD); (c): Sweep gas membrane distillation (SGMD); and (d): Vacuum membrane distillation (VMD). HE01: Heat exchanger.

According to Rahimpour *et al.* (2019), the DCMD is the oldest and most widely used process to aqueous solution concentration. As can be seen in Fig. 2.1.a, an aqueous solution at lower temperature is in direct contact with the membrane surface on the permeate side. In this configuration, the temperature difference across the membrane is capable of inducing a vapor pressure difference and, consequently, the volatile molecules transport from the feed solution towards the permeate side. Among the configurations presented, the DCMD process is considered the simplest one, although presenting a higher heat loss when compared to other configurations (RYU *et al.,* 2019; BINIAZ *et al.,* 2019; SHIRAZI *et al.,* 2016). For the second configuration, AGMD (Fig. 2.1.b), a space, usually filled with air, is established between the membrane and the lower temperature surface, so that the molecules must cross both the membrane surface and the air gap, being further condensed and recovered (EYKENS *et al.,* 2016). Due to the air gap that separates the two surfaces, an additional resistance is provided to the mass transfer process. However, the AGMD presents lower heat loss comparing to DCMD because the feed stream is not in direct contact with the cold face (permeate). Still, in general, AGMD presents smaller flux when compared to the DCMD process. As a consequence, a larger membrane area would be required in order to generate the same permeate volume under similar conditions. (TAI *et al.,* 2019; WANG and CHUNG., 2015; ASHOOR *et al.,* 2016; URAGAMI., 2017). AGMD stands out among the other MD configurations for achieving the highest energy yield and can be used in two different modules: flat sheet and hollow fiber. However, despite these advantages, this configuration presents more complex module designs which makes it difficult to extend its application (BINIAZ *et al.,* 2019). It is also noteworthy that for the DCMD and AGMD configurations spacers can be used to promote turbulence at the interface between the feed and the membrane surface, which contributes to the reduction of the concentration polarization phenomenon (JIAO, CASSANO and DRIOLI., 2004). As this polarization is one of the biggest obstacles that corroborates to DCMD heat loss, using the spacer can makes DCMD even more competitive against AGMD. In the SGMD process (Fig. 2.1.c), an inert drag gas generally at low temperatures, is used to promote the vapor molecules recovery from the membrane surface, which occurs outside the membrane module by an additional condenser (DRIOLI, ALI and MACEDONIO., 2015). The configuration achieves lower flow rates between the MD systems, thus requiring high volumes of sweep gas and condenser, making this configuration less economically competitive (BINIAZ *et al.,* 2019; ALKHUDHIRI and HILAL., 2018). For the last configuration, VMD (Fig. 2.1.d), vacuum is applied on the permeate side in order to promote a vapor pressure gradient between the membrane surfaces and thus favor the

process recovery. This configuration presents as a great advantage the small heat loss in addition to be more difficult to wet the membrane. However, VMD is more susceptible to fouling phenomenon (BINIAZ *et al.,* 2019; ALKHUDHIRI and HILAL., 2018).

2.5.2 Membrane distillation materials

MD membranes can be manufactured in different ways and materials, hence they have distinct properties regarding porosity, hydrophobicity, thermal conductivity etc. (CURCIO and DRIOLI., 2005). Among the polymers most used for the MD membranes manufacture, poly(propylene) (PP), poly(tetrafluoroethylene) (PTFE) and poly(vinylidenefluoride) (PVDF) stands out (GRAY *et al.,* 2010). PTFE has becoming more popular due to higher hydrophobicity, higher contact angle with water, good resistance to temperature and chemical oxidation. A downside to this material is the greater thermal conductivity, around 0.25 W/m·K which can cause loss of heat through the membrane (KESIEME., 2015; TAI *et al.,* 2019). On the other hand, according to Dumée *et al*. (2010) and Tai *et al*. (2019), PVDF is the most investigated material for MD application due to its simple manufacturing process compared to PTFE. PVDF presents good hydrophobicity, thermal resistance, mechanical strength and can be easily prepared into membranes with versatile pore structures by different methods. PP also exhibits good thermal and chemical resistance, presenting a thermal conductivity around 0.17 W/m·K, however, its moderate resistance at higher temperatures compromises its application to MD membranes (TAI *et al.,* 2019; SUK *et al.,* 2010). These membranes usually have the porosity in the range of 0.60 to 0.95 and the pore size in the range of 0.2 to 1.0 μm and the thickness in the range of 0.04 to 0.25 mm (TOMASZEWSKA., 1996). In this context, more recently, studies aim to develop new membranes with greater mechanical strength, hydrophobicity and porosity. Techniques such as stretching, sintering and phase inversion have been used for manufacturing new membranes containing carbon nanotubes and fluorinated copolymer materials (GROSSI., 2018; GRYTA., 2008; WANG *et al.,* 2019; XIAO *et al.,* 2019; XIAO *et al.,* 2019).

In order to minimize fouling caused by organic compounds, Chen *et al*. (2017) investigated the association of PVDF hydrophobic membrane with strongly hydrophilic zwitterionic chemicals. In this sense, a zwitterionomeric acid, 3-[[3-(tretoxyethoxysilyl)propyl]amino] propane-1-sulfonic acid (TPAPS) was grafted onto a PVDF hydroxylated microfiltration membrane. Thus, the virgin PVDF membrane (V-PVDF) was compared to the zwitterionomer acid exerted into to PVDF membrane (T-PVDF). To compare the efficiency of both membranes, the DCMD test was applied to treat a synthetic gray water effluent as a feed. The test was performed using a feed

temperature of 60 ºC and a permeate of 20 ºC, and the velocity flow of both currents was 0.11 m/s. As a result, both membranes fouled, but T-PVDF fouled more slowly, showing less decline in permeate flux throughout the process. This higher T-PVDF fouling resistance was attributed to the surface's hydrophilicity and to the charge's effect due to the chemical graft with zwitterionomer acid.

Scaling is the main fouling in membrane surfaces whose effluent to be treated presents high inorganic compound's concentrations, such as acid drainage. But, MD is not limited by the osmotic pressure difference between feed and permeate, being capable of concentrate non-volatiles solutions until their saturation point without a significant decline of the permeate flux and quality (CAMACHO *et al.,* 2013). MD has been successfully in the treatment of different effluents. In this sense, Kesieme *et al*. (2014) applied DCMD with a flat sheet PTFE membrane to recover acid from mining leach solutions containing HCl or H_2SO_4 and metals such as aluminum, copper, nickel among others. In this study an acid and salt rejection greater than 99% was found. Hull and Zodrow (2017) achieved > 99% dissolved solids rejection in acid rock drainage (ARD) demonstrating that membrane distillation can treat ARD solutions with high concentrations of dissolved compounds.

Thereby, upon reaching the saturation limit, these elements tend to precipitate on the membrane surface and this phenomenon's consequences are easy to be measured (YANG *et al.,* 2014). Among the scaling's negative effects, there is the hydrophobic membrane character's reduction making it hydrophilic and, consequently, corroborates to its wetting and to the permeate quality degradation, besides the temperature polarization's increases (YANG *et al.,* 2014; YANG *et al.,* 2015). However, how to avoid scaling remains a significant challenge in membrane technology because according to fouling in MD it occurs at three interfaces: liquid phase (feed) - gas phase created by diffusion steam (pore) - solid phase (polymer) but some operational measures can be adopted to minimize its occurrence, such as increased feed flow and air injection (WEI *et al.,* 2012; TIAN *et al.,* 2015). Although these operational changes may still be ineffective given the high salt concentration in the feed stream. Thus, an alternative is to invest in modifications to the membrane surface to be more detrimental to this fouling's type. In this sense, it is clear that the nanotechnology development, including treatment with plasma's fluorination allows the production of hyper hydrophobic membranes, with excellent antifouling properties, such as contact angle with water greater than 150º and sliding less than 10º, which induces water's repulsion and creates the self-cleaning membrane surface, because fluorinated materials have a

low surface tension (YANG *et al.,* 2014; LEE *et al.*, 2016; ALI *et al.,* 2012). The surface modification process occurs by replacing CH bonds with CF and CF_3 with the possibility of polymeric materials deposition (ALI *et al.,* 2012). According to Yang *et al*. (2014) membranes with micro-pillar arrays (MP-PVDF) and additional CF_4 plasma treatment (CF4-MP-PVDF) showed a greater contact angle (~155.3°) than the commercial PVDF membrane (C-PVDF), whose contact angle is (~130.1°). The membrane MP-PVDF has a lower water slip angle (below 10º) compared to C-PVDF (above 90º), which increases its repulsion by water droplets, which float above the polymer surface due to the low adhesion to the material. Thus, a low interaction between the effluent and the membrane surface is obtained, which was proven by using CF_4-MP-PVDF membrane in the DCMD process by applying a NaCl solution (25 %wt), which showed lower susceptibility to fouling against the MP-PVDF and C-PVDF membrane. In addition, autopsy of the membranes revealed that wetting occurred in the membrane MP-PVDF but was not observed in CF_4-MP-PVDF.

It is noteworthy that the MP-PVDF membrane achieved results linked to the direct contact and slip angles between the values obtained by C-PVDF and CF_4-MP-PVDF. However, the MP-PVDF and CF_4-MP-PVDF membranes reached higher porosity (~87% and ~86%, respectively) than the C-PVDF membrane (~52%). A bench-scale DCMD test applying the three membranes mentioned above and using a saturated $CaSO_4$ solutions as feed (2000 mg/L) on the temperature of 70 ºC and distilled water at 20 ºC was carried out. This test showed as the best result the CF_4-MP-PVDF membrane whose flux remained stable. In addition, SEM images of the three membranes indicated high precipitation of $CaSO_4$ crystals on the surface of C-PVDF and MP-PVDF, but this phenomenon was not observed in CF_4-MP-PVDF. In this sense, Warsinger *et al*. (2015) evaluated the superhydrophobic membranes manufacture by CF_4 surface gas deposition, which may lead to an increase of up to 30 % of permeate flux in DCMD processes compared to the use of membrane modification by conventional one. Although the application of the CF_4-PVDF membrane is promising, it is necessary to deepen the studies in real scale, since in large scale the material may have some relevant implications (ALI *et al.,* 2012).

Tijing *et al*. (2015) evaluated the CF_4 plasma-treated superhydrophobic membrane's performance in DCMD for two types of effluent, the first (E1) consisting of hexadecane 2,400 ppm, sodium dodecyl sulfate (SDS) 240 ppm, Sodium Chloride (NaCl) 10,000 ppm and pH (measured) 6.1 ~ 6.3. The second feed (E2) consisted of hexadecane 2,400 ppm tetradecyl dimethyl benzyl ammonium 240 ppm, sodium chloride (NaCl) 10,000 ppm and pH (measured)

6.2 ~ 6.4. It should be noted that to aim to test about oily compounds affinity with virgin PVDF (V-PVDF) and the modified membrane (T-PVDF), both were placed in contact with hexadecane, whose surface tension is 27.2 mN/m. This substance wetted the V-PVDF membrane immediately, while T-PVDF resulted in a contact angle between 90.9 ~ 95.5º, meaning the T-PVDF membrane is also oleophobic. Regarding the DCMD test, permeate fluxes were 20.5 kg/m^2h and 25.6 kg/m^2h for V-PVDF and T-PDVF, respectively. For E1, the V-PDVF presented a contact angle with water of 70º, which allowed the passage of E1 through the membrane pores, blocking them and, consequently, decreasing the flux and permeate quality. The T-PVDF membrane showed stable flux and good rejection. In relation to E2, the PVDF-V membrane was immediately wetted according to the instantaneous increase in permeates electrical conductivity (3 to 83.1%).

However, the higher membrane hydrophobicity implies the greater the susceptibility to severely occurring the temperature polarization phenomenon and decreasing evaporation efficiency due to good thermal conductivity (HE *et al.,* 2008). Thus, the superhydrophobic membrane, normally, exhibits permeate flux loss. Thus, hydrophilic membranes have characteristics opposite to those linked to hydrophobicity. Studies that consider the association of the hydrophilic layer, with CF_4 deposition treatment, to obtain a hydrophobic layer have also been highlighted. In this sense, Gryta *et al*. (2006) evaluated the super hydrophobicity process using polysulfone (PSf) hydrophilic membranes. As a result of this modification, PSf obtained twice the permeate flux with treatment compared to the commercial PVDF membrane. This occurred because the treated PSf presented less tortuosity and lower resistance to mass transfer at high water contact angle (137º). In this sense, He *et al*. (2008) used CF_4 plasma treatment on the asymmetric hydrophilic polyethersulfone flat membrane and a hollow fiber surface for the DCMD process. Modification in both membranes contributes to increase in flux and in the salts rejection with less susceptibility to wetting due to the increase in contact angle with water. Thus, the conciliation of the super hydrophobization treatment of a hydrophilic membrane may be promising in view of the increased permeate flux. Lee *et al*. (2016) evaluated the potential of the laminated PTFE membrane in bench-scale DCMD. The process performance was evaluated using a 213,33 g/L NaCl solution as feed. The feed and permeate were circulated at 600 mL/min. The results of the single layer PTFE flat membrane showed that this material had a high flux but showed fouling and wetting in a short test period, even with the simple NaCl feed composition. In addition, it was found at the end of the test that the initial contact angle (151.7°) reduced to 110° at the end of the test reducing the hydrophobic membrane character. For the double-

laminated PTFE membrane, it presented stability in relation to flux and permeate quality. However, the membrane side in contact with the effluent was contemplated by the decrease in the contact angle, which, at the end of the 28th day of the test, dropped to 90º. However, the side facing the permeate remained intact; therefore, replacing the feed interaction layer with a new layer will restore membrane performance. However, the use of multilayer membranes should be well planned not to burden the system on demand of larger areas and modules to obtain a certain flux, because the association of layers may decrease the pore size which may influence the permeated flux declines.

Another alternative for increasing the hydrophobicity of the membrane concerns of nanomaterials application. Alklaibi *et al.* (2005) found that the direct addition of TiO_2 nanoparticles in electrospinning membrane manufacturing can help to improve membrane hydrophobicity as TiO_2 particles cause a reduction in pore size of the membrane, which corroborates the increase in contact angle and LEP parameters over 194.5 kPa. Thus, the 10% TiO_2 membrane had a permeate flux of approximately 40 kg/m^2h, without any noticeable reduction in its permeability, even in seven-day operation. Moreover, Schneider et al. (1998) explored the graphene's incorporation in the PVDF membrane, which became rougher and also more hydrophobic, corroborating the MD process robustness.

Different materials used give distinct membrane properties, and these can directly affect the water production cost, Gryta *et al*. (2009) reported this specific situation. This cost was calculated as a function of membrane porosity, tortuosity, thermal conductivity, pore diameter, and thickness for a small-scale, single-stage MD process driven by waste heat. They concluded that all five membrane properties examined were found to have a significant effect on water production cost, which under optimized conditions, the water production cost can be less than 1 USD/m^3.

2.5.3 Membrane distillation fouling, temperature and concentration polarization

As with all other MSP, fouling is one of the main obstacles to be overcome, since it adds resistance to water permeation (decreasing water flux) and causes progressive membrane wetting. Thus, the effluent can permeate the membrane pores, reducing its selectivity significantly and, consequently, the permeate physical-chemical quality (XIAO *et al.,* 2019; XIAO *et al.,* 2019; SRISURICHAN *et al.,* 2005). Although complex, it is well known that fouling phenomena depend on (i) fouling agent characteristics (concentration, solubility,

diffusivity, hydrophobicity, charge, among others); (ii) membrane properties (hydrophobicity, tortuosity, pore size, surface charge, among others); (iii) operating conditions (permeate flux, temperature and recirculation rate); and (iv) feed stream physical-chemical characteristics (pH, ionic strength, inorganic concentration) (BUFFLE *et al.,* 1998).

Despite the MD membranes lower propensity for fouling compared with the classical membrane separation process (MSP), mainly nanofiltration and reverse osmosis, several fouling types can occur, for example, inorganic, organic and biological fouling (SRISURICHAN *et al.,* 2005). But, it is worth mentioning that, according to the physico-chemical characteristics of the POX effluent the present study will evaluate the inorganic fouling occurrence.

Inorganic fouling generally refers to the precipitated hard minerals deposition from the feed solution involving both crystallization and transport mechanisms (BUFFLE *et al.,* 1998). Additionally, inorganic and precipitated colloidal particles such as silica, clays among others, also contribute greatly to inorganic fouling formation. The depositions are formed when the ionic product of the weakly soluble salt exceeds the equilibrium solubility product (GUO, NGO and LI., 2012). This fouling type is one of the main challenges that prevent the MD large-scale operation for desalination (BAKER and DUDLEY., 1998). In MD processes, a supersaturated condition is mainly caused by water evaporation and temperature changes leading to nucleation and crystal growth in the feed solution and the membrane surface (VROUWENVELDER and VAN DER KOOIJ., 2001). Scaling in MD usually begin to form in the larger pores of the membrane since they are prone to accelerate wettability compared to smaller pore sizes (GRYTA., 2002). In many cases this phenomenon is considered irreversible due to the pore compaction and membrane degradation (KRIVOROT *et al.,* 2011). The crystals nucleation directly on the surface of the membrane (crystallization of the surface) is called heterogeneous crystallization, while those that nucleate in the volume (mass crystallization) are called homogeneous crystallization (Figure 2.2) (HOEK *et al.,* 2008).

However, the calcium sulphate precipitation over a membrane surface was primarily responsible for the fouling phenomena, that observed by Reis *et al.* (2018). Still, while compared to nanofiltration process, DCMD had a lower fouling potential considering the total and feed resistances. The same was observed by Kesieme and Aral (2015), in which calcium sulphate deposition on the membrane was justified by the high temperatures at which the tests were conducted.

In general, a fouling layer produces additional thermal and hydraulic resistances, which depend on its characteristics, such as porosity and thickness (BUFFLE *et al.*, 1998; QIN *et al.*, 2018). The fouling layer formation reduces the temperature difference across the membrane, or an increase in temperature polarization (BUFFLE *et al.*, 1998), which translates into lower driving force i.e. less difference in vapor pressure. If the fouling layer is not porous, it is likely to contribute to thermal and hydraulic resistances, whereas a porous layer may contribute only to thermal resistance (XIAO *et al.*, 2019; BUFFLE *et al.*, 1998). Fouling is also one of the main obstacles in MD, although it is less affected than the processes that have the pressure difference as the driving force (XIAO *et al.*, 2019; XIAO *et al.*, 2019; QIN *et al.*, 2018).

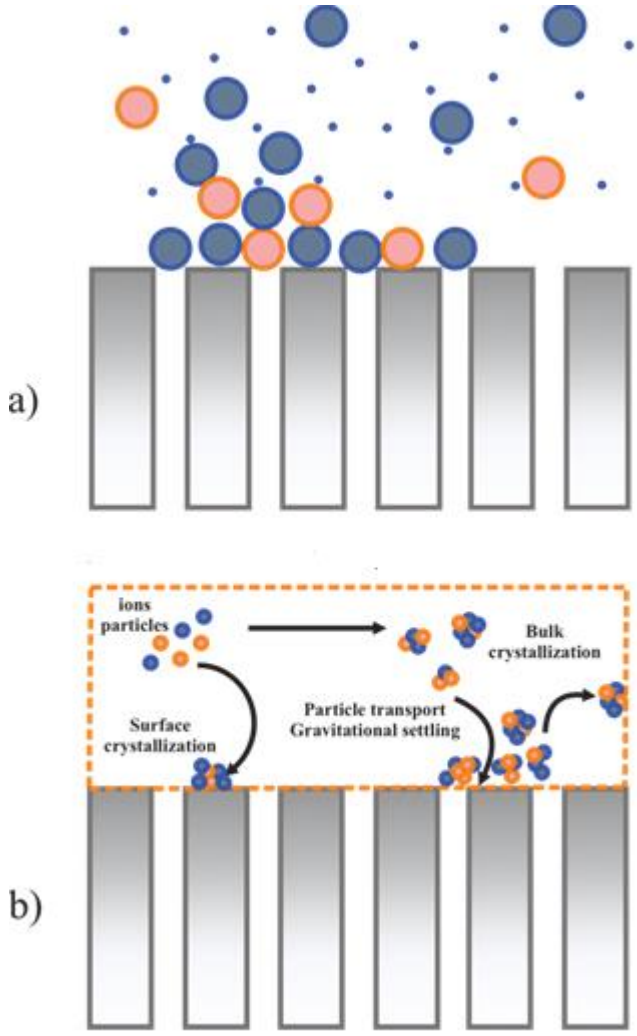

Figure 2.2 - Main fouling mechanisms in membrane distillation process for acid effluents treatment: (a) external surface fouling; (b) representation of nucleation and crystal growth in the feed solution and membrane surface.

Fouling phenomena for DCMD, SGMD, and VMD configurations were compared by Ge *et al.* (2014). According to the authors, the direct contact mode presented the highest initial flux, while the VMD presented the highest fouling rate. A membrane compression was noticed due to the vacuum requirement, occasioning a reduction in membrane permeability as well as porosity. The inorganic layer deposited over membrane surface still presented lower porosity compared to the DCMD and AGMD processes. In this case, an additional hydraulic resistance contributed to the observed flux reduction in VMD. In addition to that, SGMD and VMD were more subject to calcium carbonate deposition, which in turn had the greatest influence on the flux decay observed in these arrangements.

2.5.4 Membrane distillation wetting

Besides membrane fouling, there is another relevant problem in the MD process which is the membrane pore wetting. This phenomenon involves a complex of chemical and physical interactions (VROUWENVELDER and VAN DER KOOIJ., 2001), but essentially occurs when the transmembrane pressure surpasses the liquid entry pressure (LEP) of a membrane (LEE *et al.,* 2017). This can occur in a hydrophobic membrane employed to desalinate solutions containing amphiphilic molecules such as surfactants. These molecules attach to the hydrophobic membrane pore surface, leaving the hydrophilic portion exposed and eventually giving the membrane pores hydrophilic characteristics (WARSINGER *et al.,* 2015; GRYTA., 2007; REZAEI *et al.,* 2018; GRYTA., 2005). Besides the surfactants other mechanisms were reported such as chemical and mechanical degradation of the membrane (HULL and ZODROW., 2017), capillary condensation (FENG, WU and JIANG., 2018; GUILLEN-BURRIEZA *et al.,* 2016) and fouling (SRISURICHAN, JIRARATANANON and FANE, 2005; ULLAH *et al.,* 2018). The wetness degree of the membrane pores can be classified as on-wetted, surface-wetted, partially-wetted, and fully-wetted (BANAT and JWAIED., 2010), where wetting shifts the liquid/vapor interface inward on the membrane cross-section (LI *et al.,* 2019). The direct permeation of feed water into the distillate stream and decline in salt rejection are typical membrane wetting consequences (LEE *et al.,* 2017; WARSINGER *et al.,* 2015; ALKHUDIRI, DARWISH and HILAL., 2012). Different approaches have been applied to membrane wetting prevention, the main ones are focused on the manufacture of membranes with low affinity between the liquid and the polymeric material (LI *et al.,* 2019).

Although recurrent in MD (REIS *et al.,* 2018; GRYTA., 2007; HULL and ZODROW., 2017), the mechanisms associated with the wetting phenomenon must be further investigated and better

comprehended for acid effluents treatment. Membranes with larger pore diameter would be more subject to liquid phase introduction, as pointed out by Hausmann *et al.* (2012) and demonstrated by the Laplace-Young relationship. Consequently, membranes would be most prone to scaling inside its pores, which in turn promotes the formation of hydrophilic sites and favors the wetting process. Changes in operational conditions such as the temperature gradient between feed and permeate streams, and feed flow rate have been commonly adopted to minimize wetting effects. In general, larger temperature differences between feed and permeate streams, as well as lower feed recirculation rates, favor membrane wetting (SCHWANTES *et al.*, 2013).

2.5.5 Membrane distillation integration with renewable energies and waste heat

An important factor contributing to the MD use expansions on an industrial scale is the possibility of using the waste residual heat and integrating MD system with renewable energies, such as solar and geothermal (SOUHAIMI and MATSUURA., 2011; SCHWANTES *et al.*, 2013; LONG *et al.*, 2018; LAI *et al.*, 2018). This integration is important because MD is capable of generate high quality water, which is a resource that together with energy use are pre requisites for economic progress (KIM *et al.*, 2013; DOW *et al.*, 2017). Besides that, this association can reduce the carbon emission and extends the effluents treatment to the remote areas, where don't present a lot of energy availability (ZHANG *et al.*, 2019). In addition of this context, it is also worth mentioning the great availability of solar resource abundance and geothermal energy, the latter stands out for being constant and stable (RAHIMPUR, KAZEROONI and PARHOUDEH., 2019). Moreover, from an economic point of view, the capital cost is very sensitive to heat recovery, because the energy used to heat the feed is the most expensive in the MD process (DOW *et al.*, 2016; KABEEL, ABDELGAIED and EL-SAID., 2017). For this reason, several authors have been reporting the use of solar powered membrane distillation (SPMD) and the use of waste heat to reduce costs (KIM *et al.*, 2018; AL-OBAIDANI *et al.*, 2008; KESIEME *et al.*, 2013; TARNACKI *et al.*, 2011; TARNACKI *et al.*, 2012; KESIEME *et al.*, 2014; PABBY and RIZVI., 2009; RAVINDRA *et al.*, 2008).

Given the different configurations available, choosing the one that best fits the process in question should consider flows, energy recovery and additional investment costs for external heat exchangers, pumps and capacitors. Biniaz *et al.* (2019) evaluated the DCMD process in the treatment of acid drainage from the gold mining activity in terms of its technical-economic performance. Srisurichan, Jiraratananon and Fane (2006) reported that the water cost in a MD plant using a heat recovery system is 1.17 $\$/m^3$ being reduced to 0.64 $\$/m^3$ if the plant is operated

with lower grade waste heat. Mohammadi and Esmaeelifar (2005) showed that the cost of water produced by MD drops from 2.2 to 0.66 $/m^3$ if waste heat is used.

Benítez, Acero and Leal (2006) compared the environmental impacts of reverse osmosis and the membrane distillation process, considering different energy supplies and different methods. The highest environmental load of the use of this technology is related to the operational phase. The authors reported that, in all impact assessment methods, contribution higher than 96% of the total score were found. They also reported that change of materials, membrane lifespan or chemical consumption do not have such a strong negative impact on the environment from the life cycle point of view as the energy source and energy demand. Similar results were reported by Kaya *et al.* (2010), which detailed that more than 90% of the environmental impacts are related to energy demand, so any energy demand reductions directly influence the environmental impacts of the whole process.

2.5.6 Membrane distillation application for acid effluents

Table 2.3 presents several studies related to the application of MD to acidic effluents. Chang *et al.* (2011) applied DCMD with a flat sheet PTFE membrane to recover acid from mining leach solutions containing HCl or H_2SO_4 and metals such as aluminum, copper, nickel among others. In this study an acid and salt rejection greater than 99% was found. It is possible to observe the great tendency to use the direct contact configuration (DCMD) because (i) it is more suitable for water-based applications; (ii) does not require an external condenser; (iii) it's the simplest configuration; (iv) is easy to operate and (v) higher flux and mass transfer coefficients are achieve (CAMACHO *et al.*, 2013; SHIRAZI *et al.*, 2016; ASHOOR *et al.*, 2016; DRIOLO, ALI and MACEDONIO., 2015). The use of flat sheet PTFE material is also highlighted. Besides the PTFE material advantages discussed in section 2.5.2, some authors argue that the flat sheet membranes can be easily exchanged in the modules and present good fouling control in comparison with capillary for example (GRYTA, KARAKULSKI and MORAWSKI., 2006).

Hermia's models (TOMASZEWSKA, GRYTA and MORAWSKI., 2006; MORADI *et al.*, 2016) were considered for the fouling phenomenon elucidation in the study of Reis *et al.* (2018), in which the DCMD was considered for the treatment of an acid effluent generated in the gold beneficiation process. The phenomenon was caused mainly by the precipitation of $CaSO_4$ into the membrane surface, and the fouling mechanism was better explained by the blocking filtration model. Process flux decline was observed after 10% recovery grade and in addition to the fouling

phenomenon, the concentration by polarization has also been reported as responsible for the flux reduction. The results presented by Reis *et al.* (2018) demonstrated electrical conductivity rejections greater than 99%. However, by observing the permeate conductivity as a function of the recovery is possible to observe the passage of the solute by the increase in the conductivity after the recovery of 10%. For some authors, permeate conductivity values higher than 20 µS/cm may be considered as a membrane wetting evidence (REIS *et al.,* 2018; KESIEME and ARAL., 2015). As an alternative to reduce membrane wetting, two factors could be taken into consideration: (i) higher temperature differences between feed and permeate and (ii) lower flow rates (REIS *et al.,* 2018). Gryta Karakulski and Morawski (2006) observed a formation of salt crystallites in the feed tank when the concentration of SO_4^{2-} ions exceeded 650 mg/dm^3. Further analysis showed that these crystallites were composed of $CaSO_4$ and a mixture of salts containing silicone. These compounds hamper the efficient operation of the MD process, clogging the evaporation surface (membrane surface) and favoring a rapid wettability of the membrane pores – which contributes for increase in salts permeation and distillate contamination. It is almost consensus that the formation of salt crystallites in the feed tank, given the composition of these acidic effluents, is the major contributor to higher wetting rates and flux decline. To remediate this problem Kesieme and Aral (2015) added to the system a cartridge filter (0.5 µm) on the hot loop to collect precipitated matter prior to entering the MD module. This solution led to a more stable flux and lower wetting rates.

A flux reduction was also reported by Hull and Zodrow. (2017) in the treatment of an acid mine drainage, corresponding to 14.8% and associated with iron precipitation on the membrane. In addition, these results indicate that high iron concentrations lead to scale on the membrane surface, inside some of the pore walls, and then grows on the distillate side of the membrane (HULL and ZODROW., 2017). The wetting phenomenon was reported in the study conducted by Hull and Zodrow (2017) after observing an increase in the presence of solids dissolved in the permeate at a recovery grade of 25%. It was first confirmed by the reduction of 14.5% in the membrane LEP and later by the significant reduction in the membrane contact angle for the feed side, which decreased from 122.7° to 101.8°.

Table 2.4 - Studies involving metals recovery from acidic solutions through membrane distillation processes

Pore size (µm)	Material	Active area (cm^2)	Supplier	Flow rate (hot/cold)	Temperature (hot/cold) °C	Effluent	Metals	Acid Content	Acid rejection (%)	Sal rejec (%
0.60	Capillary PP	120.0	Accurel	0.25/0.1 m/s	70/20	Real metal pickling solution	Cu^{2+}, Fe^{2+}, Zn^{2+} and Mg^{2+}	5.5-135.25 g/dm^3	>99.9	>99
0.22	Capillary PP	193.0	Accurel	0.142/0.03 1 m/s	85/25	Cation exchanger regeneration effluent	Ca^{2+}, Mg^{2+}, Na^{+} and Si^{2+}	1080-46700 mg/L	~99	-
0.45	Flat sheet PTFE	169.0	Ningbo Chanqi, China	900/900 mL/min	60/20	Leach solutions from mining process	Al^{3+}, Ca^{2+}, Co^{2+}, Cu^{2+}, Fe^{2+}, Mg^{2+}, Mn^{2+}, Ni^{2+}, Sc^{3+} and Zn^{2+}	1.08 mol/L	>99.9	>99
0.45	Flat sheet PTFE	169.0	Ningbo Chanqi, China	900/900 mL/min	60/20	Synthetic acidic waste solution	Al^{3+}, Co^{2+}, Cu^{2+}, Ca^{2+}, Fe^{2+}, Mn^{2+}, Mg^{2+}, and Ni^{2+}	0.85 mol/L	>99.9	>99
0.20	Flat sheet PTFE	42.0	Sterlitech®	n.a.	60/25	Real mining effluent	Ca^{2+}, Mg^{2+} and As^{3+}	1.80 mol/L	>99.0	>99
0.20	Flat sheet PVDF	26.6	Pall Corp	3500/3500 mL/min	90/6	Acid Rock Drainage	Fe^{2+}, Al^{3+}, Cu^{2+} and Zn^{2+}	2.47 pH	>99.0	>99
n.a.	Capillary PP	120.0	Euro-Sep Ltd., Poland	n.a.	70/20	Synthetic solution	Fe^{2+}	18-250 g/dm^3	>99.0	>99

0.45	Flat sheet PTFE	169.0	Ningbo Chanqi, China	900/900	60/20	Synthetic solution	-	120.00 mg/L	>99.0	-
0.15	Hollow fiber PVDF/PVDF-HFP (12/6)	n.a.	-	250/40 mL/min	70/15	Synthetic solution	Fe^{2+}	20 % wt	~97.0	> 99
0.30	Hollow fiber PVDF/PVDF-HFP (12/3)	n.a.	-	250/40 mL/min	70/15	Synthetic solution	Fe^{2+}	20 % wt	~99.0	> 99

2.6 FINAL CONSIDERATIONS

One of the most important challenges in mining and metallurgic industry is to conciliate the contradictions between the economics benefits and environmental negative impacts related to the installation and operation of its projects. One of the ways to minimize the environmental impacts of this activity is to incorporate the sustainable development principles in all operation stages. Advanced mining wastewater treatment, which increases the energy uses efficiency and allows the by-products recovery as well the reuse water generation, has become an environmentally and economically viable option for industries. This practice improves both the population's environmental perception of the industry and can generate increased profits, as it introduces new products to be marketed, reduces the costs of buying treated water and decrease the dependence on local sanitation services as also reducing waste disposal costs. From the environmental point of view, this practice contributes to the reduction or non-generation of hazardous waste with potential for aqueous matrix and soil contamination as well water abstraction and effluents discharge, making available the volume saved for more noble purposes, such as public supply declining the environmental negative impacts of the mining sectors.

In this sense, MD stands out for enabling all these associated advantages in a simple operation process that can still be integrated with renewable energies or to take advantage of residual heat from industrial effluents, thus making it more sustainable and economically viable. In addition, the MD generates a high distillate quality, which can be used as industrial reuse water, which contributes to a decrease in the demand for this increasingly scarce and expensive resource. As can be seen throughout this study, the distinct MD configurations applications achieves

significant efficiencies in the acid and metal recovery. The DCMD is the most used because of its simplicity and low operating cost compared to other MD configurations in addition to being resistant to low pH when compared to traditional MSP such as NF and RO. Nevertheless, because the fact that concentrate is constituted by these elements mixing it is still necessary to apply a post treatment to separate them.

3 CHAPTER 3

TECHNICAL AND ECONOMIC POTENTIAL OF HIGH TEMPERATURA NF AND DCMD FOR GOLD MINING EFFLUENT RECLAMATION

3.1 INTRODUCTION

Gold, as well as most ores, is not used in the direct form as it is mined. Thus, throughout its beneficiation, it is necessary to change the particle size, shape and concentration of the interest species without causing chemical alteration in these compounds (LUZ *et al*., 2004). Among the auriferous ores beneficiation stages, the pressure oxidation process (POX) can be highlighted. The process is necessary when a large part of ores, that contain gold, present this element in a sulphide occluded matrix reducing gold recovery by direct leaching with cyanide (IVANNIKOV *et al*., 2018; KEFENI *et al*., 2017).

The POX stage is responsible for high water consumption and, consequently, a large volume of liquid effluent is generated, which is composed of significant sulphate, metals and high acidity concentrations at an elevated outlet temperature (JOHNSON., 2014; KAUR *et al*., 2018; LÓPEZ *et al*., 2018; SKOUSEN *et al*., 2017). Normally, this effluent is cooled and treated by neutralization followed by precipitation applying alkaline chemical products (KEFENI *et al*., 2017). Despite the simplicity of the method, it presents as a disadvantage the high alkalinizing consumption and the relevant sludge production containing high concentrations of trace metals. In the case of dissolution, they can be transported and contaminate the environment, demanding high costs for its final correct disposition (KAUR *et al*., 2018). Furthermore, the neutralization-precipitation produces a treated effluent with limited potential for reclamation.

As an alternative to treat this effluent and aiming for better use of its contents, membrane technologies have been emphasized. Among these processes, nanofiltration (NF), reverse osmosis (RO) and membrane distillation (MD) can be applied in the POX effluents treatment due to their capacity to retain dissolved substances (AMARAL *et al.*, 2018). These membranes processes permit to achieve highly valuable metals concentration and generate water with excellent physical and chemical quality as a permeate, which can be used directly as process water, thus contributing to the gold mining company economics (AMARAL *et al*., 2018; SCHAFER, FANE and WAITE., 2005).

NF membrane presents the combination of characteristics of ultrafiltration (UF) and reverse osmosis (RO), which allows higher permeate flux when compared to RO (BAKER, 2005). However, NF ions' rejection is strongly dependent on its speciation. Monovalent ions rejection is just around 70%, but it can achieve more than 99% and 90% of multivalent ions and organic matter rejection, respectively (ANDRADE *et al*., 2017; FOUREAUX *et al*., 2019). In addition,

most NF membranes have a low isoelectric point (IEP), between 3 and 6, thus becoming positively charged, which contributes to reject multivalent metallic cations (RICCI *et al*., 2015). Some results prove that the NF viability for the POX effluent treatment allowing its by-products recovery (AMARAL *et al*., 2018; RICCI *et al*., 2017, 2015). Ricci *et al*. (2017) assessed the chemical stability of the MPF-34 membrane by measuring its permeability at regular intervals of two-week, for two months. A maximum rejection reduction of 33% was observed for nickel and cobalt, however still generating a concentrate rich in metal ions and sulfuric acid for further processing. After eight weeks of exposure, a decrease in the selectivity of the MPF-34 was verified, being related to the increase of the solute convective flux contribution caused by the increase of pores sizes of the membrane, resulting from its degradation.

Previous studies address the POX effluent treatment at room temperature (25 °C) according to these promising results. However, the POX effluent reaches temperatures around 200 °C, followed by an initial cooling stage and reaching 50 to 80 °C. Therefore, the treatment of POX effluents at higher temperatures by nanofiltration can be a way to avoid an additional cooling stage, reducing energy consumption. NF membranes and modules can be designed to operate in temperatures up to 45-70 °C (DUPONT, 2019a, 2019b; GE., 2019) largely due to the materials used in the spiral-wound membrane elements. High temperatures increase the permeability of NF membranes and reduce the scaling potential over the membrane. However, since salts solubility is higher at higher temperature conditions, it can also decrease membrane rejection. Moreover, as the POX is composed of significant sulphate, metals and high acidity concentrations, its osmotic pressure and scaling potential are high. So, when pressure-driven membrane processes are used, the energy consumption is intensified by the increasing pressures requirement (COUTO *et al*., 2017).

Membrane distillation (MD) is an emerging process with great potential to treat concentrated effluents. In MD, the mass transfer is driven by the vapor pressure gradient obtained by the vapor pressure difference between feed and permeate (ZARE and KARGARI., 2018). Generally, in this process, gradients of temperature between 10 and 20 °C may be sufficient to produce distilled water. Therefore, the residual heat associated with the effluent could be used to drive the membrane distillation (MD) system, thus avoiding the need for a heating stage, which can drastically reduce the energy costs. Also, since mass transfer occurs in the vapor phase, MD is not limited by the osmotic pressure difference between feed and permeate, being capable of concentrating non-volatiles solutions until their saturation point without a significant decline of

the permeate flux and quality (CAMACHO *et al.*, 2013). MD has been successfully demonstrated in the treatment of different effluents. Kesieme *et al*. (2014) applied DCMD with a flat sheet PTFE membrane to recover acid from mining leach solutions containing HCl or H_2SO_4 and metals such as aluminum, copper, nickel among others. In this study an acid and salt rejection greater than 99% was found. Hull and Zodrow (2017) achieved > 99% dissolved solids rejection in acid rock drainage (ARD) demonstrating that membrane distillation can treat ARD solutions with high concentrations of dissolved solids.

In this study, NF and MD were compared to treat POX effluent by measuring the permeate flux, acid and metals rejection, specific energy consumption and costs considering the capital expenditure (CAPEX) and the operational expenditure (OPEX). The high-temperature NF, as an alternative treatment to POX effluent, was investigated and the temperature-induced changes of NF selectivity and productivity were discussed. Differences in fouling behavior and its impacts on NF and MD performance were also evaluated. At the end, this research allowed for a better comprehension of these membrane technologies while exploring a case of a real effluent, which can be extrapolated to other applications involving acid, metals-rich and heated effluents.

3.2 MATERIALS AND METHODS

3.2.1 POX effluent and pretreatment process

The wastewater used in this study came from the POX stage of a gold mining plant located in the state of Minas Gerais (Brazil). It is worth mentioning that these wastewater collections were carried out at the same point, but on different dates. The first POX wastewater sample was collected in 2014 and was destined to UF's feed. The second sample took place in 2016 and was destined to feed the DM. Table 3.1 presents its main characteristics. Before NF tests, a pretreatment with UF was carried out in order to prevent damages to the NF membranes caused by the presence of suspended solids from the raw effluent. The PVDF UF fiber membrane (ZeeWeed 500) had a mean pore diameter of 0.04 μm, with a membrane area of 0.9 m^2 (SUEZ., 2021). The system was operated at 0.7 bar and a maximum flow rate of 138 L/h, until a recovery grade of 90%.

Table 3.1 - POX effluent samples chemical characteristics for UF and DCMD feed

Parameter	Sample	
	UF Feed	**DCMD Feed**
pH	1.5	0.7
Acidity (g/L)	5.3	38.1
Electrical conductivity (mS/cm^2)	34.1	56.0
SO_4^{2-} (mg/L)	17,240	21,377
Al^{3+} (mg/L)	571.0	550.3
As^{3+} (mg/L)	7.6	244.7
Ca^{2+} (mg/L)	272.5	415.0
Mg^{2+} (mg/L)	733.8	500.9
Fe^{2+} (mg/L)	598.1	2,075.3
Mn^{2+} (mg/L)	95.3	73.0
Co^{2+} (mg/L)	28.3	37.0
Cu^{2+} (mg/L)	123.6	139.1
Ni^{2+} (mg/L)	127.1	181.8

3.2.2 NF and DCMD Systems

Before tests, NF membrane (DK membrane) was properly cut to be placed in the cell. The stainless-steel membrane module diameter (2r) was 9 cm, providing a 64.0 cm^2 filtration area. A feed spacer (711 μm) was placed over the membrane to promote flow distribution. In all tests were conducted in the batch operating mode, where the permeate was continuously collected and the retentate was recycled back to the feed tank. Firstly, distillate water permeability was determined by measuring its volume at regular time intervals of every 5 minutes of filtration. In sequence, the feed was replaced by 2 L of the POX effluent whose temperature was maintained at 25 ± 2 °C using a chiller (Gelaqua® 1/3 HP), and the permeate flux continued to be monitored for 24 h. The feed flow rate (Qf) was maintained at 2.4 L/min and transmembrane pressure (ΔP) was controlled at 10 bar by varying the rotary vane pump speed and a needle valve to ensure constant pressure during the test.

To achieve the highest recovery grade for NF, 6 L of the effluent was used in the same operating conditions described above. Its scheme can be observed in Fig. 3.1.

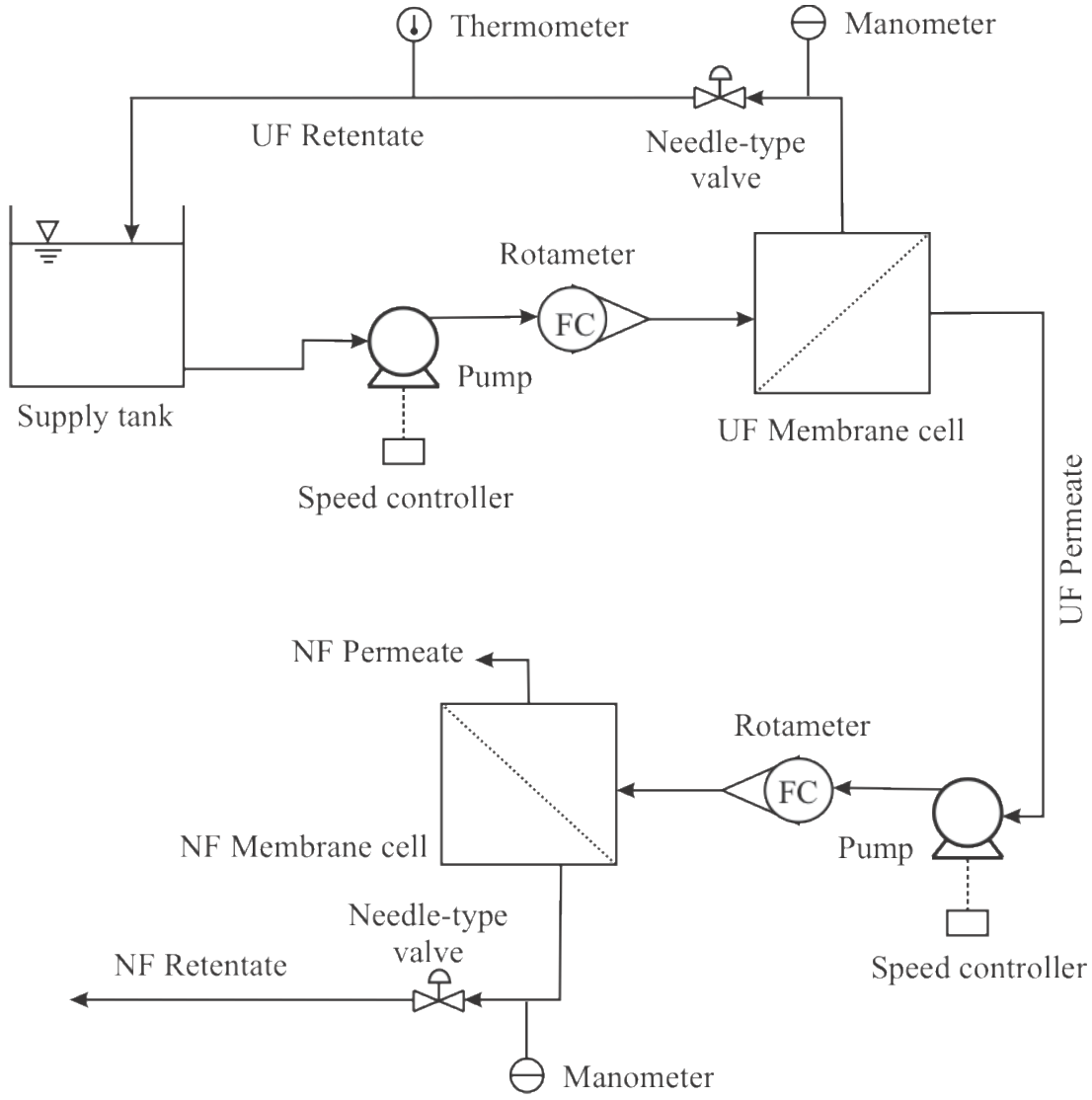

Figure 3.1 - NF bench-scale unit scheme that was considered in the POX treatment process

3.2.3 DCMD Process

The direct contact membrane distillation (DCMD) process was evaluated in a bench-scale unit as represented in Fig. 3.2. A MD cell model CF042 provided by Sterlitech® was used, providing an effective filtration area of 42 cm^2. Peristaltic pumps (Provitec GA5200 MB) were used for the permeate. 2 L of the effluent sample was added to the feed tank, which was heated to a temperature of 60 °C with a hot plate with magnetic stirrer (Solab SL-91). In the permeate tank, 1 L of distilled water was added and maintained at a constant temperature of 20 °C by a chiller, and the parameters pH and electrical conductivity of feed and permeate were monitored at regular intervals of 20 min. For the membrane flux measure, the accumulated distilled water mass was periodically measured by using a semi-analytical balance (Shimadzu UX6200H).

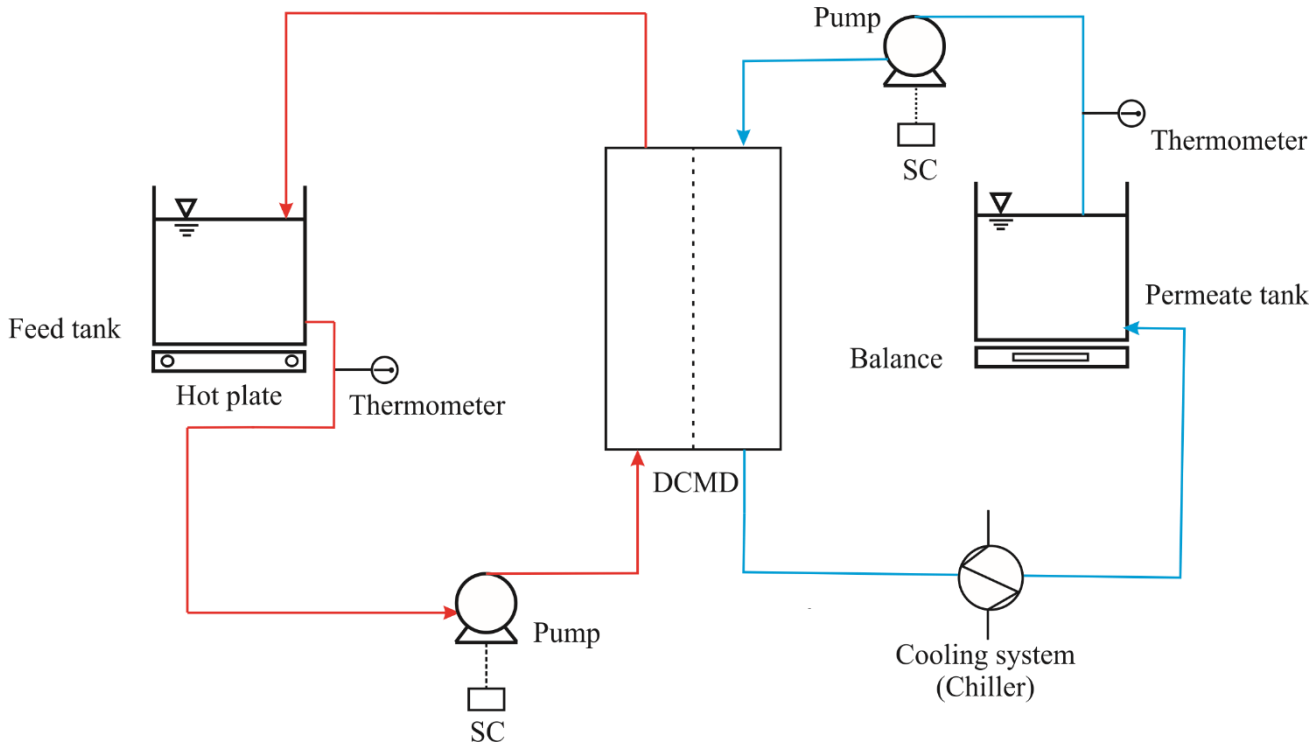

Figure 3.2 - The DCMD system diagram that was considered in the POX treatment process

3.2.4 Membrane Cleaning

3.2.4.1 NF Cleaning

Physical cleaning was performed by circulating water, without pressurizing, in order to remove reversible membrane fouling (fouling due to concentration polarization and reversible cake). Chemical cleaning was carried out using citric acid (pH 2.5) followed by a NaOH (0.4% w/w) solution. The cleaning solutions were recirculated for 30 minutes each. Between chemicals and at the end of the procedure, water was recirculated for 5 minutes.

3.2.4.2 DCMD Cleaning

Before the tests, the membranes passed through a cleaning procedure in which they were submerged in a hydrochloric acid (HCl) 0.1% v/v solution for 20 minutes and then washed with distillate water. After chemical cleaning, distilled water was used as feed and its permeability was measured until reaching a steady permeate flux.

3.2.5 Calculations

For the NF membrane, the permeate flow rate was measured through the permeate collection volume during 60 s. This permeate flux at temperature (T) was calculated by applying Eq. 3.1.

$$J(T) = \frac{\Delta V}{a_m * \Delta t} \quad (3.1)$$

Where $J(T)$ (L/m^2·h) is the permeate flux obtained at a temperature T, ΔV (L) is the permeate collected volume, Δt (h) is the collection time and a_m (m^2) is the membrane filtration area.

As the viscosity of the water is related to the temperature it was necessary to apply a correction factor. This factor is obtained by the ratio between the water dynamic viscosity at the permeation temperature T and at 25 °C for the values generated during the tests, as can be seen in Eq. 3.2.

$$J(25°C) = \frac{\mu(T)}{\mu(25°C)} * J(T) \quad (3.2)$$

Where $\mu(T)$ (N·s/m^2) and $\mu(25\ °C)$ (N·s/m^2) are the water dynamic viscosity at the permeation temperature and at 25 °C, respectively, and $J(25\ °C)$ (L/m^2·h) is the permeate flow corrected to 25 °C.

The observed rejection can be defined by Eq. 3.3.

$$R(\%) = \frac{C_f - C_p}{C_f} * 100 \quad (3.3)$$

Where C_f (mg/L) and C_p (mg/L) represent the solute content in the feed and permeate streams, respectively. In order to calculate the total flux decline (FD) Eq. 3.4 was used.

$$FD = \frac{(J_w - J_f)}{J_w} \quad (3.4)$$

Where J_w (L/m^2·h) is a pure water volume permeate flux through the membrane before effluent filtration and J_f (L/m^2·h) is the permeate flux with final effluent (after two hours of permeation). The FD has a couple of components, (i) concentration of polarization or the loose accumulation of solutes (CP, Eq. 3.6) and (ii) fouling that can be either reversed or not chemically or physically (FO, Eq. 3.5) (SCHAFER, FANE and WAITE., 2005). Flux declines due to fouling (FO) and concentration polarization (CP) was calculated trough Eq. 3.5 and Eq. 3.6 respectively, where J_{pc} (L/m^2·h) is the permeate flux with water after physical cleaning.

$$FO = \frac{(J_w - J_{pc})}{J_w} \quad (3.5)$$

$$CP = \frac{(J_f - J_{pc})}{J_w} \quad (3.6)$$

Process cleaning efficiency was evaluated through Eq. 3.7, considering the water flux after physical ($J_{cleaned} = J_{pc}$) or chemical ($J_{cleaned} = J_{cc}$) cleaning.

$$Cleaning\ efficiency\ (\%) = \frac{J_{cleaned}}{J_w} \quad (3.7)$$

The osmotic pressure difference ($\Delta\pi$) between the permeate and concentrate can be estimated by the Van't Hoff Equation (Eq. 3.8), as follows (REIS *et al.*,2018; AMARAL *et al.*, 2018; GROSSI *et al.*, 2021):

$$\Delta\pi = RT \sum(C_C - C_p) \quad (3.8)$$

In which R corresponds to the ideal gas constant, T to the temperature and C_p and C_C to the permeate and concentrate main dissolved species concentration, respectively. The specific energy consumption (SEC) (kWh/m^3 of permeate) was estimated as in Eq. 3.9.

$$SEC = \frac{W}{Q_p} \quad (3.9)$$

$$W = \frac{\Delta P * Q_f}{3.6 * 10^6} \quad (3.10)$$

Where W (Eq. 3.10) corresponds to the rate of work done by the pump (kW) considering a pump efficiency of 0.7 (SETHI and WIESNER, 2000), Q_p and Q_f the permeate and feed flow rate (m^3/s), respectively.

To assess scaling potential, calcium sulfate was chosen as representative of salt precipitation because it has low solubility therefore, greater precipitation potential. For this, calcium sulfate supersaturation index was calculated on the bulk solution (S_b) and in the membrane surface (S_m). Detailed calculations are shown by Ricci *et al.* (2015).

The Reynolds number was calculated for the DCMD feed side as in Eq. 3.11, in which D_H (0.003 m) corresponds to the module hydraulic diameter, A (0.00635 m) to the pipe's cross-sectional area and ν (m^2/s) to the kinematic viscosity of liquid water (KESTIN *et al.*, 1978).

$$Re = \frac{Q_f * D_H}{\nu * A} \quad (3.11)$$

For DCMD tests, the permeate flux (J_p) (L/m^2·h) and the water recovery grade (RR_{MD}) were calculated using Eq. 3.12 and Eq. 3.13, respectively, in which t_i is time (h), m_i is the mass corresponding at t_i (kg), a_m membrane area (m^2), v_{fi} initial feed volume (L), v_{Pi} initial permeate

volume (L), v_{Pt} permeate volume in t_i (L). Mass transfer resistance associated with DCMD ($R_{fouling}$ and R_{total}) and temperature polarization effect (τ) (Eq. 3.14) were calculated as described by Grossi *et al.* (2020).

$$J_p = \frac{m_2 - m_1}{(t_2 - t_1) * a_m} \tag{3.12}$$

$$RR_{MD}(\%) = 100 * \frac{[v_{fi} - (v_{Pi} - v_{Pt})]}{v_{fi}} \tag{3.13}$$

$$\tau = \frac{\mathrm{Tw,f - Tw,p}}{\mathrm{Tf - Tp}} \tag{3.14}$$

Where T_f; $T_{w,\,f}$; $T_{w,\,p}$; and T_p are the temperatures at bulk feed, membrane surface facing the feed, membrane surface facing the permeate and at the bulk permeate, respectively.

3.2.6 Analytical methods

The raw effluent and streams generated during tests were analyzed according to the following physical-chemical parameters: pH (pHmeter Qualxtron QX 1500), electrical conductivity (Hanna conductivity meter HI 9835), free acidity, and suspended solids - in accordance with the Standard Methods for the Examination of Water and Wastewater (APHA, 2017). Additionally, sulfate (ion chromatograph Dionex ICS-1000 equipped with AS-22 and ICS 12-A columns) and metals concentration (ICP-OES, Varian 720-ES) were also quantified.

3.2.7 Preliminary economic aspects

The UF – NF and DCMD membrane system costs to treat the POX effluent were estimated evaluating their capital and operational expenses (Capex and Opex). All calculations were made considering treating 60 m³/h of POX effluent in the operational conditions that were found to the optimized recovery grade of each system.

The effluent cooling to 25 °C was considered for NF while for DCMD the use of the effluent residual heat was taken into consideration. The electrical energy required for both systems were calculated using the Eq. 3.9, where ΔP was replaced by 10 bar for the NF system and 1.752×10^{-3} bar (mean gauge pressure of the experimental data) for the DCMD system. A pump efficiency of 70% was considered for these calculations. A large commercial membrane supplier in Brazil provided the prices for NF and DCMD units, 8750 U\$/m^3·h and 3321,03 U\$/m^3·h, respectively. The capital cost (C_{cap}) was calculated per cubic meter of effluent (C_{cap/m^3}) (Eq. 3.15), where Am is the amortization factor, calculated as in Eq. 3.16, i_r the investment (2.0 % in Brazil (BCB., 2021)) and PL the design plant life.

$$C_{cap/m^3} = \frac{Am * C_{cap/m^3}}{Q_{cap}} \quad (3.15)$$

$$Am = \frac{i_r*(1+i_r)^{PL}}{(1+i_r)^{PL}-1} \quad (3.16)$$

Several aspects have been taken into account to calculate OPEX for NF and DCMD systems, among them are the energy requirement, maintenance (5% of C_{cap/m^3}), cleaning agent, membrane replacement, alkalizing agent (calculated based on the volume of NaOH solution used to NF DK and DCMD cleaning process), and capital cost amortization. Considering an exchange rate of US$1 = R$5.42, the energy requirement cost was estimated considering the energy tariff currently paid by the mining company in Brazil, which is around 0.05 US$/kWh. Table 3.2 shows the characteristics and considerations of the DCMD and NF system used for treatment cost estimation.

Table 3.2 - System characteristics considered for the cost estimation of the NF and DCMD treatment system for POX gold mining effluent. [a]Corresponding value for February 2021; [b]Dollar currency exchange US$ 1 = R$ 5.42

	Description	NF System	DCMD System	Units
System Characteristics	System capacity	60	60	m^3/h
	Annual system capacity	525,600	525,600	$m^3/year$
	Average permeate flux	0.010	0.016	$m^3/h \cdot m^2$
	Recovery grade	48	52	%
	Effluent temperature	60	60	ºC
	Operating temperature	25	60	ºC
	Required membrane area	2,959.92	1,789.01	m^2
	Design plant life	15	15	years
	Membrane lifespan	1-5	1-5	years

Cleaning frequency	1	1	weekly
Brazil investment rate[a]	2.0	2.0	%
Expenses taken into consideration[b]			
Membrane cost per square meter	50	12	US$/m^2
NaOH price	0.53	0.53	US$/kg
Citric Acid price	9.10	9.10	US$/kg
Energy price	0.05	0.05	US$/kWh

3.3 RESULTS AND DISCUSSION

3.3.1 NF processes evaluation

3.3.1.1 Effect of feed temperature

The temperature limit for the operation of the DK membrane is 50 °C. Thus, the maximum temperature achieved in NF experiments was 40 °C. Fig. 3.3 shows the results for SEC (including feed cooling) and membrane overall flux for operation at four different temperatures. Regarding the permeate flux, it was seen that it increased from 12.8 to 19.2 L/m^2 h when temperature was raised from 25 °C to 40 °C. The observed increase in water flux due to the temperature rise is related to the decrease of an intra-pore water viscosity with the increasing in temperature. The variations in membrane structural properties, such as pore radius and effective thickness, with temperature (from 25 to 40 °C), can account for the residual temperature dependence (BEN AMAR *et al*., 2009, 2007). Consequently, even accounting with the smallest value of osmotic pressure, SEC at 25 °C was 34% higher when compared to other temperatures. From 30 °C onwards, no significant change in SEC was observed.

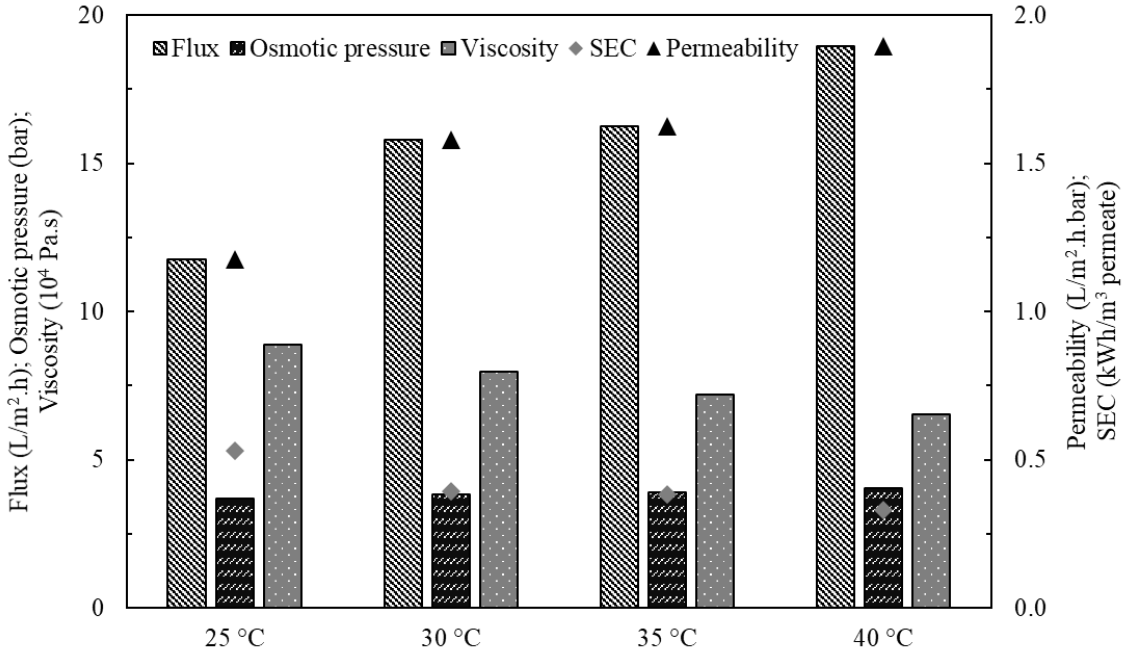

Figure 3.3 - Temperature effect on NF performance.

In addition to flux, at higher temperatures, the solutes mass transfer coefficients are also increased, along with the thermal expansion of the polymer. Since the ion diffusivity is dominant over the decrease in solvent viscosity, the net effect of temperature increase is to augment permeate solutes concentration (ROY and LIENHARD., 2019). This increase, however, can be less prominent in charged solutes, since the membrane surface charge is most responsible for retention (BEN AMAR *et al*., 2009, 2007; NILSSON *et al*., 2008). As a consequence, it can counteract the diffusivity increase commonly observed, thus making the difference in retention of charged solutes at a range of temperatures not very expressive, as seen in Table 3.3.

Table 3.3 - Physical chemical characterization of NF DK membrane permeate for different feed temperatures. In grey and italics are the respectively ion rejection in comparison with the feed

Parameters	Units	Permeate Sample								
		Feed	T = 25 ºC		T = 30 ºC		T = 35 ºC		T = 40 ºC	
pH	-	1.3	1.4	-	1.2	-	1.4	-	1.2	-
Acidity	(g/L)	4.9	3.9	*20.4%*	4.3	*12.2%*	4.3	*12.2%*	4.2	*14.3%*
Electrical conductivity	(mS/cm^2)	33.53	24.15	*28.0%*	25.81	*23.0%*	25.28	*24.6%*	24.34	*27.4%*
Al^{3+}	(mg/L)	546.03	3.50	*99.4%*	5.24	*99.0%*	6.93	*98.7%*	12.60	*97.7%*
Ca^{2+}	(mg/L)	270.00	5.63	*97.9%*	6.49	*97.6%*	8.94	*96.7%*	13.31	*95.1%*
Mg^{2+}	(mg/L)	2380.0	23.8	*99.0%*	35.2	*98.5%*	50.6	*97.9%*	73.8	*96.9%*
Fe^{2+}	(mg/L)	588.0	7.6	*98.7%*	10.3	*98.2%*	13.4	*97.7%*	19.2	*96.7%*
Mn^{2+}	(mg/L)	66.20	0.69	*99.0%*	1.36	*97.9%*	1.88	*97.2%*	0.73	*98.9%*
Co^{2+}	(mg/L)	21.50	0.22	*99.0%*	0.34	*98.4%*	0.49	*97.7%*	0.72	*96.7%*
Cu^{2+}	(mg/L)	122.02	1.97	*98.4%*	4.39	*96.4%*	4.98	*95.9%*	9.33	*92.4%*
Ni^{2+}	(mg/L)	121.00	2.43	*98.0%*	2.99	*97.5%*	3.08	*97.5%*	4.03	*96.7%*

Given the balance between the observed phenomena, the membrane overall rejection was kept above 92% for all metals. since the permeate obtained in all cases can potentially be used as process water, the discussion regarding the operating temperature should take into account the costs of cooling the feed before entering the system and membrane stability under each

circumstance. In this context, as expected, Fig. 3.3 shows a reduction in SEC by the increase of the temperature, once the cooling costs are diminished. However, the difference between SEC from 30 °C to 40 °C is not very prominent. Combining this with the recommendations that membranes should work close to the room temperature, at 30 °C an interesting threshold point was attained. In this case, working at higher temperatures does not bring energetic gains to the system. Besides, operating conditions at 30 °C can favor a longer membrane lifespan, while providing water with quality for reuse and enabling the recovery of byproducts on a next stage.

3.3.1.2 Membrane fouling and water recovery grade

In Table 3.4 it is possible to observe the significant reduction comparing the permeate flux using as feed the distilled water (J_w) and the POX effluent. This reduction occurs due to the concentration polarization phenomenon (CP = 0.64), which is very prominent because of the effluent characteristics. It is important to mention that the NF performance is more sensitive to the CP effects, comparing to DCMD, due to the NF's ion rejection (ZHANG *et al*., 2018; AGUIAR *et al*., 2016). In addition, a reduction of flux during operation can be attributed to the fouling phenomenon, which is inherent in the pressure-driven membrane separation process and it is directly connected with the solution interaction with the membrane surface (HOEK and ELIMELECH., 2003). Despite this flux reduction, a combination of physical and chemical cleaning was able to restore the membrane initial flux. This indicates that most of fouling has reversible characteristics and can be managed. However, it is worth mentioning that the higher the frequency of membrane cleaning, the smaller its lifespan and the higher the operational costs (ZHAO and YU., 2015).

Table 3.4 -Type of flux decline and cleaning efficiency for NF DK membrane. Jw: permeate flux with distillated water; Jo: permeate flux with initial effluent; Jf: permeate flux with final effluent (after two hours of permeation); Jpc: permeate flux with with water after physical cleaning; J_{cc}: permeate flux with water after chemical cleaning; (FD) total flux decline; (FO) flux decline due to fouling

Flux decline type								**Cleaning efficiency (%)**	
J_w (L/m^2.h)	**J_o (L/m^2.h)**	**J_f (L/m^2.h)**	**J_{pc} (L/m^2.h)**	**J_{cc} (L/m^2.h)**	**Total (FD)**	**Fouling (FO)**	**Concentration polarization (CP)**	**Physical**	**Chemical**
46.0	20.2	16.1	36.0	45.5	0.65	0.012	0.64	78.26	98.91

Long-term filtration tests (feed temperature 30 °C) were carried out to investigate membrane fouling by increasing the permeate recovery grade. NF membranes are more permeable to water than to solutes, and by increasing the recovery grade, the salt concentration in the retentate is also enlarged, therefore increasing both solute flux, fouling potential, and osmotic pressure. Thus, for a fixed operating pressure, an increase in the recovery grade leads to a reduction in the permeate flux and membrane rejection (Table 3.5). Otherwise, high recovery grades allow a larger amount of permeate production. It can be seen in Fig. 3.4(a) that the permeate flux decay occurred in a practically linear manner (R^2 of the linear adjustment = 0.95) after 20%. By increasing the permeate recovery grade in 1%, a reduction of approximately 0.25 $L/h \cdot m^2$ was observed. Considering the high osmotic pressure of the effluent (4.6 bar at the beginning of operation), it was necessary to operate the system at 10 bar to maintain the permeate flux, requiring more energy and consequently higher operational costs.

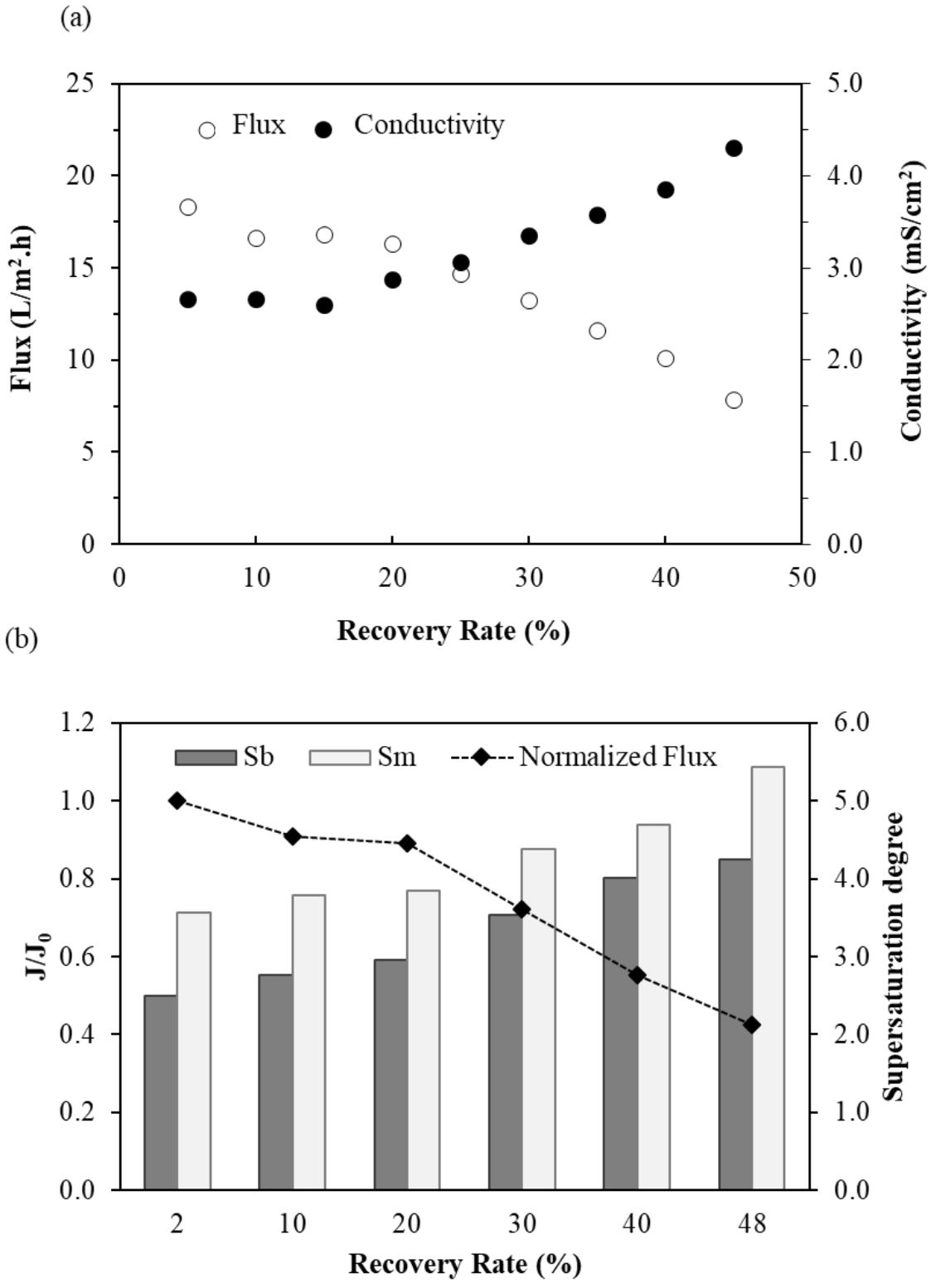

Figure 3.4 - (a) Permeate flux and electrical conductivity as a recovery function of for NF DK membrane ; (b) Bulk (S_b) and membrane (S_m) calcium sulfate supersaturation index.

In addition to flux decline, the electrical conductivity increased prominently during the test, which indicates the constant passage of solutes to the permeate side from 20% of recovery

afterwards. When considering the supersaturation index of Ca^{2+} in the solution – chosen as a representative of salt precipitation due to its low solubility in the form of $CaSO_4$ and high concentration in the effluent – it can be seen that the effluent was already saturated before tests (Fig. 3.4(b)). This, however, might not necessarily mean scaling from the first moment, since kinetics and metastability effects increase the supersaturation index very prominently. Also, the presence of other cations in the solution can hinder the formation of $CaSO_4$ due to the complexation of sulfate ions (LE GOUELLEC., 2002; WAITE *et al.*, 2005). In this case, considering the sharp flux decay experienced from RR_{NF} = 20%, it can be inferred that salts start to precipitate from a S_m > 4.0 or S_b > 3.0, thus favoring membrane scaling.

Metals overall retention continued to decrease by the increase of the recovery fraction, but rejection was still kept above 90% in most cases. To this matter, arsenic rejection can be highlighted due the inability of NF membranes to retain this species. The NF achieved lower removal efficiency for arsenic. According Qu *et al.* (2009) NF membranes do not reach high efficiency in arsenic rejection, mainly As^{3+}. This lower rejection can be explained by their speciation in the pH condition evaluated, since for a pH value as in the NF stage feed, trivalent and pentavalent arsenic are in the forms of the neutral species H_3AsO_4 and H_2AsO_3, respectively (Fig. 3.5).

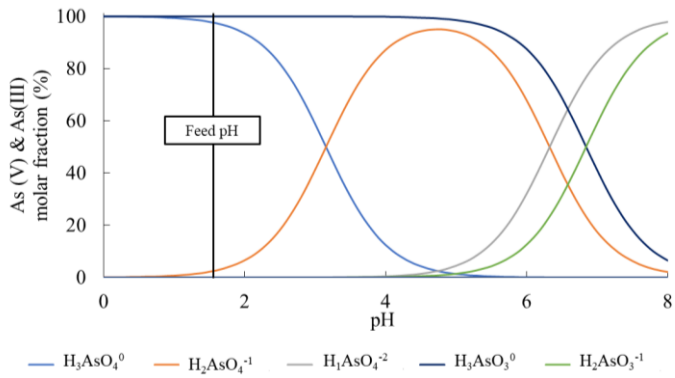

Figure 3.5 - As^{3+} and As^{5+} species distribution in a pH function. Adapted from Chemicalize (ChemAxon., 2018).

For neutral species, the main retention mechanism in the NF membranes is size exclusion, so that the higher the ratio between the molecular weight of the species to be removed and the molecular cut-off of the membrane (MWCO), the greater the expected rejection (FOUREAUX *et al.*, 2019; KOŠUTIĆ *et al.*, 2005; VAN DER BRUGGEN *et al.*, 1999). The molecular H_3AsO_4 and H_2AsO_3 weights are, respectively, 141.94 g/mol and 125.94 g/mol, which are smaller than

NF MWCO, which corresponding to values between 200-400, thus, a smaller rejection is expected for such species, as observed in the present study.

Table 3.5 - Nanofiltration and membrane distillation performance for sulfuric acid and metals rejection for different recovery grades

	pH	Acidity (g/L)	Electrical conductivity (mS/cm^2)	SO_4^{2-} (mg/L)	Al^{3+} (mg/L)	As^{3+} (mg/L)	Ca^{2+} (mg/L)	Mg^{2+} (mg/L)	Fe^{2+} (mg/L)	Mn^{2+} (mg/L)	Co^{2+} (mg/L)	Cu^{2+} (mg/L)	Ni^{2+} (mg/L)
Nanofiltration													
UF Permeate (NF feed)	1.85	3.93	21.64	17065	197.00	7.03	202.00	586.00	258.00	72.46	15.20	76.28	71.41
Permeate recovery grade 10%	1.95	1.76	10.70	2673	5.52	4.50	15.70	24.38	12.81	2.68	0.64	22.09	3.25
Permeate recovery grade 20%	1.83	1.78	10.93	2645	5.59	4.05	14.43	26.29	11.40	2.77	0.69	8.19	3.38
Permeate recovery grade 30%	1.80	1.82	11.70	2719	6.41	4.44	17.30	29.12	12.23	2.94	0.80	7.90	4.15
Permeate recovery grade 40%	1.77	1.76	11.48	2847	7.50	5.08	17.42	37.30	16.77	3.43	0.96	12.03	4.86
Permeate recovery grade 50%	1.77	1.86	11.87	3024	10.76	5.36	20.13	50.05	18.39	4.08	1.36	13.45	7.05
Permeate recovery grade 60%	1.77	1.99	13.63	3625	15.72	6.05	28.47	74.42	25.96	5.40	1.97	18.92	10.42

Permeate recovery grade 70%	1.77	2.16	14.73	4400	-	-	-	-	-	-	-	-	-
NF Concentrate recovery grade 50%	-	6.00	31.40	31106	383.20	8.70	383.90	1122.00	497.60	140.80	29.00	139.10	135.80
NF Concentrate recovery grade 70%	-	8.10	37.80	46616	620.00	9.30	606.90	1779.70	799.40	228.90	46.10	210.10	213.70
Retention 50%	-	*52.6%*	*45.1%*	*82.3%*	*94.5%*	*23.8%*	*90.0%*	*91.5%*	*92.9%*	*94.4%*	*91.1%*	*82.4%*	*90.1%*
Membrane distillation													
Permeate recovery grade 50%	3.37	1.51	0.11	-	6.69	1.44	3.03	12.5	15.14	0.73	0.32	1.32	1.51
Retention	-	*96.1%*	*99.8%*	*-*	*98.8%*	*99.4%*	*99.3%*	*97.5%*	*99.3%*	*99.0%*	*99.2%*	*98.8%*	*99.2%*

3.3.2 DCMD process evaluation

It is possible to observe in Fig. 3.6(a) the permeate flux behavior during the recovery test as well as how sulfuric acid was concentrated in the retentate stream, which was evaluated until the recovery grade of 70%. The permeate flux remained relatively stable until the recovery grade of 52% where permeation flux decay is practically linear (R^2 of the linear adjustment = 0.9), with a reduction of approximately 1.55 L/h·m² for each increase of 1% degree of recovery. At the same recovery , an increase in fouling resistance contribution to the total resistance was noticed, which could be explained by solutes accumulation on the membrane surface, therefore provoking salts to precipitate (scaling) (GRYTA., 2007). Although it is a process less susceptible to fouling and scaling, the increase in solute concentration affects the driving force of the process as the vapor pressure is linked to the solution activity. An increase in feed concentration leads to a decrease in solution activity, therefore a decrease in vapor pressure related to feed side. Then, the flux of distillation processes is expected to decay while increasing the recovery if they operate at constant temperature. An increase in concentration still reflects on the process-associated resistance as solutions of higher metal ions concentrations has also higher viscosity and density. The change in feed phase physicochemical properties also affects the temperature polarization , where higher recovery grades lead to stronger effects (τ=0.69 at 66% recovery grade). Conversely, the temperature polarization effect was weaker in low recovery (τ=0.81 at 10% recovery). These conditions hamper the vapor diffusion and the heat transfer from bulk feed to the membrane surface since the heat and mass transfers directly correlates to Reynolds number, which in turn has an inverse correlation with viscosity (ALI *et al*., 2013).

The application of UF as a pre-treatment of the POX effluent allowed the reduction of approximately 25% of Ca^{2+} and Mg^{2+} concentration, in addition to suspended solids, which are the main elements to contribute to the scaling formation on the membrane surface (SCHAFER, FANE and WAITE., 2005; TZOTZI *et al*., 2007). Although UF membranes were not designed for divalent ions retention, electrostatic repulsion and additional contribution by the cake layer formed, allowed calcium and magnesium ions retention.

The POX effluent that served as a feed for DCMD besides not having undergone this pretreatment, presented twice the calcium concentration when compared to the UF permeate, that was used as NF DK feed. However, this significant DCMD permeate flux reduction occurred from the recovery grade of 52% because from this recovery grade, an increase in the

concentration of physical-chemical parameters in the permeate of DCMD was observed. On the other hand, the NF permeates flux decay from the 10% recovery grade, when it is noted that from this recovery grade there is a reduction in the retention of metals and acid solution present in the feed, corroborating the passage of these elements to the permeate of the NF as can be seen in Fig. 3.6.

For the DCMD process, when the permeate electrical conductivity value grows significantly, it demonstrates the occurrence of the membrane pore's wetting phenomenon, which allows the feed current's passage degrading the permeate physicochemical quality. Once membrane wetting was observed, the values corresponding to the time required for the phenomenon to occur and the wetting rate were estimated, which was obtained by evaluating the increased concentrations of metals and or acid solution (consequently increase in electrical conductivity) in the permeate throughout the test, corresponding to 20-30 min and 0.307, the last one estimated by the angular coefficient of the curve correlating the electrical conductivity and time. As higher wetting time is desirable, and in order to increase this value, two factors could be taken into account: operating with (a) higher temperature difference between the permeate and feed stream and (b) lower flow rate. In Fig. 3.6(b) it can be observed the electrical conductivity's increased that was occurred throughout the test up to a recovery grade of 70%, which is equivalent to 800 min after its start.

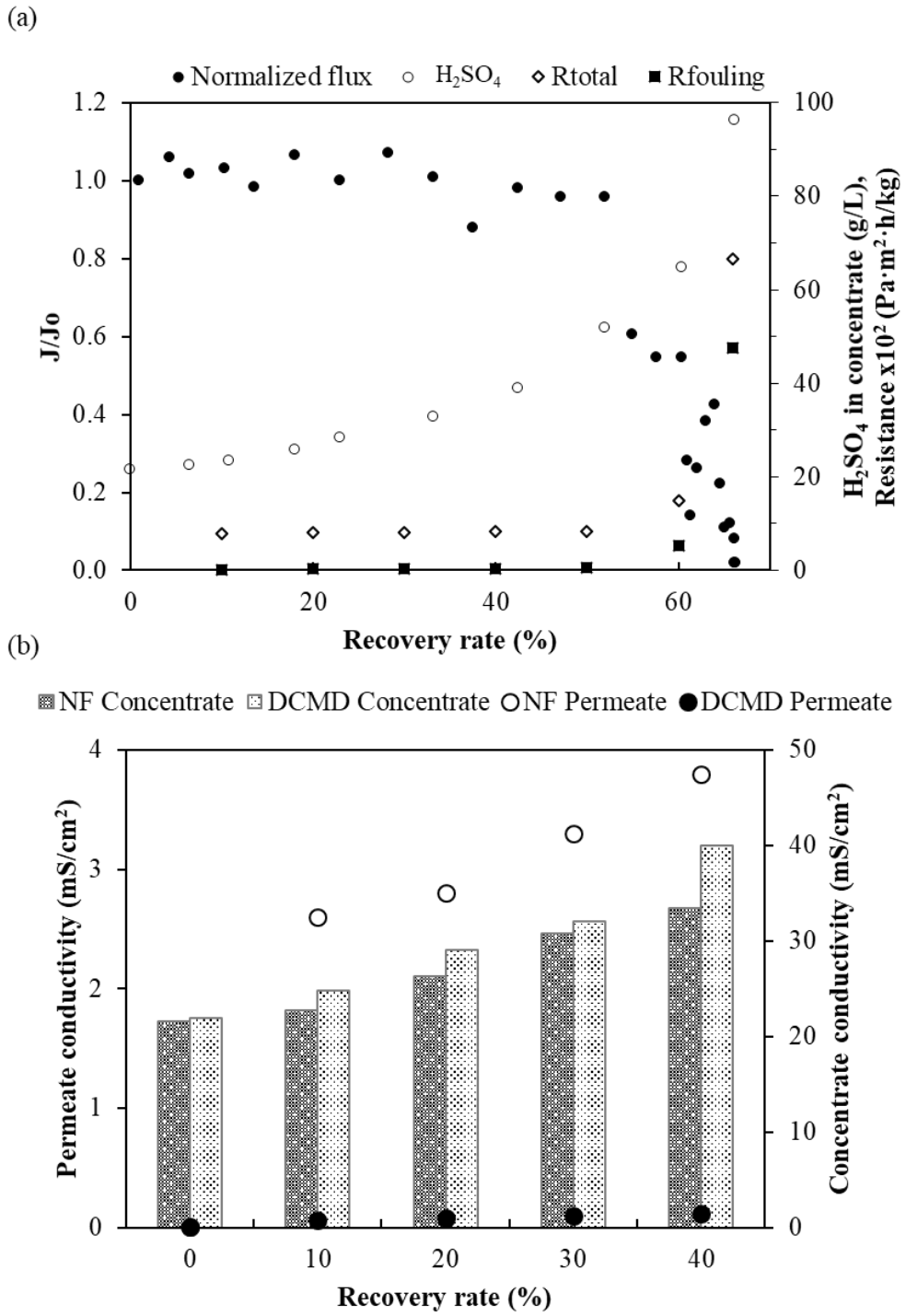

Figure 3.6 - a) Normalized permeate flow, in the left y-axis, and sulfuric acid concentration, in the right y-axis, as well as resistance due to fouling ($R_{fouling}$) and total resistance (R_{total}) observed throughout the DCMD test; (b) Electrical conductivity comparison for permeate, in the left y-axis, and concentrate, in the right y-axis, from DCMD and NF process.

A satisfactory result in terms of salt rejection is observed after comparing the permeate quality from DCMD and NF in Fig. 3.6 (b). As a characteristic of the DCMD process, only volatile

compounds that make up the feed solution are capable of permeating the hydrophobic MD membrane. Therefore, the process exhibits theoretical rejection of 100% for salts, which explains the high rejection observed, resulting in a high permeate quality. The sulfuric acid concentration is also observed during the distillation process resulting in a final concentration of 96.2 g/L in the retentate, equivalent to a 4.5 of concentration factor. For the permeate, a sulfuric acid concentration of 0.02 g/L was observed, corresponding to a rejection factor >99.9%

The overall results emphasize the DCMD robustness for the treatment of high temperature and acid effluents, since its permeate flux was less sensitive to fouling compared to NF (GRYTA., 2007). The low electrical conductivity values observed (mean value of 0.03 mS/cm^2) in the permeate compared to the feed solution (54.8 mS/cm^2) reinforces its feasibility for reuse water obtainment. Table 3.5 presents the membrane distillation results evidencing the process performance in metals retention.

In this way the DCMD process is an alternative for the treatment of the POX effluent, producing two streams, the permeate that presents quality for reuse and the concentrate, a liquor that can be destined for the metals and sulfuric acid recovery.

3.3.3 DCMD and UF-NF techno-economic comparison for POX effluent treatment

It was observed from the experimental data that the DCMD system had an average permeate flux (0.016 $m^3/h.m^2$) higher when compared to the NF process (0.009 $m^3/h.m^2$). That implies in a smaller membrane area (1,789.01 and 2,959.9 m^2, respectively) and therefore, lower costs associated with its acquisition and replacement considering a membrane life span of 5 years (Table 3.6). In addition, the lower Capex also implies in a lower capital amortization cost per cubic meter of treated effluent, when compared to NF. For the experimental conditions employed in this study, the energy cost related to the DCMD process was significantly lower when compared to the NF process as seen in Fig.3.6, since the first operates at higher temperatures and close to those in which the effluent is generated, dispensing a cooling feed step as in the nanofiltration process.

Table 3.6 - Capital and Operational Expenditure for the NF and DCMD systems, considering a 5 years lifespan

Description	UF-NF System	DCMD System	Units

CAPEX	Membrane Replacement	29,599.17	2,081.93	US$/y
	Membrane Replacement	0.056	0.004	US$/$m^3$
	Amortization	0.051	0.026	US$/$m^3$
OPEX	Price of NaOH per cubic meter	0.188	0.119	US$/$m^3$
	Price per weight of citric acid	9.100	9.100	US$/kg
	Required weight of citric acid	0.777	0.777	kg/cleaning
	Cleaning Agent	0.001	0.001	US$/$m^3$
	Energy Requirement	1.901	0.008	US$/$m^3$
	Maintenance	0.003	0.001	US$/$m^3$
	Total	2.200	0.160	US$/$m^3$

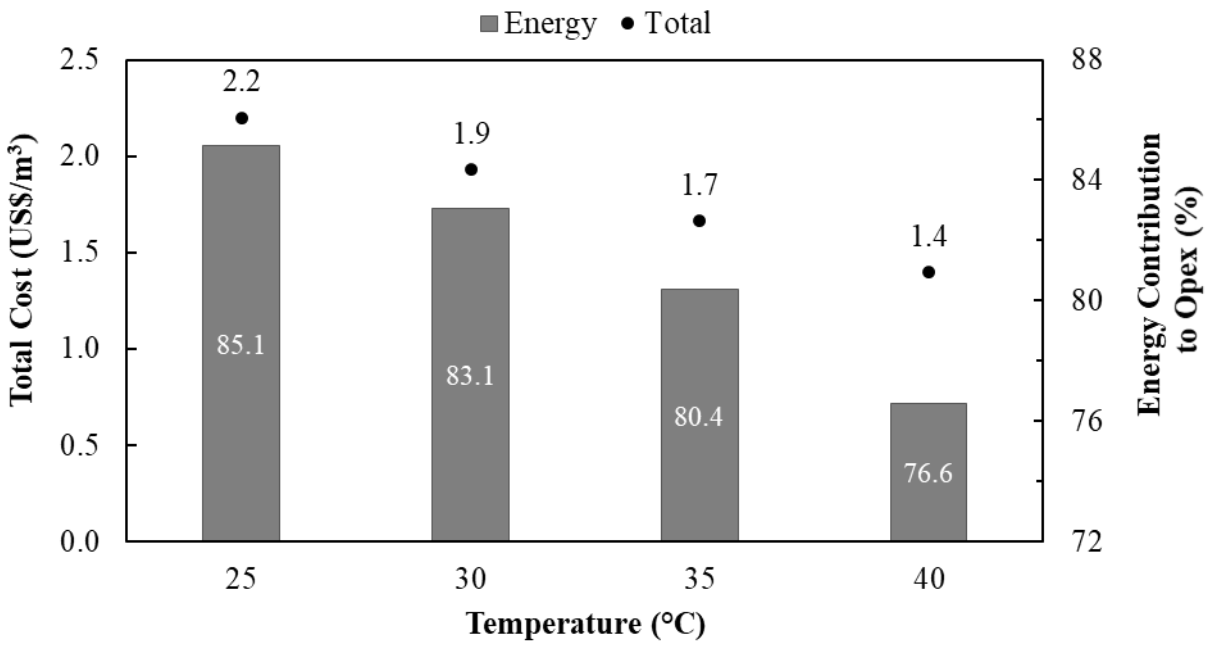

Figure 3.7 - Energy contribution to Opex and total cost for the NF system.

Although the NF system operating temperature was set at 30 ºC, other values were compared, since the energy cost associated with the process is the main contributor to the total cost (Fig. 3.8). Thus, temperatures of 30, 35 and 40 ºC were also considered, observing a 36% reduction in total cost for a system operating at a 40 ºC (from 2.2 to 1.4 US$/$m^3$), corresponding to approximately 74% of the total cost. This saving, however, might not compensate due to a very likely decrease in membrane lifespan when working at higher temperatures. Since membrane replacement accounts for the second highest share of total expenditures, the influence of temperature on NF membrane ageing when treating this effluent should be further understood.

Unlike the nanofiltration system, the DCMD process does not require prior effluent cooling in order to be treated. Considering a permeate flux of 0.016 $m^3/h \cdot m^2$, the system would be capable of supplying 121,584.6 m^3 of high-quality water for reuse annually. Considering an acquisition cost of industrial high-quality water (US$ 0.18/m^3), the DCMD system implementation would represent a saving of US$ 21,885.23.

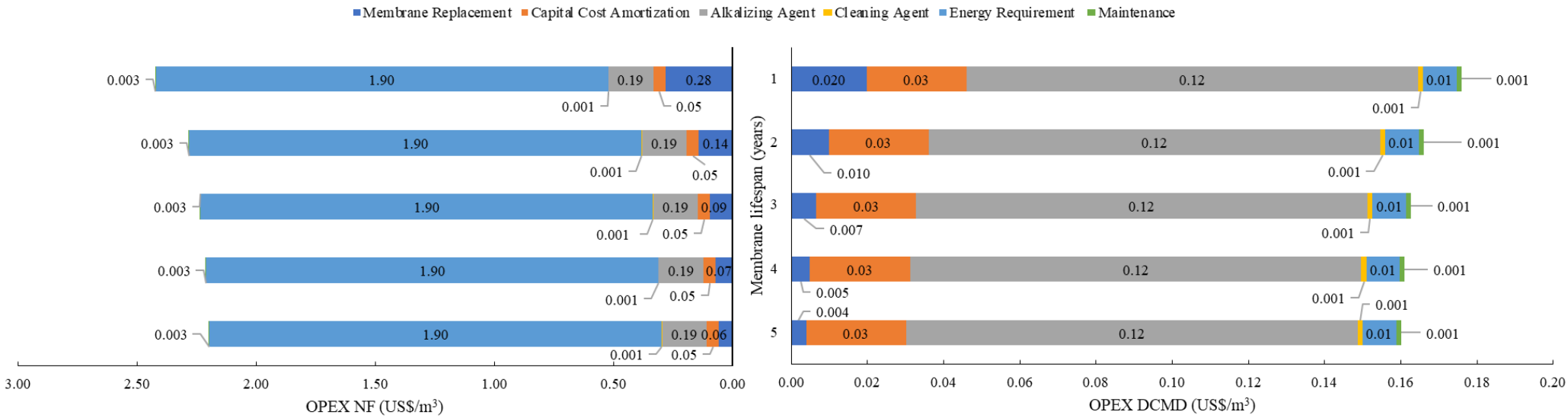

Figure 3.8 - Operational expenditure comparison for both NF and DCMD process.

3.4 FINAL CONSIDERATIONS

The NF and the DCMD process presented promising alternatives to the treatment of the POX effluent. Under the investigated conditions, both processes generated a permeate with physical-chemical quality that allows its reuse as process water. Despite the success of both technologies, DCMD should be highlighted by its robustness, since it was submitted to a more concentrated effluent and nevertheless generated a better quality permeate, as well as higher retention. In addition, the DCMD was less susceptible to the fouling phenomenon throughout the test at a recovery grade higher than that achieved by NF. Furthermore, the DCMD presented the lowest operating costs, a fact that relates to the advantage of this system to use the residual POX effluent heat as the system driving force. As a consequence, the cooling stage - which contributed to the NF operational cost increase, was dismissed for DCMD, thus affecting costs.

4 CHAPTER 4

WATER REUSE GENERATED FROM POX EFFLUENT APPLYING THE DCMD

4.1 INTRODUCTION

Fresh water is a renewable, but finite resource, that is indispensable for the human consumption, hygiene and food supply while guaranteeing the ecosystem essential functions (BERGER and FINKBEINER., 2010). Furthermore, this resource is essential for the performance of various economic activities, such as agriculture, mining, power generation, among others (VOULVOLIS., 2018).

Despite the fact that the industry is not the largest water consumer, this sector has a greater polluting potential due to the use of different raw materials and inputs, that contributes to dangerous waste and effluents generation. This situation is aggravated by population and industrial growth. From this perspective and according to Prisciandaro *et al*. (2016), in 2050 half of the world population will live under severe water scarcity.

In this context, the mining industry stands out as an activity that present an evident water demand and environmental impact. Among the minerals, gold is highlighted due to its high economic value. However, gold and most ores are not directly used as they are mined and require further physical and chemical processing. These steps are essential to achieve higher recoveries since most gold ores are occluded in a matrix composed mainly of pyrite, arsenopyrite and pyrrhotite (KEFENI, MSAGATI and MAMBA., 2017). This condition contributes to the low yield in conventional cyanide leaching and requires a prior oxidation treatment to promote the sulfides crystalline structures rupture (GUZMAN, THORPE and PAPANGELAKIS., 2018; FRASER, WALTON and WELLS., 1991).

The oxidation under pressure (POX) process stands out among the pre-oxidative treatments available, being widely used since the 1980s. This hydrometallurgical process takes place in autoclaves at high pressure (~21 atm) and at temperatures between 200 °C and 220 °C. This condition promotes the sulfides oxidation into sulfates, soluble metals and sulfuric acid generation. After the POX, the gold, previously occluded in the mineral matrix, is released and reaches prominent recovery values in the next stages (RICCI *et al.*, 2015; IVANNIKOV *et al.*, 2018).

However, the POX process is responsible for high water consumption and, consequently, for a large volume of aqueous effluent generation (63 m^3/h), which is composed of sulfuric acid and several metal ions in high concentrations (FOUREAUX *et al*., 2020; NAIDU *et al*., 2019). It is

worth mentioning that the negative environmental impacts caused when this effluent is disposed in nature without a proper treatment can be persistent, even when the mining company's activities cease (RAMBABU *et al*., 2020). Thus, the high demand for water, as well as the management of acidic effluents from gold mining, is one of the greatest challenges faced by this sector.

Water recycling has been progressively increasing in order to supply part of industrial water demand, contributing to reduce water stress. It is also worth mentioning that the expenses related with fresh water acquisition is increasing due to its scarcity; therefore, the adoption of water reuse also accounts as an economical advantage (PRISCIANDARO *et al*., 2016; GHERNAOUT *et al*., 2019). However, it is a consensus that the centralized treatment for industrial wastewater is not effective, since the industrial centers tend to be more distant and the cost associated with transportation would be high. Thus, the implementation of decentralized treatments becomes more interesting, as they can be applied in the same place where the effluent is produced (LACKEY *et al*., 2020).

In this perspective, the direct contact membrane distillation (DCMD) application stands out. DCMD consists of a thermal process whose driving force is generated by the vapor pressure gradient obtained through the difference in temperature of the heated feed (represented by the effluent in this study) with the permeate (distillate), that remains at room temperature (SALLS *et al.*, 2018; TAI *et al.,* 2019). In this process, the mass transfer occurs through a hydrophobic microporous membrane that establishes a direct interface between the hot and cold streams. Due to a surface tension between the liquid and the membrane surface, a liquid–vapor interface is established at the entrance of the membrane pores and permits only a vapor to permeate. Since only volatile compounds passes through the membrane pores, the DCMD has a theoretical rejection of 100% of metallic ions and other non-volatile compounds (RAHIMPOUR, KAZEROONI and PARHOUDEH., 2019). In addition, DCMD is an example of decentralized and modular treatment, which increases its flexibility in relation to the effluent volume to be treated and allows its application in the same location in which the effluent is produced. Another factor that contributes to the DCMD expansion on an industrial scale is the possibility of using the residual heat from the effluents (KHAYET and MATSUURA., 2011; ULLAH *et al.,* 2018). Therefore, it prevents extra expenses with heating/cooling systems for the feed stream and reduce carbon emissions when fossil fuels are considered for energy supply (ZHANG *et al.,* 2019). These advantages endorse the DCMD application for POX treatment once this effluent reaches temperatures around between 50 and 80°C after sedimentation and dispenses additional heating

stages (ALKHUDHIRI, DARWISH and HILAL., 2012). Recently, a review by Foureaux *et al*. (2020) showed that DCMD can be successfully applied to effluents with similar characteristics to the POX effluent.

For these reasons, this study proposes a DCMD process for POX effluent treatment and reuse water generation. Different operational conditions as feed temperature (50–70 °C) and recirculation flow rate (0.3–1.5 L/min) were investigated using a PTFE membrane. After the best conditions were defined, PVDF and PTFE membranes were compared, with and without spacer, in terms of distillate flux, recovery and metallic compounds rejection. The produced distillate's physical-chemical properties were compared to an actual mining industry process to evaluate its application as reuse water. Lastly, membranes were exposed to the effluent for eight months at similar temperature conditions in order to assess its integrity in prolonged treatment processes.

4.2 MATERIALS AND METHODS

4.2.1 Sample collection and characterization

The POX effluent was collected, in 2019, from a local mining site located in the state of Minas Gerais (Brazil). The company has an open pit mine for gold beneficiation and employs the POX process. The samples were stored at 4 °C and brought to room temperature prior to use. The effluent collected and all the permeates and concentrates generated by DCMD, were characterized according to the parameters listed in Table 4.1. The H_2SO_4 concentration analysis were adapted according to Gromov *et al*. (2018) and arsenic analyzes were performed adapting the method proposed by Dhar *et al*. (2004).

Table 4.1 - Physico-chemical analysis of POX effluent samples and DCMD's permeate and concentrated streams

Analysis	N° of Standard Methods 2017	Equipment
Electric conductivity	2510 B	Conductivimeter Hanna HI 9835
pH	4500 B	pHmeter Qualxtron QX 1500

SO_4^{2-}	-	Ion chromatograph Dionex ICS-1000
Metals atomic absorption (Fe^{3+}, Mg^{2+}, Ca^{2+}, Co^{2+}, Cu^{2+} and Ni^{2+}) by acetylene flame	3111 B	Shimadzu AA-7000
Metals atomic absorption (Al^{3+}) by nitrous oxide flame	3111 D	Shimadzu AA-7000

4.2.2 DCMD experiments and metals recovery

DCMD tests were carried out in triplicate, on a lab-scale set up, as represented in Figure 4.1. Before the tests, the membranes passed through a cleaning procedure in which they were submerged in a hydrochloric acid (HCl) 0.1% v/v solution for 20 minutes and then washed with distillated water. After chemical cleaning, distilled water was used as feed and its permeability was measured until reaching a steady permeate flux.

POX effluent was used as feed solution (2 L) while distilled water (1 L) was initially added in the distillate tank. The process was investigated in three different feed temperatures (50, 60 and 70 °C) to simulate the effluent outlet temperature in the mining plant, which leaves the autoclave at a temperature of approximately 180 °C. However, this effluent is washed by water in the counter-correct flux to proceed to the sedimentation step. After the washing, the effluent presents a temperature between 50 and 80 °C, which justifies the choice of this temperature range. The distillate temperature was maintained at 25 °C. The recirculation flowrate was maintained the same for both feed and distillate streams and varied from 0.3 – 1.5 L/min, which did not exceed the membranes liquid entry pressure. A flat sheet poly(tetrafluoroethylene) (PTFE) and poly(vinylidenefluoride) (PVDF) membranes, both commercially available and provided by Sterlitech®, with an effective area of 42.09 cm^2, were compared. The main properties of membranes are presented in Table 4.2.

An additional spacer (CF042 Low Foulant Spacer, PTFE 31Mil – 0.787 mm; provided by Sterlitech) was also considered under optimum feed temperature and circulation flowrates. After

each test, membrane cleaning was performed once with distilled water (physical cleaning) and with HCl (0.1 %v/v – chemical cleaning) recirculation (4 L/min) for 30 min at 60 °C. All tests were performed until an expressive increase in electrical conductivity was observed, which represents that the membrane was fully wetted, corresponding to approximately 120 h on average. Furthermore, the maximum recovery before wetting was defined when the permeate electrical conductivity increased by 20 µS/cm. All experiments were conducted in steady-state conditions regarding recirculation rate and temperature of feed and permeate.

Table 4.2 - PTFE and PVDF membranes properties

Parameter	PTFE	PVDF
Membrane porosity	0.70	0.64
Pore size (µm)	0.2	0.1
Membrane overall thickness (µm)	170	121
Contact angle (°)*	125	114
Liquid entry pressure (bar)	>4.0	>3.0
Polymer thermal conductivity (W/m·K)	0.250	0.180
Air thermal conductivity (W/m·K)	0.020 – 0.022	0.020 – 0.022
Membrane thermal conductivity (W/m·K)	0.092	0.079

*(REHMAN *et al*., 2019)

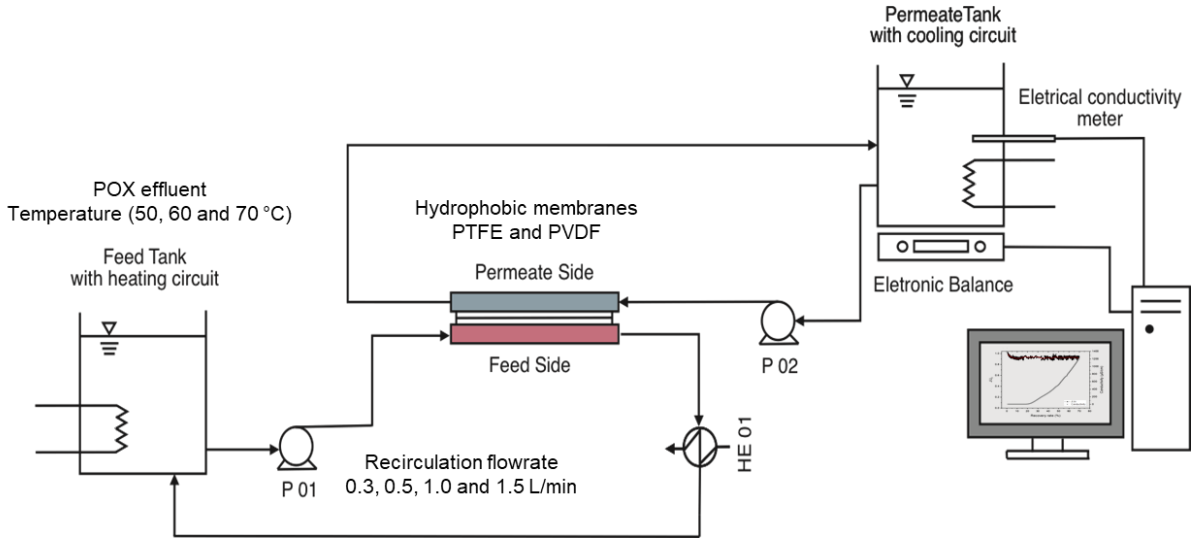

Figure 4.1 - Lab-scale DCMD system. P01 and P02: peristaltic pumps. HE01: heat exchanger.

PTFE and PVDF membranes were immersed in the effluent and kept under a constant temperature of 60 °C in order to assess their stability and integrity in POX effluent treatment over prolonged exposure. Distillate flux and NaCl rejection (initial NaCl concentration: 2,000 mg/L) were monitored every 30 days in a 6 h test, for eight months. The DCMD experimental conditions were similar to that described in section 2.2 except for feed temperature, which was kept constant at 60 °C, and recirculation flow rate, maintained at 0.30 L/min. The use of a NaCl solution was to assess the membrane integrity, and given that this is a monovalent salt with a low hydrated radius, it should provide a fair estimative of the membrane integrity and provide a reference point to the literature that report rejection of NaCl with DCMD.

Prior to the experiments, both PTFE and PVDF membranes were rinsed with distilled water. They were also characterized prior to the experiments and after 240 days immersed in the effluent, in order to observe possible degradation in terms of their morphology and composition. For that, a scanning electron microscopy (SEM) and energy dispersive X-ray spectroscopy (EDS), (JEOL JSM IT300) were used.

4.2.3 Calculations

The permeate flux (J, L/m^2·h) was calculated using Eq. (4.1), where t_1 and t_2 are the time; $m_2 - m_1$ is the increase in the permeate mass between times t_1 and t_2; a_m is the active membrane area and ρ_{H_2O} is the water density at the permeate temperature.

$$J = \frac{(m_2 - m_1)}{(t_2 - t_1) \cdot a_m \cdot \rho_{H_2O}} \quad (4.1)$$

The DCMD recovery grade (RR_{MD}) was calculated by Eq. (4.2), where v_{Ai} is the initial feed volume (L), v_{Pi} initial permeate volume (L) and v_{Pt} the permeate volume in t_2.

$$RR_{MD}(\%) = 100 \times \frac{[v_{Ai} - (v_{Pi} - v_{Pt})]}{v_{Ai}} \quad (4.2)$$

The resistances associated with the DCMD process, namely, membrane (R_m); permeate boundary layer (R_{pb}); feed boundary layer (R_{fb}); fouling layer (R_f) and total (R_t) resistances ($Pa \cdot m^2 \cdot h/kg$) were calculated according to previous studies (SRISURICHAN, JIRARATANANON and FANE., 2006), as the following equations Eqs.(4.3-4.7).

$$R_m = \frac{P_1 - P_2}{J} \quad (4.3)$$

$$R_{pb} = \frac{P_2 - P_p}{J} \quad (4.4)$$

$$R_{fb} = \frac{P_f - P_1}{J} \quad (4.5)$$

$$R_f = R_t - R_m - R_{pb} - R_{fb} \quad (4.6)$$

$$R_t = \frac{P_f - P_p}{J} \quad (4.7)$$

Where P_f, P_1, P_2 and P_p are the vapor pressure (Pa) at bulk feed, membrane surface facing the feed, membrane surface facing the permeate and at the bulk permeate, respectively. According to Ali *et al*. (2013), these pressures were calculated using Antoine's equation Eq. (4.8) where T (K) is the temperature. Furthermore, the P_f was corrected using the water activity coefficient, as shown in Eq. (4.9), where P_w is the water vapor pressure and α_f the feed water activity coefficient.

$$P = EXP\,(23{,}238 - \frac{3841}{T - 45}) \quad (4.8)$$

$$P_f = P_w \alpha_f \quad (4.9)$$

The α_f was estimated using the Pitzer model through the software "PHREEQC". The software allows to perform a variety of calculations related to aqueous media, such as the water activity coefficient and saturation index (PARKHURST and APPELO., 2013). The model was preferred over specific ion interaction theory (SIT theory) due to its better fit for complex electrolyte solutions and was already validated in previous study (PÉREZ-VILLASEÑOR, IGLESIAS-SILVA and HALL., 2002; CUI *et al.*, 2007).

In this present study, α_f was greater than 0.98, which shows that this effluent has low propensity to form polarization effects, specially, concentration polarization effects. Due to this fact and the difficulty to estimate ions mass transfer coefficients in complex electrolytes solutions, the concentration polarization effect was not considered in this study. Guan *et al.* (2020) demonstrated that significant water activity coefficients (α_f<0.95) and concentration polarization effects were only pronounced at salts (KCl, NaCl, $MgSO_4$ and $MgCl_2$) concentrations >1 mol/L. Furthermore, similar behavior was reported by Quist-Jensen *et al.* (2016) while recovering lithium from high-concentrated aqueous solutions. In this present study the sum of all ions never surpassed 0.5 mol/L.

The temperature in the bulk feed and permeate were monitored using thermometers. To estimate the temperatures at the membrane surface facing the feed and permeate an energy balance was considered for the system, leading to the following equations (Eqs. 4.10-4.11) (GROSSI *et al.*, 2020; SRISURICHAN, JIRARATANANON and FANE., 2006).

$$T_{w,f} = \frac{h_m\left(T_p+\left(\frac{h_f}{h_p}\right)T_f\right)+h_p\,T_p-J\Delta Hv}{h_m+hf\left(1+\frac{h_m}{hp}\right)} \quad (4.10)$$

$$T_{w,p} = \frac{h_m\left(T_f+\left(\frac{h_p}{h_f}\right)T_p\right)+h_f\,T_f-J\Delta Hv}{h_m+h_p\left(1+\frac{h_m}{h_f}\right)} \quad (4.11)$$

Where T_f; $T_{w,f}$; $T_{w,p}$; and T_p are the temperatures at bulk feed, membrane surface facing the feed, membrane surface facing the permeate and at the bulk permeate, respectively. The, h_m , h_p and h_f (W/m^2 ·h) are the convective heat transfer coefficient of the membrane, permeate and feed. Lastly, ΔHv stands for the water vaporization heat calculated by Eq. (4.12) (PHATTARANAWIK, JIRARATANANON and FANE., 2003).

$$\Delta Hv = 1.7535 \cdot T + 2024.3 \quad (4.12)$$

Considering the module geometry, the following Nusselt correlations Eqs. (4.13-4.14) were used to calculate h_p and h_f Eq.(4.15) (GROSSI *et al.*, 2020; PHATTARANAWIK, JIRARATANANON and FANE., 2003).

$$Nu_F = 15(RePr)^{0,23}(D_h/L)^{0,5} \quad (4.13)$$

$$Nu_P = 11{,}5(RePr)^{0,23}(D_h/L)^{0,5} \quad (4.14)$$

$$h_{p,f} = k_{p,f} Nu_{P,F}/D_h \quad (4.15)$$

Where Re is the Reynolds number Eq. (4.16), Pr the Prandtl number Eq. (4. 17), $k_{p,f}$ the permeate or the feed thermal conductivity, D_h the hydraulic diameter, μ and ν are the water dynamic and kinematic viscosity and A the pipe's cross-sectional area.

$$Re = \frac{Q*D_h}{\nu*A} \quad (4.16)$$

$$Pr = C_p \mu / k_{p,f} \quad (4.17)$$

The temperature polarization effect on the reduction of vapor pressure gradient across the membrane was evaluated. For that, the temperature polarization coefficient was estimated using Eq. (4.18).

$$\tau = \frac{T_{w,f} - T_{w,p}}{T_f - T_p} \quad (4.18)$$

The observed rejection efficiency for each physical-chemical parameter by DCMD was determined by Eq. (4.19), in which $C_{i,f}$ (mg/L) corresponds to the component concentration in the feed solution whereas $C_{i,p}$ (mg/L) to the component concentration in the permeate.

$$R\ (\%) = 100 \times \frac{(C_{i,f} - C_{i,p})}{C_{i,0}} \quad (4.19)$$

Cleaning efficiency Eq. (4.20) was estimated by comparing the permeate flux with a pristine membrane with the flux with the membranes and after physical (J_{pc}) or chemical (J_{cc}) cleaning,

both using distilled water as feed solution. J_w (L/m^2·h) is a pure water volume permeate flux before effluent distillation.

$$Cleaning\ efficiency = 100 \times \left(\frac{J_w - J_{pc,cc}}{J_w}\right) \quad (4.20)$$

4.3 RESULTS AND DISCUSSION

4.3.1 Membrane distillation performance

4.3.1.1 Feed temperature effect

Initial tests with circulation rate at 0.3 L/min (test monitoring shown in Figure 4.2) demonstrated that temperature increase led to a Reynolds number increase (Table 4.3). This can be attributed

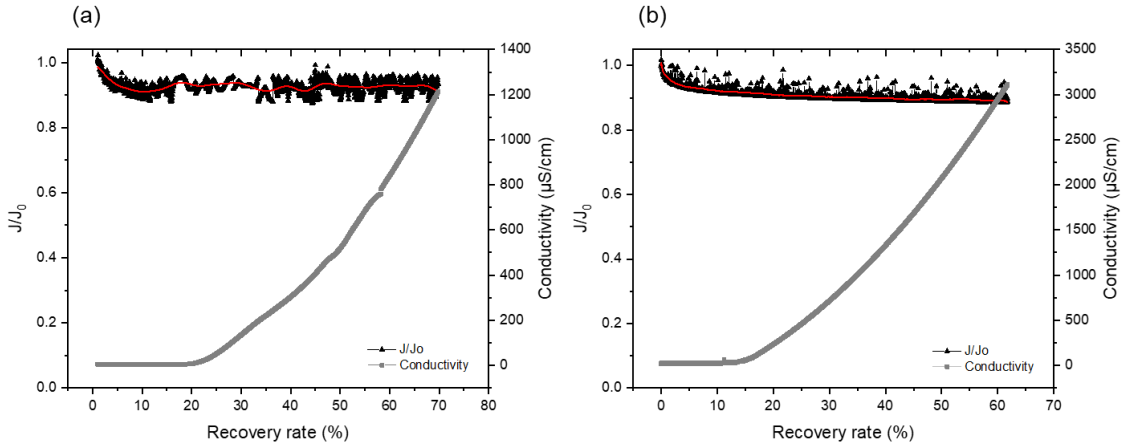

Figure 4.2 - Temperature effect over distillate flux decay and electrical conductivity at a constant recirculation flowrate (0.3L/min): (a) 60 °C and (b) 70 °C.

to the fact that, although the circulation rate has remained the same, the fluid properties such as density and viscosity change significantly with temperature. The permeate flux with distillate water (J_w) and the permeate flux with the effluent also increases with the temperature, led by the elevate in driving force across the membrane ($\Delta P_{interface}$). However, the initial flux when the effluent was fed (J_0) is reduced due to the introduction of the feed osmotic pressure and temperature polarization effects.

Table 4.3 - DCMD performance summary for different operational conditions and cleaning efficiency

	Feed Temperature (°C)	Reynolds (Re)	Flux (L/m²·h) J_w	J_0	J_f	J_f/J_0	J_{pc} *(Efficiency)*	J_{cc} *(Efficiency)*	Recovery at wetting (%)
Feed flow rate 0.30 L/min (PTFE)	50	4154	0.56	*	*	*	*	*	*
	60	4481	5.87	2.58	2.40	0.93	5.50 *(93.7 %)*	5.64 *(96.1 %)*	22.71 ± 1.75
	70	5156	20.43	16.47	15.15	0.92	19.21 *(94.0 %)*	19.86 *(97.2 %)*	13.65 ± 1.03
	Feed flow rate (L/min)								
Feed temperature 60 °C (PTFE)	0.30	4481	5.87	2.58	2.40	0.93	5.50 *(93.7 %)*	5.70 *(97.1 %)*	22.71 ± 1.75
	0.50	7468	15.65	9.11	8.47	0.93	14.55 *(92.9 %)*	15.36 *(98.1 %)*	12.05 ± 2.83
	1.00	14937	27.75	18.19	16.73	0.92	25.80 *(92.9 %)*	27.00 *(97.3 %)*	10.42 ± 1.36
	1.50	22405	34.77	24.91	23.17	0.93	32.53 *(93.5 %)*	33.70 *(96.9 %)*	9.46 ± 0.94
	Membrane type								
	PTFE	4481	5.87	2.58	2.40	0.93	5.50 *(93.7 %)*	5.70 *(97.1 %)*	22.71 ± 1.75

Feed temperature 60 °C; Flow rate 0.30 L/min	PTFE + Spacer	4481	8.38	7.03	6.61	0.94	7.55 *(90.0 %)*	8.19 *(97.7 %)*	33.91 ± 2.69
	PVDF	4481	21.37	16.03	15.07	0.94	19.50 *(91.2 %)*	20.48 *(95.8 %)*	17.49 ± 1.50
	PVDF + Spacer	4481	34.43	23.51	22.33	0.95	31.10 *(90.3 %)*	33.80 *(98.1 %)*	25.82 ± 1.08

*There was no driving force under that experimental condition. In grey and italics are the cleaning efficiency. Standard deviation for flux and cleaning efficiency were <3%.

An increase in feed solution temperature resulted in lower permeate recovery percentage due to a higher wetting grade. This occurs because, usually, liquids surface tension reduces with the increment in temperature which also changes the membrane morphology as pore structure and size distribution (SAFFARINI *et al.*, 2013). These phenomena are the largest contributors to a $\Delta P_{interface}$ greater than the membrane liquid entry pressure (REZAEI *et al*., 2018), leading to membrane wetting. Other mechanisms responsible for wetting, such as the absence of a temperature gradient and vapor condensation within the pores were discarded as the process operated continuously and temperatures were precisely controlled.

The main results obtained for temperature polarization and DCMD resistances were summarized in in Table 4.4. Considering that heat and mass transfer occurs simultaneously across the membrane, the thermal boundary layer, located adjacent to the membrane surface, creates a heat resistance and results in temperature polarization effects. The temperature polarization coefficient (τ) relates to the fraction of the total thermal driving force that contributes to the heat transfer. For a rapid heat transfer in the liquid phases, $\tau \rightarrow 1$; in this case the process rate is completely controlled by the transmembrane mass-transfer resistance. Conversely, in cases that $\tau \rightarrow 0$, the process is completely controlled by the heat transfer resistance in the liquid phases. For an increase in feed temperature from 60 to 70 °C, the temperature polarization became more pronounced whereas the resistances of both feed and permeate bulk reduced. Under these conditions, τ varied from 0.62 – 0.59 demonstrating that both heat and mass transfer resistance played an important role in the total resistance (R_t).

Table 4.4 - DCMD temperature polarization and resistances for different recirculation flow rates and feed temperature

	Temperature (°C)	Prandtl (Prf)	Nusselt (Nuf)	Reynolds (Re)	Temperature polarization (τ)	Resistances (Pa.m^2.h/kg)				
						R_{fb}	R_m	R_{pb}	R_f	R_t
Feed flow rate 0.30 L/min (PTFE)	50	3.25	24.13	4154	*	*	*	*	*	*
	60	2.99	24.10	4481	0.62 ± 0.01	1289.9	5935.7	404.0	222.6	7852.2
	70	2.56	23.99	5156	0.59 ± 0.02	470.8	1401.9	116.0	61.1	2049.9
	Feed flow rate (L/min)									
Feed temperature 60 °C (PTFE)	0.30	2.99	24.10	4481	0.62 ± 0.01	1289.9	5935.7	404.0	222.6	7852.2
	0.50	2.99	27.10	7468	0.68 ± 0.03	394.2	1642.5	126.2	62.1	2224.9
	1.00	2.99	31.79	14937	0.72 ± 0.02	212.6	809.1	69.4	35.3	1126.4
	1.50	2.99	34.90	22405	0.72 ± 0.04	160.8	577.8	53.3	21.4	813.3
	Feed temperature	Reynolds				Resistances (Pa.m^2.h/kg)				

	(°C)	(Re)	Temperature polarization coefficient (τ)	R_{fb}	R_m	R_{pb}	R_f	R_t
	Membrane type							
Feed temperature 60 °C; flow rate 0.30 L/min	PTFE	4481	0.62 ± 0.01	1289.9	5935.7	404.0	222.6	7852.2
	PTFE + Spacer	4481	0.67 ± 0.03	526.1	2088.9	169.6	66.4	2851.0
	PVDF	4481	0.79 ± 0.05	306.1	794.3	124.9	25.3	1250.5
	PVDF + Spacer	4481	0.87 ± 0.03	232.4	501.7	96.6	13.3	843.9

*There was no driving force under that experimental condition. Standard deviation for resistances were <1.

The decrease in τ for an increase in T_f is a well-known phenomenon and an accepted trend in membrane distillation studies (ALI *et al.,* 2013; QTAISHAT *et al.,* 2008). That is a result of higher convective heat transfer coefficients (Figure 4.3), since the fluid viscosity and density reduce whereas the thermal conductivity increase. The overall results lead to a higher heat exchange rate between the feed and permeate streams at the membrane interface. Consequently, the feed temperature at the membrane surface reduces while the permeate temperature at the membrane surface increases, therefore, leading to a lower temperature difference across the membrane and pronounced temperature polarization effects. It is also important to consider the exponential growth in vapor pressure and distillate flux for a slightly increase in feed temperature. Ricci *et al.* (2019) pointed out that these higher fluxes would also contribute for an increased temperature gradient in the boundary layers, intensifying the temperature polarization. In that case, the increase in the heat transfer coefficients would not be enough to diminish the heat exchange occurring in membrane surface.

An increase in feed temperature also affected the overall process resistance (R_t), mainly because membrane, feed bulk and permeate bulk resistances decreased. In this context, the Rm decreases stand out due to temperature increases. This fact can be attributed to the inverse relationship between Rm and the membrane mass transfer coefficient (K_m), because K_m is proportional to the diffusivity (PD_{wa}) and consequently to the temperature, since $PD_{wa} = 4.46 \times 10^{-6}T^{2334}$ (GROSSI *et al*., 2020). However, it is worth mentioning that, among all, membrane resistance was the main contributor opposing to mass transfer (68.4 – 75.6%), whereas fouling had a minor contribution (2.8 – 2.9%).

Vapor transport through the membrane pores relies on the pore size and its mean free path for transport. Therefore, as membrane morphology changes and pores become wider at higher temperatures, its resistance to vapor transport decreases (ALI *et al*., 2013). Moreover, as convective heat transfer increases, thermal boundary layer reduces and lead to lower feed and permeate bulk resistances.

The low fouling contribution to total process resistance was attributed to the effluent physico-chemical composition. Due to the absence of organic matter in POX effluents, the propensity to form a cake layer or biofouling is negligible (BOGLER, LIN and BAR-ZEEV., 2017). Additionally, scaling from $CaCO_3$ and $CaSO_4$ precipitation was discarded as Langelier Saturation Index (LSI) was <0 (WARSINGER *et al.*, 2015). Under the experimental conditions,

these two main precipitates would not form or accumulate over membrane surface, but rather stay dissolved in the bulk solution. Due to those reasons, the normalized flux reported in Table 4.3 was close to one regardless of the operating condition, indicating that there was no flux decay throughout the monitoring period.

Organic and inorganic fouling can be efficiently removed from the membrane surface through physical and chemical cleaning. In this study there was no significant influence in the cleaning efficiency when there was an increase in feed temperature (Table 4.3), but, because the effluent is composed mainly of inorganic compounds, chemical cleaning had better efficiencies. Furthermore, the lower fouling propensity suggested that, when or if occurs, the fouling is reversible, which corroborate for long-term operations and reduced costs with maintenance.

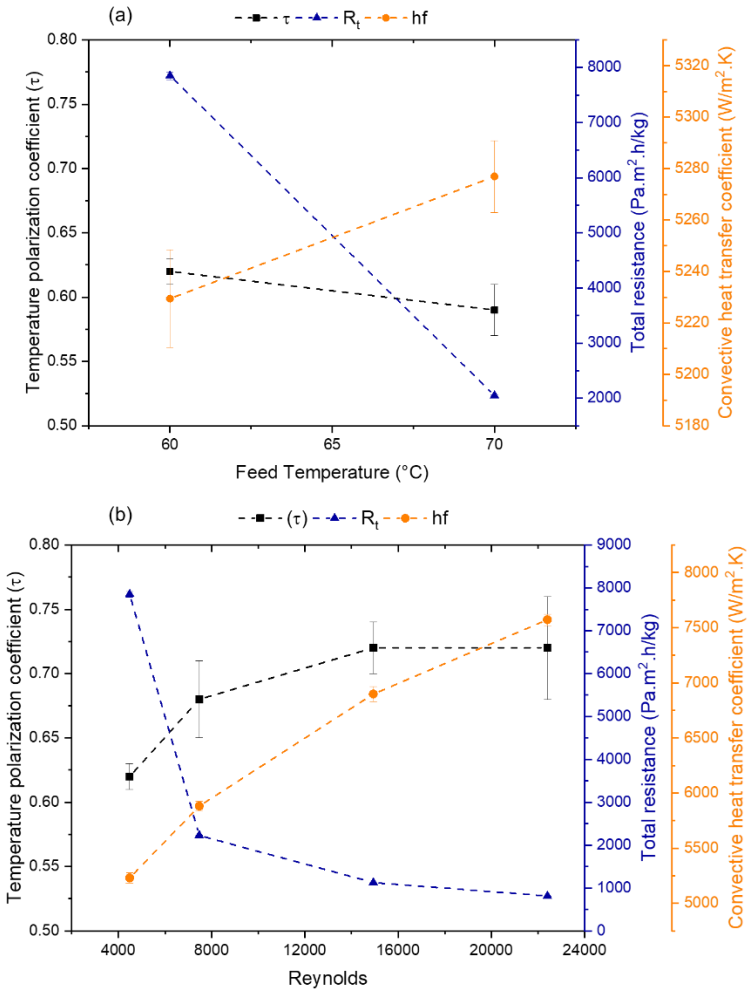

Figure 4.3 - (a) Temperature and (b) recirculation flowrate effect over temperature polarization coefficient (τ), total resistance (R_t) and convection heat transfer coefficient (h_f).

Because 60 °C as feed temperature showed better performance, higher recovery grade and less flux decline, it was selected as feed temperature to assess the feed flow rate effect. The results are shown in Tables 4.3-4.4 and Figure 4.4.

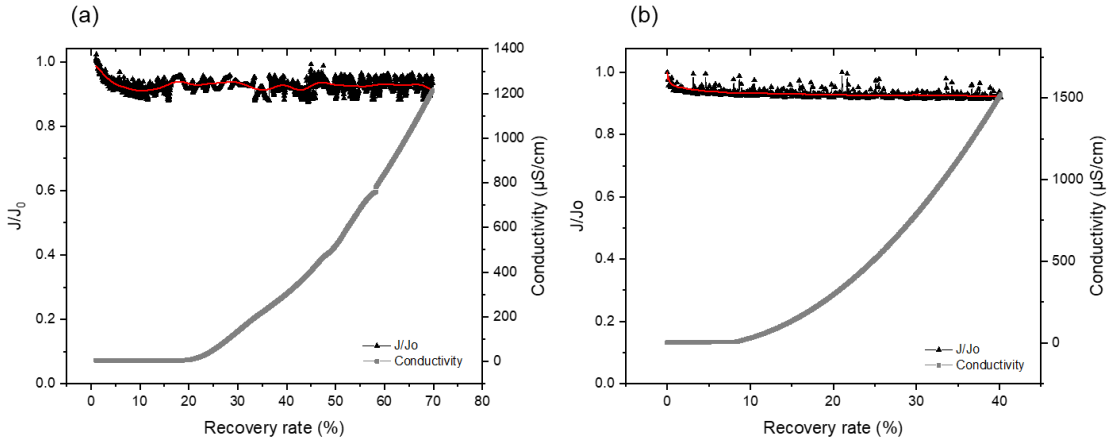

Figure 4.4 - Recirculation flowrate effect over distillate flux decay and electrical conductivity at a constant temperature (60 °C): (a) 0.3 L/min and (b) 1.5 L/min.

With the increase in flow rate, there was an increase in Reynolds number, which led to higher J_w and J_0. This increase in flux can be due to an enhancement of the feed boundary heat transfer coefficient (h_f; Figure 4.3b) which resulted in increased membrane surface temperature ($T_{w,f}$) Ali *et al.* (2013). Consequently, both temperature polarization and resistance to mass transfer offered by the boundary layer reduces as a result of a lower thermal resistance. In that case, convective heat transfer overcomes the effects of heat loss due to water vaporization at membrane interface. In fact, the energy associated to vaporization decreases with increment in volumetric flow rate as reported by Ali *et al.* (2013) and reinforces the benefits of improving thermal efficiency at greater hydraulic conditions.

However, a reduction in the recovery grade at greater flowrates was observed, suggesting that the higher shear conditions favor the membrane wetting. This can happen because at higher feed flow rates there is a significantly increase in permeate flux and, therefore, higher concentration of acids and metals dissolved are found in the feed stream, which presents a shear force with the membrane surface (QUIST-JENSEN *et al*., 2016). The electrical charge of these compounds, as well as the membrane surface, can also interfere in the occurrence of membrane wetting. Several

studies reported a negative charge on polymeric membrane surface, which is due to the electronegative charge of C-F moiety (GUO *et al*., 2018).

Lastly, there was no significant effect of feed flow rate on membrane cleaning efficiencies, as happen on the feed temperature effects. Furthermore, the J_f/J_0 values were close to one, independently of the feed flow rate, once again highlighting the minimal effects of fouling phenomena when DCMD is applied in this effluent treatment.

4.3.1.2 Membrane type and spacer effect

The operational condition that led to higher recovery grade until this point was 60 °C as feed temperature and 0.3 L/min as circulation flow rate. This operational condition was then applied to assess the performance difference between two different membrane materials and the spacer addition, and these results are shown in Table 4.3.

DCMD membranes can be manufactured with different materials, which leads to different mechanical, physical and separation properties. Among the most used materials for DCMD membranes are PTFE and PVDF (FOUREAUX *et al.,* 2020). PTFE membranes are usually more hydrophobic, with higher contact angle with water, and offer good resistance to temperature and chemical oxidation (FOUREAUX *et al*., 2020; TAI *et al*., 2019). PVDF, on the other hand, shows good hydrophobicity – but less than PTFE, and can be easily manufactured into membranes with versatile pore structures by different methods (TAI *et al*., 2019). These properties allowed the PTFE membrane to achieve higher recovery grades. However, due to its higher polymer thermal conductivity compared to PVDF, it had a slightly lower energy efficiency and, therefore, more pronounced temperature polarization effects.

For PTFE, the τ varied from 0.62 – 0.67 when spacer was considered, whereas for PVDF, these values varied from 0.79 – 0.87 (Table 4.4). Not only temperature polarization was less significant, but reductions in overall process resistances were also observed. As a result of higher temperatures over the membrane surface at the feed side and lower resistances, a higher permeate flux was also obtained. The results obtained for the permeate's flux and electrical conductivity monitoring using both PTFE and PVDF membranes, with and without spacer considering the most appropriate temperature (60 ºC) and recirculation flow rate (0.30 L/min) were presented in Figures 4.5 and 4.6, respectively.

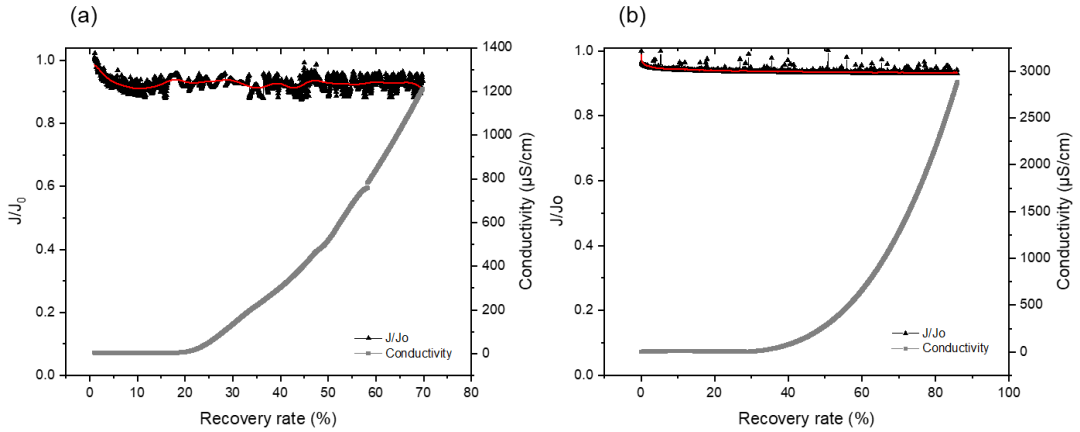

Figure 4.5 - PTFE membranes: spacer contribution to distillate recovery grade. (a) without spacer (b) with spacer and.

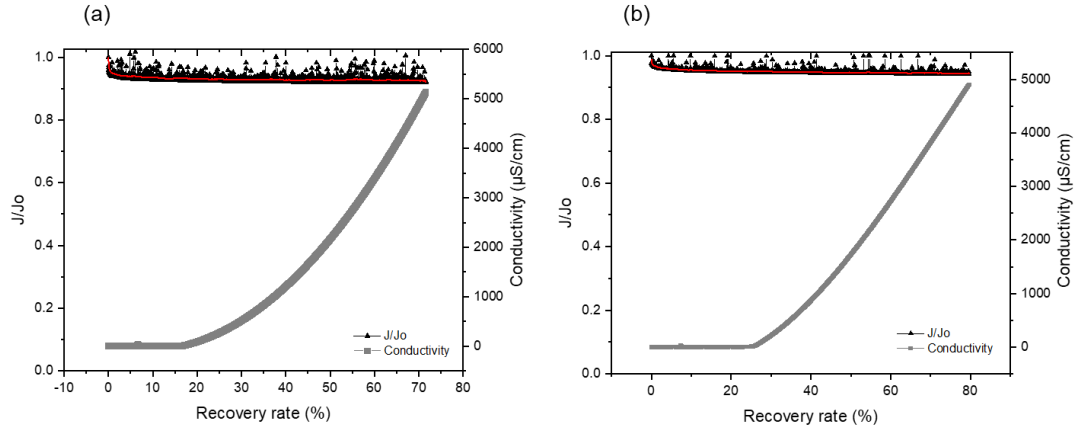

Figure 4.6 - PVDF membranes: spacer contribution to distillate recovery grade. (a) without spacer and (b) with spacer.

Previous studies have reported the effect of including mixers and spacers in the bulk feed and the membrane respectively (ALWATBAN *et al*., 2019; KATSANDRI., 2017). The consensus is that spacers add extra mechanical support to the membrane as well as reduces the level of the temperature polarization. That is a result of a turbulence promotion when spacers are added, changing the flux characteristics, and enhancing the boundary layer heat and mass transfer coefficients. Kayvan *et al.* (2015) studied the operational conditions effect in DCMD to desalinate sea water. The authors reported that the spacer utilization enhanced the momentum, heat, and mass transfer. In their case the distillate flux was enhanced by around 51% when a

spacer was used which shows the significance of spacers as an enhancement tool to the overall DCMD performance.

Therefore, among all operational variables discussed, and considering process water reclamation as the main objective of the current work, the optimum DCMD conditions were defined as 60 °C for feed temperature, using a membrane with PTFE as base polymer, with spacer. Under the mentioned conditions, higher distillate flux was obtained and allowed for a greater recovery grade.

4.3.1.3 DCMD desalting ability

The results regarding DCMD desalting ability for the various operational conditions is presented in Table 4.5. The ions characterization near the wetting point showed the DCMD desalting ability. Removal efficiencies did not vary significantly (coefficient of variation < 1%), and the membrane guarantees values close to the theoretical retention of 100% in DCMD processes. The slightly increase in permeate electrical conductivity was attributed to iron, sulphate and magnesium ions transported through the membrane and detected at higher concentrations in the distillate stream. Partial and surface wetting may occur prior to membrane full-wetting and could be responsible for these ions transport across the membrane (REZAEI *et al.,* 2018). In that case, the liquid-vapor interface is encountered within the membrane pores rather than its surface, which makes the distillate reclamation possible although favoring the ions transport (REZAEI *et al.,* 2018). Furthermore, in fully wetted membranes the ions transport is more favorable than water, thus the permeate flux in this study, after the membrane was fully wetted, in all cases, remained stable while the permeate electrical conductivity increased significantly. Similar behavior was previously reported (GE *et al*., 2014; KIM *et al*., 2019). In that case, the liquid-vapor interface is encountered within the membrane pores rather than its surface, which makes the distillate reclamation possible although favoring the ions transport (REZAEI *et al.,* 2018).

Due to the low concentration of metallic ions and a neutral pH, the permeate generated represents a promising alternative for industrial reuse water at relatively low costs, especially when the residual heat from the effluent is used as driving force. It is noteworthy the process ability to retain highly toxic metallic compounds as As^{3+} and $As^{5,+}$ which retention efficiency is considerably low in conventional and advanced treatments (MONDAL *et al*., 2013). Furthermore, it is important to note that, the operational condition with PTFE membrane with spacer at 60 °C feed temperature and recirculation rate at 0.3 L/min showed comparable removal

efficiencies to other operational conditions, while maintaining a higher permeate flux and achieving an overall higher recovery grade.

Most of the physic-chemical properties would attain the required process water quality reported by Silva *et al.* (2020). The authors studied the DCMD effectiveness for treating another effluent from the mining industry and characterized the process water used by the mining industry. For the previously mentioned operational condition, which showed concentrations lower than the process water, the distillate could be used as reuse water in the same industry, contributing to costs cut down and reducing environmental impacts. In a different research, the costs associated with DCMD for water reclamation were taken into account and compared with nanofiltration costs (REIS *et al*., 2019). The authors proposed a sensitive analysis taking into consideration the membrane lifespan and the temperatures in which the effluent is generated, concluding that the residual heat characteristic of POX effluent accounts for major savings in membrane distillation process (treatment cost: 0.364 – 0.466 US$/$m^3$).

Moreover, the concentrated stream generated after all process could be easily disposed due to its low volume, but also be processed for value-added compounds recovery. These also accounts as advantages to DCMD since most process as ion-exchange and solvent extraction has the concentration as the driving force and would present higher efficiencies for concentrated solutions (KESIEME and ARAL., 2015; ABBASI, MCKEVITT and DREISINGER., 2018).

Table 4.5 - DCMD removal efficiencies for different operational conditions

Parameter	Effluent	Process water[a]	PTFE membrane						PVDF membrane	
			60 °C 0.3 L/min	60 °C 0.5 L/min	60 °C 1.0 L/min	60 °C 1.5 L/min	70 °C 0.3 L/min	Spacer 60 °C 0.3 L/min	60 °C 0.3 L/min	Spacer 60 °C 0.3 L/min
			RR[b]=25%	RR=15%	RR=15%	RR=10%	RR=15%	RR=35%	RR=20%	RR=30%
pH	1.37	6.80	--	--	--	--	--	--	--	--
Electrical conductivity (µS/cm)	16808.33	30.81	99.7	99.1	99.4	99.8	99.6	99.8	99.4	99.8
H_2SO_4 (mg/L)	8367.70	--	>99.9	>99.9	>99.9	>99.9	>99.9	>99.9	>99.9	>99.9
SO_4^{2-} (mg/L)	10724.00	17.85	99.9	98.1	99.8	99.9	99.9	99.9	99.8	99.9
Cl^- (mg/L)	35.35	4.07	99.9	98.0	99.8	99.9	99.9	99.9	99.9	99.9
As $^{3+}$ (mg/L)	269.88	0.02	97.5	>99.9	99.6	99.8	99.7	99.9	99.7	99.8
As $^{+5}$ (mg/L)	29.59	0.19	99.8	>99.6	>99.6	>99.6	>99.6	99.4	99.3	99.4
As Total (mg/L)	299.48	0.21	97.7	>99.9	99.6	99.8	99.7	99.8	99.6	99.7

Fe Total(mg/L)	829.20	--	99.6	>99.9	99.7	99.8	99.6	99.8	99.6	99.9
Ca^{2+} (mg/L)	37.61	3.26	>99.2	98.6	98.6	98.6	98.1	>99.2	98.3	98.6
Al^{3+} (mg/L)	484.65	--	99.3	99.6	98.7	99.3	99.6	99.6	99.8	>99.8
Cu^{2+} (mg/L)	171.57	--	>99.9	99.7	99.4	99.7	>99.9	>99.9	98.4	99.6
Mg^{2+} (mg/L)	2662.10	3.12	99.9	99.9	99.9	99.9	>99.9	99.9	>99.9	99.9
Ni^{2+} (mg/L)	169.30	--	99.4	99.7	98.6	99.7	>99.9	>99.9	95.7	99.6
Mn^{2+} (mg/L)	85.48	--	>99.9	99.4	99.1	99.4	>99.9	>99.9	>99.9	99.6
Co^{2+} (mg/L)	33.07	--	>99.5	>99.5	>99.5	>99.5	>99.5	>99.5	98.8	98.4

[a]Reference (SILVA *et al*., 2020). [b]RR is the recovery grade in which the ions concentration was measured. Rejection efficiencies standard deviation were <0.5%

4.3.1.4 Membrane stability and integrity

Due to the chemical and thermal resistance of PTFE and PVDF, no significant modification on its microstructure is excepted under harsh conditions (high temperature and acidic media) (SAFFARINI *et al.*, 2013; AWANIS HASHIM. LIU and LI., 2011). For that reason, they have been considered in a few attempts of acidic effluents treatment, focusing on their treatment (HULL and ZODROW., 2017) and by products recovery (TOMASZEWSKA, GRYTA and MORAWASKI., 1998). What would be observed, though, is a slightly increase in pore size which may favors wetting phenomenon at higher temperatures as already reported by Saffarini *et al.* (2013) and discussed previously.

Both membranes presented a stable distillate flux and maintained their high rejection rate to NaCl (Figure 4.7). For PVDF membranes, the mean distillate flux and electrical conductivity rejection were respectively 19.13 ± 0.09 L/m^2·h and 99.2 ± 0.1 %, whereas for PTFE membranes they were 4.26 ± 0.11 L/m^2·h and 99.7 ± 0.1 %. These values are close to those reported in Table 4.3, suggesting that membrane remained intact over the exposure period. The results reinforce the DCMD is a feasible process for POX effluent treatment and water reclamation, even under high temperature and acidic concentrations. As shown in Figure 4.8 membrane morphology and composition were also maintained passed the period of 240 days and no relevant difference was observed. After exposure, additional peaks from magnesium, iron, copper and calcium were observed, however not correlated with scaling given the unfavourable conditions for salt precipitates formation.

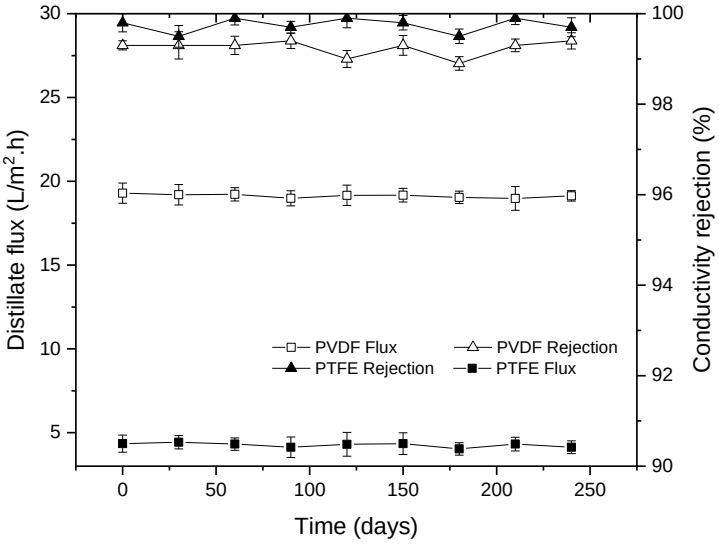

Figure 4.7 - Distillate flux and electrical conductivity rejection in eight months of monitoring.

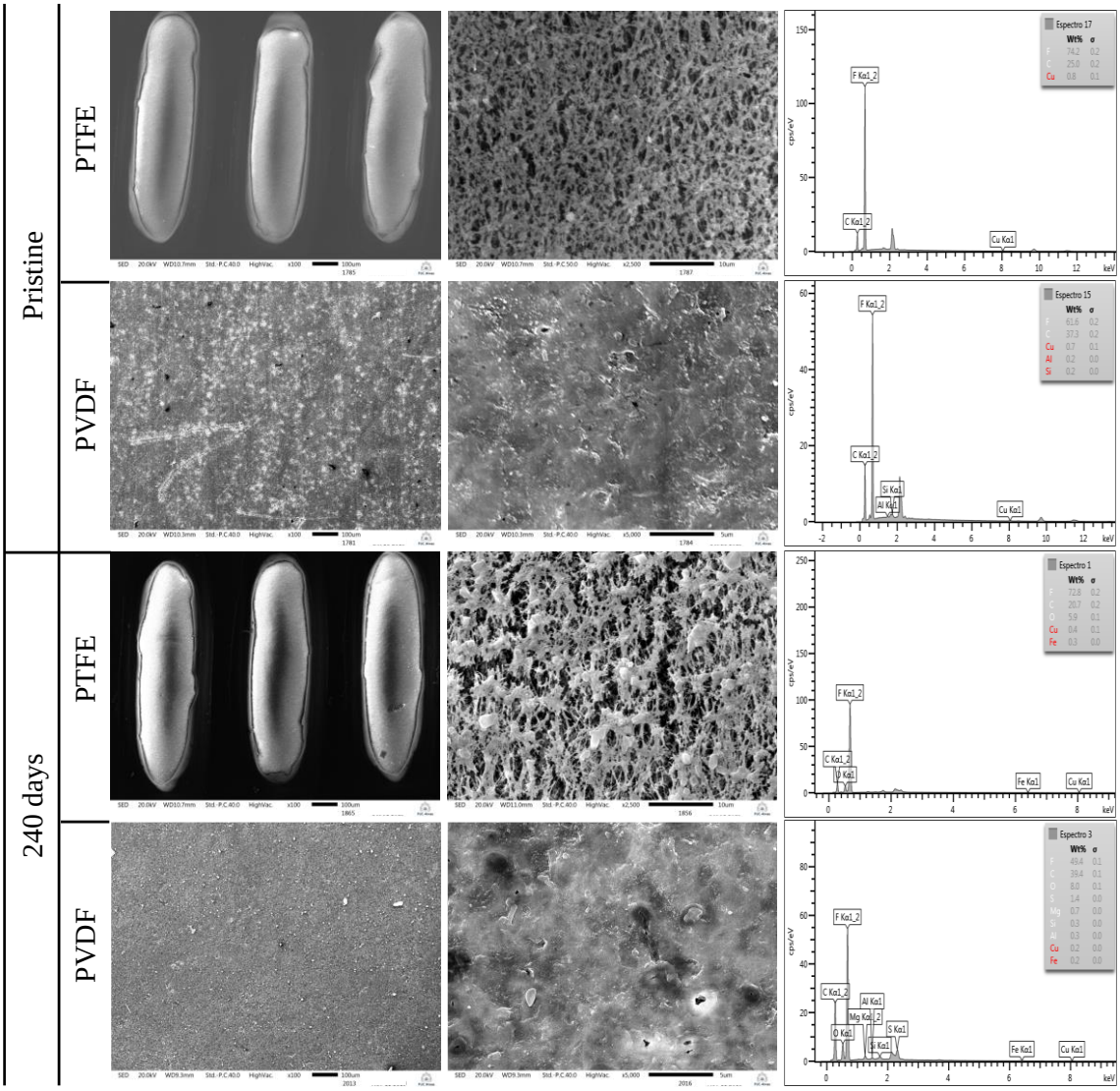

Figure 4.8 - PTFE and PVDF membrane morphology and composition before and after exposure characterized by scanning electron microscopy (SEM) and energy dispersive X-ray spectroscopy at different magnitudes (from left to right, for PTFE: x100 and x2500; for PVDF: x100 and x5000).

4.4 FINAL CONSIDERATIONS

Membrane distillation was investigated for its suitability in process water reclamation. Different operational conditions were assessed, including different membranes and the contribution of an additional spacer. The total resistance was lower, and the process had a higher energy efficiency, for higher feed temperature and recirculation flowrates. In contrast, higher wetting rate and lower recovery grades were obtained for the same conditions, compromising the permeate physic-chemical quality. Under the best condition assessed (PTFE membrane with spacer, feed

temperature: 60ºC and recirculation flow rate: 0.3 L/min), retention rates greater than 95.7% was achieved, allowing for a high-quality reuse water reclamation. The average permeate flux corresponded to: 6.82 L/m^2.h, whereas the recovery grade achieved was 33.9%. The process feasibility was reinforced by the membrane stability and integrity even after exposed to the effluent for 8 months. In that case, both PVDF and PTFE membranes maintained their higher rejection to NaCl (99.2 %) and no significant flux change was observed. Due to the possibility of reuse the POX residual heat, which prevents extra expenses with heating systems, DCMD was pointed out as a promising technology for water reclamation.

5 CHAPTER 5

METALS RECOVERY BY ION EXCHANGE RESINS

5.1 INTRODUCTION

There is a growing need for the adoption of treatments which can be applied to gold mining effluents in order to meet increasingly restrictive environmental legislation and, moreover, allow their byproducts recovery. Increasingly, mining seeks to adopt practices that are in accordance with the circular economy principles (DINIZ *et al.*, 2005; FOUREAUX *et al.*,2020). One type of effluent that is generated in gold mining refers to this metal beneficiation processes by oxidation under pressure (POX), since most of the gold is in the refractory category due to its association with sulfide elements, which compromises its recovery (FOUREAUX *et al*., 2021). In this sense, Yu *et al*. (2019) reported that for sulfide-rich matrices, gold recovery by the conventional leaching process varies between 55 - 70% and after POX, recoveries up to 86 % could be achieved. However, the POX wastewater contain elevate concentrations of dissolved metals in the extremely acid environment (FOUREAUX *et al.*, 2020). This effluent offers opportunities for the recovery of metals of economic interest such as Nickel (Ni^{2+}), Copper (Cu^{2+}) and Cobalt (Co^{2+}).

In this sense, Nickel global consumption in 2019 was around of 2.4 million tonnes and its global demand is expected to grow by 3-4% over the next five years (ERAMET., 2020). Cobalt plays an important role in the composition of the majority alloys developed since the 19^{th} century, and the increase in its demand is estimated to be approximately 83% in 2030 (FU *et al*., 2020). In addition, nickel and cobalt are considered by the European Union as critical materials, which are the most economically important raw materials with high supply risk, what is related to their use in batteries (UNION., 2020). According to WANG *et al*. (2020), due to the significant increase in world, copper consumption in the last 30 years it is estimated that there will be in a deficit of 600 k tonnes in 2021. In view of the high consumption of these metals, their recovery becomes even more essential because it adds value to POX effluent as well as reducing the negative environmental impact by meeting water quality standards, reducing solid waste and decreased demand for new raw materials.

In this context, some techniques are used to promote these metals recovery. One technique can be employed for this purpose is the electrodialysis (ED). ED is composed by a set of intercalated cationic (cation exchange membrane - CEM) and anionic membranes (anion exchange membranes - AEM) that form individual cells, delimited by two electrodes at the stack ends. The driving force required derives from a difference in the electric potential between the cells

(GALUCHI ., 2010). The membranes used in the ED are ion-selective, separating cations and anions that are present on the feed composition. What defines the permeation or retention of these chemical elements is their electrical charge and interaction with the membrane. Cationic membranes are contemplated by negatively charged groups in their polymer matrix; thus, it is permeable to the cations whereas it retains the negatively charged elements. Conversely, the membranes contemplated with a positive charge are called anionic, which repel positively charged elements but allow the negatively charged compounds permeation (BAKER., 2000). In this way, the feed entering the system by the central cell is subjected to an electrochemical separation, forming two different currents. One of them is the concentrate, constituted by the electrically charged compounds, and the other by the desalinated solution, absent or of lower ions concentration (SHETH and. NATH., 2018; ARAHMAN *et al*., 2017).

ED has become a promising alternative in the effluent's treatment due to its effectiveness and low energy expenditure compared to the classical MSPs. Scarazzato (2013) applied ED in the effluent generated during the metals galvanization and obtained 99.7% copper removal. Aiming for ions recovery from a coal mine acid drainage, Buzzi *et al*. (2011) applied ED and achieved 93% in electrical conductivity removal, which also achieved retention values of 97% for F^-, 98% for SO_4^{2-}, 99% for NO_3^-, Fe^{3+}, Cl^- and Na^+, while the other ions were > 99.9% retained.

Another technique that can be applied to metal recovery is the solvent extraction (SX) process, that consists in a shift in the equilibrium between the extractions and stripping stages. In order to consider the SX as an advantageous technology, it is necessary to develop viable process and economic techniques for the recovery of metals such as Cd^{2+}, Co^{2+}, Cu^{2+}, Cr^{2+}, Ni^{2+}, and Zn^{2+}, which are present in mixtures that also contains aluminum and iron, the latter considered to have a lower added value and, therefore, unwanted in most cases.

It is known that several parameters affect the recovery efficiency in the extraction process of metal ions, such as: composition, pH, extractor type and concentration, temperature, organic to aqueous ratio (O:A), among others (GUIMARÃES *et al*., 2014). The equilibrium pH dependence on the selective zinc, copper, iron, nickel and chromium recovery, all present in the real mix electroplating wastewater, was investigated by Kul and Oskay (2015) by varying the medium pH and considering different extractants. For zinc extraction, for example, pH values between 2.05 and 3.05 were tested observing the coextraction of Iron was when considering D2EHPA and Cyanex 272 as extractive agents. On the other hand, when considering the extractant 10 vol%

Aliquat 366, with two-stage extraction at equilibrium pH 1.50 and an organic and aqueous phase ratio of 1:1, 99.9% of the zinc in the wastewater was recovered with practically 100% selectivity. The stripping study results showed that two stages of stripping were necessary to successfully strip more than 99% of the zinc from the loaded organic using 2 mol L^{-1} NaOH at an O:A phase ratio of 1:1.

Moreover, considering the metals recovery from the mining acid effluent, the ion-exchange (IX) method stands out. According to KOŁODYŃSKA *et al*. (2014), the IX uses have been growing in recent years to remove metal ions from effluents from hydrometallurgical processes, mainly in acidic solutions.

The IX process consist of a chemical interaction between ions in a liquid phase and ions in a solid phase. Certain ions in the solution are preferentially sorbed onto the solid substrate, and because electroneutrality must be maintained, the solid substrate releases replacement ions back into the solution, this concept is shown in Fig. 5.1. The interactions involved in the IX process are stoichiometric, they obey the law of mass action and can be irreversible or reversible, the latter being more interesting because the IX can be reused many times (REYNOLDS and RICHARDS., 1977; HUBICKI and KOODYNSK., 2012).

In this sense, is important to highlight that, during the adsorption process, there is a combination of physical forces (physisorption), which is weaker, and the chemical force (chemisorption), that occurs through the electrons exchange or sharing between the adsorbate molecules and the adsorbent surface, resulting in a new chemical bond. It should be noted that although the concepts of chemisorption and physisorption are different, these two mechanisms are not completely independent. Moreover, the chemical adsorption is more specific and physical adsorption is unspecified and not located since it this type of adsorbent does note present active sites (DO NASCIMENTO *et al*., 2014).

The efficiency of this process depends on several factors, such as the adsorbent (resin) and the adsorbent (elements of interest) physical-chemical characteristics, as well the operational conditions. Among the adsorbent characteristics, stands out the surface area, pore size, functional groups and the material hydrophobicity. The adsorbate nature is linked to the polarity, the molecule size, the solubility and the fluid's pH. In addition, regarding operational conditions,

temperature and pH are highlighted (BONILLA-PETRICIOLET, MENDOZA-CASTILLO and REYNEL-ÁVILA., 2017).

It is also worth highlighting these operational parameters relevance, given that the temperature increment provides an increase of adsorbate molecules diffusion rate. This occurs because the temperature elevation corroborates the decrease in the solution viscosity that includes the elements of interest, which can contribute to the kinetic energy and these species mobility increase (DO NASCIMENTO *et al*., 2014; BONILLA-PETRICIOLET , MENDOZA-CASTILLO and REYNEL-ÁVILA., 2017) .The pH interferes in the adsorption efficiency since this parameter is related to the degree of chemical species distribution according to the adsorbent surface loads and functional groups, governing, therefore, the electrostatic interactions between this material and the elements of interest (BONILLA-PETRICIOLET, MENDOZA-CASTILLO and REYNEL-ÁVILA., 2017). This relationship is relevant to the adsorption process, since the adsorbent and adsorbate charges must be opposed so that the electrostatic interaction between these compounds is favored until equilibrium is reached, i.e., until the solute concentration, present in the liquid phase, remains constant. Therefore, if the charges are the same, the adsorption process will be impaired, since there will be electrostatic repulsion (DO NASCIMENTO *et al*., 2014).

Moreover, the ion-exchange advantages can be summarized as follows: (i) the treatment (sorption/desorption) occurs at room temperature and pressure; (ii) low toxicity risks (compared to solvent extraction); (iii) high load capacity (adsorption); (iv) high metal ions recovery and (v) applied commercially worldwide (KESIEME., 2015). In addition, the minerals industry has successfully used ion-exchange for the following reasons: (i) wastewater demineralization; (ii) metals recovery; (iii) acid recovery and (iv) polishing effluents (KESIEME., 2015).

The IX process was first described in 1850 as occurring naturally in aluminosilicates minerals, such as clays, ultramarines and aerolites (NIKOLOSKI and ANG., 2014; KUNIN., 1958; KICHENER., 1957; SIMON., 1991). Although these natural materials are relatively abundant, they had very low exchange capacity and decomposed irreversibly in acid solutions (NIKOLOSKI and ANG., 2014). IX started to become a viable processing option in 1944, when synthetic polymeric IX materials where introduced (ZAINOL., 2005).

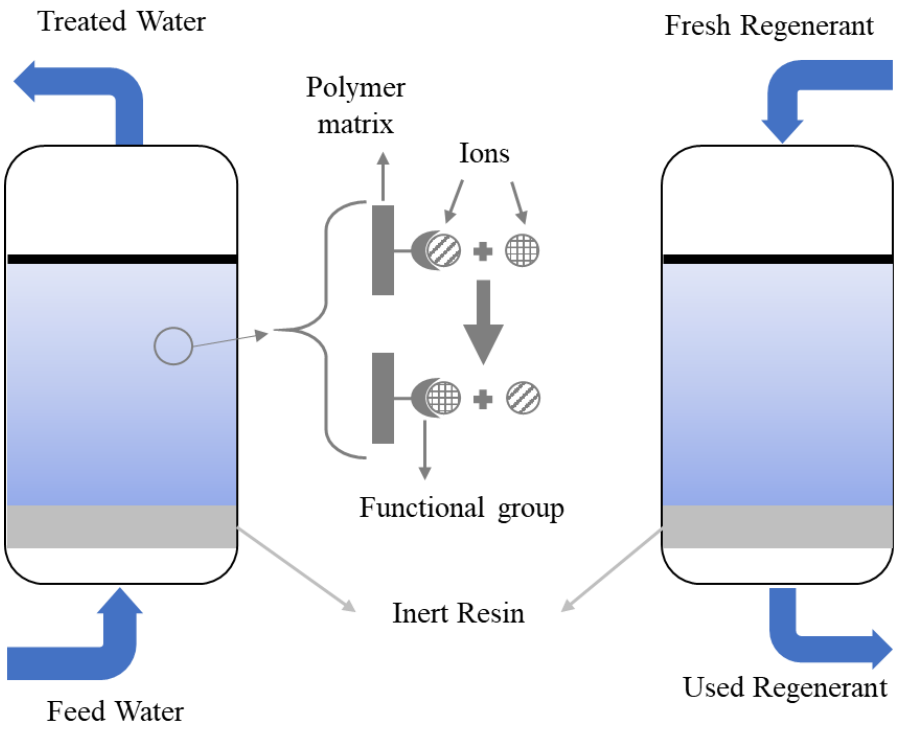

Figure 5.1 - A scheme for IX on resin operating in a counter-current configuration.

The Union of Soviet Socialist Republics, in the 1970s, applied IX resins instead of activated carbon to recover gold and silver from cyanide leach solutions (BOLINSKI and SHIRLEY., 1996). Even so, the IX resins had lower selectivity for the target metal ions and were generally smaller in particle size than activated carbon, making them not so attractive to the mining industry as they appeared more expensive and substantially more difficulty to handle (NIKOLOSKI and ANG., 2014).

Generally IX resins are manufactured in the spherical, stress and strain free form to resist physical degradation (HUBICKI and KOODYNSK., 2012). They are stable at high temperatures, applicable over a wide pH range, insoluble in water and in some organic solvents. They often consist of a cross-linked organic copolymers containing functional groups built into the matrix due to a chemical modification (CYGANOWSKI, JERMAKOWICZ-BARTKOWIAK and WILKOWSKI., 2013; SHERRINGTON., 1998).

The IX resins can be classified according to the functional groups attached to the polymer matrix and their dissociation capability. IX resins exchanging anions are called strong base or weak base anion exchangers, while IX resins exchanging cations are called strong acid or weak acid cation

exchangers (CYGANOWSKI, JERMAKOWICZ-BARTKOWIAK and WILKOWSKI., BESTER., 2012). There are other classifications which are more related to the chemical modification carried out for the introduction of specific functional groups on the resin surface, an example is the chelating resins.

Many process variations and resins properties adaptations have been made to suit different applications for these materials. Today, there are a large number of IX resins commercially available and these are used with for various purposes such as in water treatment, pharmaceutics and medicines, petroleum refining, chemical plants, hydrometallurgical separation and purification, isotope separation, biochemical production and the nuclear industry (ZAINOL., 2005; ZAGORODNI., 2007; LUCA, VLAD and BUNIA., 2009). A list containing some of the commercially available resins along with their properties is given in Table 5.1.

Table 5.1 - Different commercially available ion exchange resins and their physical and chemical characteristics

Functional group	Resin	Supplier	Type	Selectivity	Ionic-form shipped	Matrix	Structure	Bead Size (µm)	Bulk density (g/L)	Total capacity	Moisture retention (%)	Ref
Bis-Picolylamine	XUS43578	DOW, Germany	Chelating	n.a.	Sodium	Styrene-DVB	Macroporous	410	670	1.8 eq/L Na^+	40-60	EDEBALI and PEHLIVAN., 2016.
	Lewatit MonoPlus TP 220	Lanxess	Chelating	$Cu^{2+}>>Ni^{2+}>UO_2^{2+}>Fe^{3+}>Zn^{2+}>Co^{2+}>Cd^{2+}>Fe^{2+}$	Fully protonated	Cross linked polystyrene	Macroporous	615-625	690	29 g/L Cu^{2+}	48-60	LEWATIT-LENNTECH., 2019.
	Dowex® M4195	DOW, Germany	Chelating	$Cu^{2+}>>Ni^{2+}>U^{6+}>Fe^{3+}>Zn^{2+}>Co^{2+}>Cd^{2+}>Fe^{2+}$	Partially protonated	Styrene-DVB	Macroporous	300-850	673	35-42 g/L Cu^{2+}	40-60	DOWEX-LENNTECH., 2019.
Iminodiacetic acid	CR11	Mitsubishi, Japan	Chelating	n.a.	Sodium	Styrene-DVB	Macroporous	300-1180	730	n.a.	55-65	EDEBALI and PEHLIVAN., 2016.
	S930	Purolite, UK	Chelating	n.a.	Sodium	Styrene-DVB	Macroporous	425-1000	1130	2.9 eq/L Na^+	55-65	PUROLITE-LENNTECH., 2019.

	Amberlite™ IRC748	DOW, Germany	Chelating	$Fe^{3+}>Hg^{2+}>Cu^{2+}>Pb^{2+}>Ni^{2+}>Zn^{2+}>Cd^{2+}>Co^{2+}>Fe^{2+}>Mn^{2+}>Ca^{2+}>>Na^{+}$	Sodium	Styrene-DVB	Macroporous	500-650	750	1.35 eq/L Na^{+}	60-65	LENNTECH., 2019.
	Chelex-100	Bio-Rad Laboratories	Chelating	$Cu^{2+}>>Pb^{2+}>Fe^{3+}>Al^{3+}>Cr^{3+}>Ni^{2+}>Zn^{2+}>Ag^{+}>Co^{2+}>Cd^{2+}>Fe^{2+}>Mn^{2+}>Ba^{2+}>Ca^{2+}>>>Na^{+}$	Sodium	Styrene-DVB	Macroporous	300-1180	650	0.4 eq/L $Cu(NH_3)_4^{2-}$	n.a.	BIO-RAD., 2019.
	Lewatit TP 207	Lanxess	Chelating	$Cu^{2+}>VO^{2+}>UO_2^{2+}>Pb^{2+}>Ni^{2+}>Zn^{2+}>Cd^{2+}>Co^{2+}>Fe^{2+}>Be^{2+}>Mn^{2+}>>Ca^{2+}>Mg^{2+}>Sr^{2+}>Ba^{2+}>>>Na^{+}$	Sodium	Styrene-DVB	Macroporous	400-1250	720	2.2 eq/L Na^{+}	53-58	LANXESS., 2019.
	D-401	Suqing Group, China	Chelating	n.a.	Sodium	n.a.	Macroporous	400-1250	750	123.91 mg/g Cu^{2+}	52-58	SIU *et al.*, 2016; WONG *et al.*, 2014.
Sulfonic Acid	Dowex® HCR-W2	DOW, Germany	Strongly acidic	n.a.	Sodium	Styrene-DVB	Macroporous	420-1200	785	1.8 eq/L Na^{+}	48-54	EDEBALI and PEHLIVAN., 2016.
	C160	Purolite, UK	Strongly acidic	n.a.	Sodium	Styrene-DVB	Macroporous	300-1200	820-860	2.3 eq/L Na^{+}	35-40	EDEBALI and PEHLIVAN., 2016.

	Lewatit MonoPlus SP 112	Lanxess	Strongly acidic	n.a.	Fully protonated	Cross linked polystyrene	Macroporous	670	710	1.6 eq/L Na^+	56-60	LEWATIT-LENNTECH., 2019.
	Amberlite™ IRN77	DOW, Germany	Strongly acidic	n.a.	Fully protonated	Styrene-DVB	Macroporous	650	800	1.9 eq/L H^+	49-55	DOW., 2019.
Aminophosphonate	Amberlite™ IRC747	DOW, Germany	Chelating	$Pb^{2+}>Cu^{2+}>Zn^{2+}>Mg^{2+}>Ca^{2+}>Cd^{2+}>Ni^{2+}>Co^{2+}>Sr^{2+}>Ba^{2+}$	Sodium	Styrene-DVB	Macroporous	520-660	1100-1140	1.75 eq/L Na^+	64-69	LENNTECH., 2019.
Bis-(2,4,4-trimethylpentyl)-phosphinic acid	Lewatit TP 272	Lanxess	-	$Fe^{3+}>Zn^{2+}>Al^{3+}>Cu^{2+}>Co^{2+}>Mg^{2+}>Ca^{2+}>Ni^{2+}$	n.a.	Cross linked polystyrene	Macroporous	300-1600	530	12.5 g/L Zn^{2+}	28-35	LEWATIT-LENNTECH., 2019.
Tertiary amine	Amberlite™ IRA96	DOW, Germany	weakly basic	n.a.	Free base	Styrene-DVB	Macroporous	550-750	670	1.25 eq/L Na^+	57-63	LENNTECH., 2019.
Quaternary amine	Dowex® 1×8	DOW, Germany	strongly basic	n.a.	Chloride	Styrene-DVB	Fine mesh	75-37		1.2 eq/L Na^+	39-45	EDEBALI and PEHLIVAN., 2010

n.a. (Not available)

Many attempts have been made to engineer ion exchange resins with superior properties. The successful development of chelating resins, also known as complexing or specific ion resins, was considered a breakthrough because they have a greater selectivity for a particular ion or ions groups than conventional resins (NIKOLOSKI and ANG., 2014; ZAINOL., 2005). These types of IX resins adsorb metal ions through a combination of ionic and coordinating interactions instead of the simple electrostatic interactions in conventional cation or anion ion exchange (ZAINOL., 2005; EDEBALI and PEHLIVAN., 2016; HARLAND., 1994). The metals list which are recovered and purified on an industrial scale using ion-exchange include: chromium, uranium, thorium, nickel, rare earth elements, gold, platinum metals, copper, zinc, silver, cobalt and tungsten (HUBICKI and KOODYNSK., 2012). For comparison purposes, the results concerning the efficiency and sorption capacity obtained in different studies are presented in Table 5.2.

Table 5.2 - Comparison of different studies aiming metallic ions recovery by ion extraction process

Metallic Ion	Effluent	Resin	Functional Groups	Chemical type	pH	Sorption capacity / Removal efficiency	Ref.
Cu^{2+}	Single-metal ion solutions	Dow XUS43578, Dow Chemicals	Bis-Picolylamine	Chelating resin	1-5	166.29 mg/g	EDEBALI and PEHLIVAN., 2016.
	Single-metal ion solutions	Diaion CR11, Mitsubishi Chemical	Iminodiacetic acid	Chelating resin	1-5	167.38 mg/g	EDEBALI and PEHLIVAN., 2016.
	Single-metal ion solutions	Dowex® HCR W2, Lenntech	Sulfonic acid	Strongly acidic	1-5	166.99 mg/g	EDEBALI and PEHLIVAN., 2016.
	Single-metal ion solutions	Purolite C160, Purolite	Sulfonic acid	Strongly acidic	1-5	165.98 mg/g	EDEBALI and PEHLIVAN., 2016.
	Leach pulps of low-grade sulfide ores	Purolite S930	Iminodiacetic acid	Chelating resin	2.7-3	184.91 mg/g	KUZ'MIN and KUZ'MIN., 2014.
	Single-metal ion solutions	poly(glycidyl methacrylate) containing aspartate groups	Aspartate groups	Chelating resin	3-5	88.96 mg/g	CHEN, LIN and HSU., 2008.
	Single-metal ion solutions	110, Nankai University, China	Acid carboxylic	Weakly acidic	5.28	336.00 mg/g	JIA *et al.*, 2013.
	Single-metal ion solutions	Lewatit MonoPlus TP-220	Bis-Picolylamine	Chelating resin	2-4	9.12-9.98 mg/g	WOLOWICZ and HUBICKI., 2012.

	Single-metal ion solutions	Dowex® M4195	Bis-Picolylamine	Chelating resin	2-5	50.77 - 135.98 mg/g	GAO *et al*., 2013.
	Single-metal ion solutions	D-401	Iminodiacetic acid	Chelating resin	3.5	144.88 mg/g	SIU *et al*., 2016.
	Single-metal ion solutions	Amberlite™ IRC748	Iminodiacetic acid	Chelating resin	4.5	62.2 mg/g [a]	LIN, LI and JUANG., 2008.
Ni^{2+}	Leach pulps of low-grade sulfide ores	Purolite S930	Iminodiacetic acid	Chelating resin	2.7-3	154.95 mg/g	KUZ'MIN and KUZ'MIN., 2014.
	Single-metal ion solutions	Lewatit MonoPlus TP-220	Bis-Picolylamine	Chelating resin	2-4	4.68-6.24 mg/g	WOLOWICZ and HUBICKI., 2012.
	Single-metal ion solutions	Dowex® HCR S/S	Sulfonic acid	Strongly acidic	2-8	156.25 mg/g [a]	ALYÜZ and VELI., 2009.
	Laterite leach tailings	Lewatit MonoPlus TP-220	Bis-Picolylamine	Chelating resin	1.9-2-4	> 95%	LITTLEJOHN and VAUGHAN., 2013.
	Industrial tailings and synthetic pulp	Lewatit MonoPlus TP 207 XL	Iminodiacetic acid	Chelating resin	4	< 89%	LITTLEJOHN and VAUGHAN., 2014.
	Single-metal ion solutions	Amberlite™ IRC748	Iminodiacetic acid	Chelating resin	3-5	33.45 - 35.80 g/L	ZAINOL and NICOL., 2009.

Rinsing bath water from filter industry	Lewatit MonoPlus SP 112	Sulfonic acid	Strongly acidic	6	158.48 - 170.94 mg/g [a]	DIZGE, KESKINLER and BARLAS., 2009
Metal plating industry	Lewatit TP 207	Iminodiacetic acid	Chelating resin	6	1.24 mg/g	SILVA *et al*., 2008.
Synthetic nuclear power plant coolant water	Amberlite™ IRN77	Sulfonic Acid	Strongly acidic	2.75	15.00 mg/g	RENGARAJ *et al*., 2002.
Single-metal ion solutions	Amberlite™ IRC748	Iminodiacetic acid	Chelating resin	4.5	62.20 mg/g [a]	LIN, LI and JUANG., 2008.
Single-metal ion solutions	Ionac® SR-5R	Iminodiacetic acid	Chelating resin	1	73.37 mg/g [a]	MENDES and MARTINS., 2004.
Single-metal ion solutions	Dowex® M4195R	Bis-Picolylamine	Chelating resin	1	95.39 mg/g [a]	MENDES and MARTINS., 2004.
Single-metal ion solutions	Amberlite™ IRC748	Iminodiacetic acid	Chelating resin	4	73.50 mg/g [a]	MENDES and MARTINS., 2004.
Single-metal ion solutions	Purolite S930	Iminodiacetic acid	Chelating resin	1	117.40 mg/g [a]	MENDES and MARTINS., 2004.

Cd^{2+}	Single-metal ion solutions	poly(glycidyl methacrylate) containing aspartate groups	Aspartate groups	Chelating resin	3-5	143.89 mg/g	CHEN, LIN and HSU., 2008.
	Single-metal ion solutions	D-401	Iminodiacetic acid	Chelating resin	2.5-5	80.70-131.09 mg/g [a]	WONG *et al*., 2014.
Pd^{2+}	Single-metal ion solutions	Dowex® M4195	Bis-Picolylamine	Chelating resin	2-4	342.30 mg/g [a]	WOLOWICZ and HUBICKI., 2010.
	Single-metal ion solutions	Lewatit MonoPlus TP-220	Bis-Picolylamine	Chelating resin	2-4	9.44-9.93 mg/g [a]	WOLOWICZ and HUBICKI., 2012.
Cr^{3+}	Single-metal ion solutions	Chelex-100	Iminodiacetic acid	Chelating resin	4.5	14.98 mg/g [a]	GODE and PEHLIVAN., 2003.
	Single-metal ion solutions	Lewatit TP 207	Iminodiacetic acid	Chelating resin	4.5	17.72 mg/g [a]	GODE and PEHLIVAN., 2003.
	Industrial effluents	Amberlite™ IRC 748	Iminodiacetic acid	Chelating resin	2-6	23.37 mg/g [a]	CAVACO *et al*., 2009.
	Industrial effluents	Diaion CR 11	Iminodiacetic acid	Chelating resin	2-6	24.70 mg/g [a]	CAVACO *et al*., 2009.

	Industrial effluents	Diphonix	Diphosphonic and sulfonic acid	Strongly acidic	2-6	24.13 mg/g [a]	CAVACO *et al.*, 2009.
	Synthetic nuclear power plant coolant water	Amberlite™ IRN77	Sulfonic Acid	Strongly acidic	2.75	14 mg/g	RENGARAJ *et al.*, 2002.
Cr^{4+}	Single-metal ion solutions	Amberlite™ IRA96	Tertiary amine	weakly basic	1-3	1198.12 mg/g [a]	EDEBALI and PEHLIVAN., 2010.
	Single-metal ion solutions	Dowex® 1×8	Quaternary amine	strongly basic	1-4	1891.46 mg/g [a]	EDEBALI and PEHLIVAN., 2010.
Pt^{4+}	Single-metal ion solutions	Lewatit MonoPlus TP-220	Bis-Picolylamine	Chelating resin	2-4	963.8 mg/g [a]	WOLOWICZ and HUBICKI., 2012.
Au^{3+}	Single-metal ion solutions	Lewatit MonoPlus TP-220	Bis-Picolylamine	Chelating resin	2-4	9.84-9.96 mg/g	WOLOWICZ and HUBICKI., 2012.
Zn^{2+}	Single-metal ion solutions	Lewatit MonoPlus TP-220	Bis-Picolylamine	Chelating resin	2-4	1.96-9.49 mg/g	WOLOWICZ and HUBICKI., 2012.
	Single-metal ion solutions	Dowex® HCR S/S	Sulfonic acid	Strongly acidic	2-8	222.22 mg/g [a]	ALYÜZ and VELI., 2009.

	Single-metal ion solutions	Purolite C-100 MH	Sulfonic acid	Strongly acidic	6	46.08 - 64.10 mg/g [a]	ABDELWAHAB, AMIN and EL-ASHTOUKHY., 2013.
Co^{2+}	Single-metal ion solutions	Lewatit MonoPlus TP-220	Bis-Picolylamine	Chelating resin	2-4	9.12-9.98 mg/g	WOLOWICZ and HUBICKI., 2012.
	Laterite leach tailings	Lewatit MonoPlus TP-220	Bis-Picolylamine	Chelating resin	1.9-2.4	> 80%	LITTLEJOHN and VAUGHAN., 2013.
	Industrial tailings and synthetic pulp	Lewatit MonoPlus TP 207 XL	Iminodiacetic acid	Chelating resin	4	< 67%	LITTLEJOHN and VAUGHAN., 2014.
	Single-metal ion solutions	Lewatit TP272	Bis-(2,4,4-trimethylpentyl-)phosphinic acid	-	5.5	18 mg/g	VAUGHAN *et al.*, 2016.
	Single-metal ion solutions	Amberlite™ IRC748	Iminodiacetic acid	Chelating resin	3-5	27.10-35.35 g/L	ZAINOL and NICOL., 2009.
	Synthetic nuclear power plant coolant water	Amberlite™ IRN77	Sulfonic Acid	Strongly acidic	2.75	15 mg/g	RENGARAJ *et al.*, 2002.

Mg^{2+}	Single-metal ion solutions	Amberlite™ IRC748	Iminodiacetic acid	Chelating resin	3-5	6.81 - 13.37 g/L	ZAINOL and NICOL., 2009.
Mn^{2+}	Single-metal ion solutions	Amberlite™ IRC748	Iminodiacetic acid	Chelating resin	3	14.28 g/L	ZAINOL and NICOL., 2009.

[a]Langmuir maximum adsorption capacity

The Dowex M-4195 is very promising and has been used since the 1970s, when it was developed and has been used in commercial applications mainly to heavy metals adsorption. This resin presents a microporous structure with a polystyrene-divinylbenzene matrix and a weak basic chelation bispicolyl amine (bis (2-pyridylmethyl) amine) group (Diniz *et al*., 2005). Diniz *et al*. (2005) evaluated the adsorption of Pb^{+4}, Mn^{2+}, Cu^{2+}, Ni^{2+}, Co^{2+} and Fe^{2+}, from a manganese chloride leach solution using Dowex M-4195 achieving the metals affinity sequence: Cu^{2+}> Ni^{2+}> Pb^{4+}> Fe^{2+}> Co^{2+}> Mn^{2+}. Other relevant chelating resin is the Amberlite IRC747, that presents a macroporous structure whose contains aminophosphonic groups, which allow the formation of complexes with metal ions. The relative affinity of this resin for the various cations decreases in that order: Fe^{3+}> Pb^{2+}> Cu^{2+}> Zn^{2+}> Mg^{2+}> Ca^{2+}> Cd^{2+}> Ni^{2+}> Co^{2+}> Sr^{2+}> Ba^{2+} (SILVA *et al*., 2019). Fernández, Roeckel and Aspe (2014) evaluated the removal of copper and zinc using Amberlite IRC747 achieving a 0.025 meq /g of removal capacity and, moreover, they detected that this capacity does not depend on the solution's pH. Pang and Yung (2013) analyzed the nickel adsorption capacity, present in gold electroplating solutions, by Amberlite IRC747 resin and obtained ~98% of this metal recovery. On the other hand, the Amberlyst A26 OH presents a quaternary ammonium functional groups and its use is known for the paladium recovery from the acid solutions (WOŁOWICZ and HUBICKI., 2011).

However, it is important to stand out the fact that IX interactions involve the stoichiometric obeying the law of mass action (MOREIRA *et al*., 2021). Therefore, the adsorbent concentration increase contributes to improve the adsorption efficiency. In this context, the direct contact membrane distillation (DCMD) highlights, since this process uses the vapor pressure gradient as a driving force, which can be obtained by taking advantage of the residual heat from the POX effluent, generates two streams: permeate and the concentrate stream, which makes the integration between the DCMD and IX more attractive. Foureaux *et al.* (2021) proposed the treatment of POX effluent using DCMD and they obtained a distillate flux of 6.82 L/m^2 h and a permeate recovery grade of 33.91% with high values of metals retention >99% generating a permeate that can be used directly as an industrial reuse water in the mining plant. In this concentrate, the presence of high value-added metals due to their growing price and wide industrial applications, makes their recovery from this stream interesting (ULLOA *et al*., 2020).

Therefore, this study aims to promotes the POX effluent beneficiation by integrating membrane distillation (MD) and ion exchange (IX) process. The MD promotes the metals concentration

while produces reuse water. Cu^{2+}, Ni^{2+}, Co^{2+} recovery from MD concentrate was evaluated applying the Dowex M-4195 and the Amberlite IRC747, which are chelating resins and the Amberlyst A26 OH. In addition, this research will contribute to reduce the deficit of studies in relation to the DCMD's concentrate treatment using a real acid mining effluent.

5.2 MATERIALS AND METHODS

5.2.1 Wastewater sampling and MD concentrate generation

The POX wastewater was collected in the gold mining site, located in the state of Minas Gerais (Brazil). Once collected, the samples were stored at 4 °C and brought to room temperature prior to MD experiments. The concentrate was generated following the experimental conditions defined in a chapter 4. Briefly, the wastewater served as feed solution (2L) whereas distilled water (1L) was initially added in the distillate tank. The experiments were conducted using a commercial membrane (poly(tetrafluoroethylene) PTFE; provided by Sterlitech®) and spacer (CF042 Low Foulant Spacer, PTFE 31Mil – 0.787 mm; provided by Sterlitech®), with a feed and distillate temperature of 60 and 25 °C, respectively, and a recirculation flowrate of 0.3 L/min. These conditions resulted in an average distillate flux of 6.82 L/m²h and a recovery grade of approximately 34% (FOUREAUX *et al*., 2021). Raw effluent, MD concentrate and samples collected after ion exchange experiments were characterized according to the Standard Procedures for Water and Wastewater Examination (2017), as can be seen in (Table 5.3).

Table 5.3 - Raw wastewater and MD physico-chemical characteristics

Parameters	N° of Standard Methods 2017
pH	4500 B
Electrical conductivity (µS/cm)	2510 B
Iron (Fe^{2+}; mg/L)	
Magnesium (Mg^{2+}; mg/L)	
Nickel (Ni^{2+}; mg/L)	3111 B
Cobalt (Co^{2+}; mg/L)	
Copper (Cu^{2+}; mg/L)	
Aluminum (Al^{3+}; mg/L)	3111 D

5.2.2 Metals recovery by ion exchange

The potential for metals recovery was investigated for three different resins identified as (1) Amberlist™ A26, (2) Amberlite™ IRC 747 and (3) DOWEX™ M4195, all commercially available and kindly provided by the Dupont. The main characteristics of these resins can be seen in Table 5.4.

Table 5.4- Physical and chemical characteristics for the resins Dowex M4195, Amberlite IRC747 and Amberlyst A26

Functional group	Resin	Supplier	Type	Selectivity	Ionic-form shipped	Matrix	Structure	Bead Size (µm)	Bulk density (g/L)	Total capacity	Moisture retention (%)	Reference
Quaternary ammonium	Amberlyst A26	Dupont	Strongly basic	-	Hydroxide (OH)		Macroporous		41 lb/cu.ft	0.80 eq/L	45-65	DUPONT., 2020.
Aminophosphonate	Amberlite™ IRC747	Dupont	Chelating	$Pb^{2+}>Cu^{2+}>Zn^{2+}>Mg^{2+}>Ca^{2+}>Cd^{2+}>Ni^{2+}>Co^{2+}>Sr^{2+}>Ba^{2+}$	Sodium	Styrene-DVB	Macroporous	520-660	1100-1140	1.75 eq/L Na^{+}	64-69	LENNTECH., 2019.
Bis-Picolylamine	Dowex® M4195	Dupont	Chelating	$Cu^{2+}>>Ni^{2+}>U^{6+}>Fe^{3+}>Zn^{2+}>Co^{2+}>Cd^{2+}>Fe^{2+}$	Partially protonated	Styrene-DVB	Macroporous	300-850	673	35-42 g/L Cu^{2+}	40-60	DOWEX-LENNTECH., 2019.

Equilibrium assay were carried out in 250-mL erlenmeyers with 100 mL of MD concentrate containing different concentration of resin 1 – 8 g/L. The system was maintained under agitation (250 rpm, New Lab NL 01-11) and constant temperature (60 ^{o}C) during 24 h. Aliquots (1.5 mL) was collected at time intervals (1, 3, 5, 20, 30, 60, 120 and 180 minutes) and filtered using a 0.45 μm PVDF polar syringe filter.

For resin regeneration and metals recovery, three different solutions were investigated namely sulfuric acid (1 mol/L), ammonium hydroxide (1 mol/L) and hot water (60 ºC). These experiments were conducted in batch mode with 100 mL of regenerant, 8g/L of resin, at a contact time of 180 min and constant agitation (250 rpm).

5.2.3 Kinetic models

The ion exchange capacity (q_e) was calculated by Equation 5.1, where C_0 (mg.L^{-1}) is the initial ion concentration in solution; C_f (mg.L^{-1}) is the final ion concentration in solution; v (L) is the total volume used and m (mg) is the resin mass. The removal efficiency ($\%Removal$), expressed as a percentage, was calculated by Equation 5.2.

$$q_e = (C_0 - C_f).v/m \quad (5.1)$$

$$\%Removal = 100\,(C_0 - C_f)/C_i \quad (5.2)$$

After extraction, the resins were eluted by three different solutions: (i) water (60°C), (ii) sulfuric acid (H_2SO_4, 1 mol/L) and (iii) ammonium hydroxide (NH_4OH, 1 mol/L). The ions recovery was calculated considering the initial concentration of each ion in the MD concentrate.

The pseudo first order model of Lagergren (LAGERGREN., 1898) and the pseudo second order model of Ho and McKay (HO, MCKAY., 1999), were used to investigate the sorption kinetics. The Lagergren model is described by the Equation 5.3, where q_t (mg.g^{-1}) is the ion exchange capacity at a given time t (min), q_e (mg.g^{-1}) is the experimental ion exchange capacity at equilibrium, $q_{e,calc}$ is the theoretical value of ion exchange capacity at equilibrium (mg.g^{-1}) and k_1 (min^{-1}) the pseudo first order rate constant.

$$\ln(q_e - q_t) = \ln(q_{e,calc}) - k_1 t \quad (5.3)$$

Similarly, the model of Ho and McKay is described by Equation 5.4, where k_2 (g.mg^{-1}.min^{-1}) is the pseudo second order rate constant.

$$t/q_t = 1/(k_2 q_{e,calc}^2) + \left(1/q_{e,calc}\right)t \quad (5.4)$$

The graph of $\ln(q_e - q_t) - \ln(q_e)$ versus t allows estimating k_1 and the graph of t/q_t versus t allows estimating k_2 and $q_{e,calc}$.

5.2.4 Equilibrium isotherms

The equilibrium isotherms are curves that describe the distribution of metal ions between the liquid phase and the solid phase (Erdoğan *et al*. 2005). In this context, the Langmuir model is one of the most used equations to model the sorption of solutions at the solid/liquid interface (MENDES & MARTINS., 2004). This model considers that adsorption occurs on a homogeneous surface, forming monolayer, with defined number of active sites whose contain only one adsorbed molecule, where there is no interaction between adsorbed species. The Langmuir (LANGMUIR, 1918) isotherm is presented in Equation 5.5, where q_m (mg.g^{-1}) is the maximum theoretical value for the ion exchange capacity, C_e is the equilibrium concentration and k_l (L.mg^{-1}) is the Langmuir equilibrium constant. The degree of adsorption process development was evaluated by the separation factor (R_L) obtained through the Equation 5.6 (NASCIMENTO *et al.*, 2014). If 0 <R_L <1 adsorbate prefers the solid to the liquid phase and, consequently, the adsorption is favorable. When R_L> 1, there are indications that the adsorption is not favorable, since the solute prefers the phase has more preference for the liquid phase. R_L= 1 corresponds to a linear isotherm and R_L= 0 is related an Irreversible adsorption process (Erdoğan *et al*., 2005).

$$C_e/q_e = (1/k_l q_m) + (1/q_m)c_e \quad (5.5)$$

$$R_L = 1/(1 + k_l C_0) \quad (5.6)$$

Freundlich's isotherm proposes that adsorption occurs with the formation of multilayers (adsorption energies different) occurring the interaction between molecules. This model establishes the logarithmic correlation between the adsorption enthalpy and the adsorbate concentration. The adsorption energy decreases throughout this process with the increase in the resin surface coverage e by the adsorbate and this occurs due to the surface heterogeneity. The

Freundlich (FREUNDLICH., 1906) model is given by Equation 5.7, where k_f ($mg^{1-1/n}.L^{1/n}.g^{-1}$) and n are Freundlich equilibrium constants.

$$log\ q_e = log\ k_f + (1/n)\ log\ C_e \quad (5.7)$$

Another model used to investigate the adsorption process was proposed by Dubinin-Radushkevich (DUBININ., 1960) (Equation 5.8). The model allows the understanding of the average energy of adsorption (E) and the interactions involved in the process when correlating the parameter K_{DR}, obtained by the model, through the Equation 5.9:

$$\ln q_e = \ln q_s - K_{DR}[RT \ln(1 + 1/C_e)]^2 \quad (5.8)$$

$$E = 1/\sqrt{2K_{DR}} \quad (5.9)$$

Where q_s ($mg.g^{-1}$) is the theoretical isotherm saturation capacity, K_{DR} ($mol^2.kJ^{-2}$) is the Dubinin-Radushkevich isotherm constant, R (8.314 $J.mol^{-1}.K^{-1}$) is the ideal gas constant and T (K) the absolute temperature.

The last isotherm model evaluated was proposed by Temkin (TEMKIN, I., 1940) presented in Equation 5.10, in which A_t ($L.g^{-1}$) is the isotherm equilibrium binding constant and b ($J.mol^{-1}$) is Temkin's isotherm constant related to the adsorption heat.

$$q_e = (RT/b) \ln A_t + (RT/b) \ln C_e \quad (5.10)$$

5.3 THERMODYNAMIC PARAMETERS

In order to investigate the thermodynamic of the process, the parameters: Gibbs free energy change ($\Delta G°$), enthalpy change ($\Delta H°$) and entropy change ($\Delta S°$) were calculated using Equations 5.11 and 5.12 (KOUSHA *et al.*, 2012) where K_d (q_e/C_e) is the distribution coefficient. Experiments were conducted at different temperatures (30, 45 and 60 °C) once the optimal conditions of resin concentration and contact time were defined.

$$\Delta G^o = -RT\ ln\ K_d \quad (5.11)$$

$$ln\ K_d = \Delta S^o/R - \Delta\ H^o/RT \quad (5.12)$$

5.4 RESULTS AND DISCUSSION

Table 5.5 shows the concentrations of raw effluent and the DCMD's concentrate, which had an average concentration of Ni^{2+}, Cu^{2+} and Co^{2+} of 256.17, 259.60 and 50.4 mg/L, respectively, in accordance with what would be expected considering the recovery percentage of 33.91% and retention efficiency greater than 99% for these ions. In addition, the presence of unwanted metals stands out, whose recovery is not relevant because their low market value due to their abundance since the presence of several metals can interfere and cause competition with the metals of interest by the adsorption site. Among these unwanted metals, Fe^{2+}, Al^{3+} and Mg^{2+} stand out, which, presents high concentration.

Table 5.5- Concentration of raw effluent and DCMD concentrate

Parameters	Raw wastewater	MD concentrate
pH	1.37	1.19
Electrical conductivity (µS/cm)	16,808	25,627
Iron (Fe^{2+}; mg/L)	829.20	1,254.65
Magnesium (Mg^{2+}; mg/L)	2,662.10	4,027.95
Nickel (Ni^{2+}; mg/L)	169.30	256.17
Cobalt (Co^{2+}; mg/L)	33.07	50.04
Copper (Cu^{2+}; mg/L)	171.57	259.60
Aluminum (Al^{3+}; mg/L)	484.65	409.35

5.5 RESINS PERFORMANCE

The higher concentration compared to raw POX wastewater favors processes as IX that has the concentration gradient as driving force. From the three resins, Dowex-4195M achieved greater removal except for cobalt (Table 5.6), an element that was preferably adsorbed by Amberlite IRC 747. When it comes to the exchange capacity, the affinity of Dowex M-4195 for copper and nickel was confirmed ($q_{e,Cu}{}^{2+}$: 73.1 mg/g; $q_{e,Ni}{}^{2+}$: 42.4 mg/g), whereas Amberlite IRC 727 had higher affinity for cobalt ($q_{e,Co}{}^{2+}$: 61.8 mg/g).

The high selectivity observed for Dowex M4195 could be attributed to the fact that chelating resins, which are contemplated by nitrogen donor atoms presenting a tertiary amine, such as

bispicolyamine (bis-PMA), have a high affinity for divalent ions as Cu^{+2} and Ni^{+2} and selectivity in the presence of Na^{+}, K^{+}, Ca^{2+}, Mg^{2+} and Fe^{2+} even in extremely low pH conditions (ULLOA, BRINGAS and SAN-ROMÁN., 2020). The adsorption of Co^{2+} in the presence of Ni^{2+} and Cu^{2+} is reduced since occurs the competition for binding site by strong affinity with Cu^{2+} and Ni^{2+} (LENNTECH., 2019).These are interesting results that suggests the use of resin mixtures, in that case Dowex-4195M and Amberlite IRC 747, specially in continuous column experiments. In that case, it would be possible achieve great recoveries for all three elements.

For all the resins that were evaluated, the metals sorption efficiency increased when the adsorbent dose varied from 1 to 8 g/L, as can be seen in Table 5.6.

Table 5.6 - Efficiency of Cu^{2+}, Ni^{2+}, and Co^{2+} removal for each ion exchange resin. Results for the experiments with 1, 4 and 8g/L of resin, temperature of 60 °C and contact time of 24h

Metals	DCMD concentrate (mg/L)	1g/L			4g/L			8g/L		
		Amberlyst A26-OH (1)	**Aberlite IRC 747 (2)**	**Dowex M-4195 (3)**	**Amberlyst A26-OH (1)**	**Aberlite IRC 747 (2)**	**Dowex M-4195 (3)**	**Amberlyst A26-OH (1)**	**Aberlite IRC 747 (2)**	**Dowex M-4195 (3)**
Cu^{2+} Removal efficiency (%)	259.60	2.54	6.00	28.35	9.50	24.50	81.51	17.08	47.61	98.07
Ni^{2+} Removal efficiency (%)	256.17	9.44	6.31	8.66	32.86	25.84	33.64	49.25	52.37	57.06
Co^{2+} Removal efficiency (%)	50.04	9.07	2.88	3.10	33.05	11.27	12.10	21.04	55.24	23.06

This increase in removal efficiency compared to the increase in the adsorbent mass that were used was an expected result since the increase in resins concentrations implies in a greater surface area for interaction between the adsorbent and adsorbate, as well as active sites available for exchange, which ultimately favors the adsorption process (PEHLIVAN and ALTUN., 2006). Similar results have been reported by other authors that investigated IX for metals recovery. In this context, Nagib *et al*. (1999) and Lv *et al*. (2021) reported the Dowex M-4195 resin demonstrated a relevant ability in the removal of Cu^{2+} even under lower pH values as follows order of the selectivity: $Cu^{2+} > Ni^{2+} > Co^{2+}$.

5.6 EQUILIBRIUM STUDIES

The parameters obtained for the fitted isotherm models – Langmuir, Freundlich, Dubinin-Radushkevich and Temkin are presented in Table 5.7.

Table 5.7 - Isotherm parameters obtained for copper, nickel and cobalt adsorption into Dowex M-4195, Amberlyst A26-OH and Aberlite IRC 747. Experimental conditions: contact time of 24h and temperature of 60 °C

Ion	Isotherm	Parameter	Amberlyst A26-OH (1)	Aberlite IRC 747 (2)	Dowex M-4195 (3)
Copper (Cu^{2+})	Langmuir	q_m (mg/g)	15.85	48.54	75.19
		k_l (L/mg)	0.4650	0.0006	0.1496
		R_L (range)	0.01-0.02	0.86-0.88	0.03-0.57
		R^2	0.997	0.891	0.983
	Freundlich	k_f ($mg^{1-1/n}/L^{1/n}$.g)	19.02	0.05	385.92
		n	26.81	1.15	2.64
		R^2	0.213	0.997	0.699
	DR	K_{DR} (mol^2/kJ^2)	2400	4300	10
		q_s (mg/g)	304.1	383.9	96.8
		E (kJ/mol)	14.2	11.7	22.4
		R^2	0.980	0.997	0.869
	Temkin	b (kJ/mol)	7027.1	467.9	-46.3
		A_t (L/g)	0.012	0.014	0.003
		R^2	0.210	0.995	0.793
Nickel (Ni^{2+})	Langmuir	q_m (mg/g)	47.17	27.32	16.72
		k_l (L/mg)	0.005	0.019	0.166
		R_L (range)	0.48-0.64	0.18-0.31	0.02-0.04
		R^2	0.994	0.993	0.996
	Freundlich	k_f ($mg^{1-1/n}/L^{1/n}$.g)	1.09	5.38	12.53
		n	1.75	3.80	20.45

		R^2	0.990	0.914	0.401
	DR	K_{DR} (mol^2/kJ^2)	2100	1800	2300
		q_s (mg/g)	282.1	270.7	295.4
		E (kJ/mol)	15.4	16.7	14.7
		R^2	0.9707	0.9651	0.9786
	Temkin	b (kJ/mol)	217.1	472.2	3195.6
		A_t (L/g)	0.071	0.66	0.015
		R^2	0.997	0.921	0.395
Cobalt (Co^{2+})	Langmuir	q_m (mg/g)	65.23	65.23	2.09
		k_l (L/mg)	0.0051	0.0580	0.0585
		R_L (range)	0.81-0.89	0.26-0.31	0.26-0.31
		R^2	0.999	0.999	0.997
	Freundlich	k_f (mg$^{1-1/n}$/L$^{1/n}$.g)	1.04	0.48	0.48
		n	2.57	3.51	3.51
		R^2	0.989	0.992	0.981
	DR	K_{DR} (mol^2/kJ^2)	432	512	233
		q_s (mg/g)	2.6	72.3	72.3
		E (kJ/mol)	16.5	15.7	17.6
		R^2	0.968	0.996	0.996
	Temkin	b (kJ/mol)	1626.6	6286.1	6286.1
		A_t (L/g)	0.475	0.652	0.769
		R^2	0.995	0.994	0.983

The model that better fitted the adsorption of copper onto the Dowex M-4195 was the Langmuir (higher R^2), which suggests that this adsorption forms a monolayer onto the resins and that there is no interaction between the copper ions in the resin surface and each site comprising only one molecule (LEBRON *et al.*, 2018). Furthermore, the maximum sorption capacity of this model (75.19 mg/g) is in accordance with the experimental value found (83.13 mg/g). Another point that can be noticed is that the separation factor (R_L) was between zero and one, which suggests that the adsorbate prefers the solid phase to the liquid and thus the adsorption is said to be favorable (DO NASCIMENTO *et al.*, 2014). However, considering the Cu^{2+} adsorption applying the Aberlite, the best fitted model was the Freundlich isotherm, it possible indicates that adsorption occurs in a multilayer on heterogeneous surface. Moreover, this model establishes that a favorable adsorption tends to have a value of n (Freudlich's constant) between 1 and 10, which happened for Amberlite, that presented n = 1.15, which reinforces the Cu^{2+} interaction with the resin.

Regarding the adsorption of nickel and cobalt, the Dowex M-4195 resin and the Aberlite IRC 747 were the ones that that showed better performance, respectively. In both cases, the equilibrium data also better fitted the Langmuir model, suggesting the previously described implications. However, it is necessary to emphasize that although the Langmuir model has presented the best fit for these metals adsorption, it is noticed that other models have also presented adjustments greater than 0.98, which shows the adsorption processes complexity since they can be interpreted by different isotherms models.

Besides the better fitted models, the Dubinin–Radushkevich isotherm allows the understanding about the nature that is involved in the adsorption process as it considers the non-homogeneous surface of the resin. The mentioned model is commonly used to differentiate a physical from a chemical biosorption process by the E values obtained (DO NASCIMENTO *et al.*, 2014). For values smaller than 8 kJ/mol there is a predominance of physical interaction, while higher values suggest chemical interaction (MITROGIANNIS *et al.*, 2015). In cases, the E values suggests that chemical interactions are predominant. Furthermore, the high values of the constant related to the heat of adsorption in the Temkin model (b) reinforces the chemical interaction already indicated by the Dubinin–Radushkevich isotherm.

5.7 ION EXCHANGE KINETICS

The fitting results for pseudo-first and pseudo-second order for copper, nickel and cobalt adsorption are presented in Table 5.8. When these models are analyzed by means of their correlation coefficient, it is observed that the uptake of three elements are better described by a pseudo-second-order kinetics which confirms a process guided by chemical interactions. In addition to the proper adjustment (R^2>0.98) to the experimental data, the adsorption capacity calculated ($q_{e,calc}$) for the model was closely related to the experimental value ($q_{e,exp}$). In that case, the concentration of the species in the medium and over the resins surfaces affects the exchange reaction, being the adsorption capacity directly proportional to the number of active surface sites (RENGARAJ *et al*., 2007).

Table 5.8 - Pseudo-first order and pseudo-second order fitting for copper, nickel and the three different resins tested. Experimental conditions: contact time of 1 - 180 min, resin concentration of 8 g/L and temperature of 60°C

Element	**Models and parameters**		**The results regarding the**	**Aberlite IRC 747 (2)**	**Dowex M-4195 (3)**
Copper (Cu^{2+})	Pseudo-first order	k_1 (1/min)	0.0036	0.0126	0.0207
	parameters	$q_{e,calc}$ (mg/g)	5.49	4.35	12.35
		R^2	0.908	0.947	0.989
	Pseudo-second order	k_2 (g/mg.min)	0.0098	0.0167	0.0661
	parameters	$q_{e,calc}$ (mg/g)	22.96	20.86	31.26
		R^2	**0.988**	**0.998**	**0.997**
		$q_{e,exp}$ (mg/g)	23.75	20.92	30.91
Nickel (Ni^{2+})	Pseudo-first order	k_1 (1/min)	0.0045	0.0200	0.0138
	parameters	$q_{e,calc}$ (mg/g)	1.30	3.60	5.54
		R^2	0.475	0.908	0.945
	Pseudo-second order	k_2 (g/mg.min)	0.054	0.023	0.075
	parameters	$q_{e,calc}$ (mg/g)	19.84	19.53	24.33
		R^2	**0.999**	**0.999**	**0.999**
		$q_{e,exp}$ (mg/g)	19.73	19.77	24.42
Cobalt (Co^{2+})		k_1 (1/min)	0.028	0.014	0.008

Pseudo-first order	$q_{e,calc}$ (mg/g)	1.51	0.87	1.00
parameters	R^2	0.902	0.939	0.847
Pseudo-second order	k_2 (g/mg.min)	0.0594	0.0838	0.0621
parameters	$q_{e,calc}$ (mg/g)	4.04	3.49	4.05
	R^2	**0.997**	**0.997**	**0.995**
	$q_{e,exp}$ (mg/g)	3.99	3.49	4.11

Among the three resins, Dowex M4195 presented a better performance for copper and nickel uptake, whereas for cobalt the resin that showed the greatest affinity was the Aberlite IRC 747. For these resins, the pseudo-second order rate constant (k_2) was greater for copper, nickel and ultimately cobalt, same order of concentration that they appear in the DCMD concentrate, which reinforces the dependence on the ion exchange process on the initial concentration of these metals. The plateau observed in Figure 5.2 (a,b and c) reveals that, for copper and nickel, a contact time of 180 min was sufficient to ensure that the equilibrium was reached. Despite the lower adsorption capacity observed for cobalt, the equilibrium for this element was achieved right after 60 min of reaction time regardless of the resin. This lower contact time represents an advantage compared to the other two elements copper and nickel.

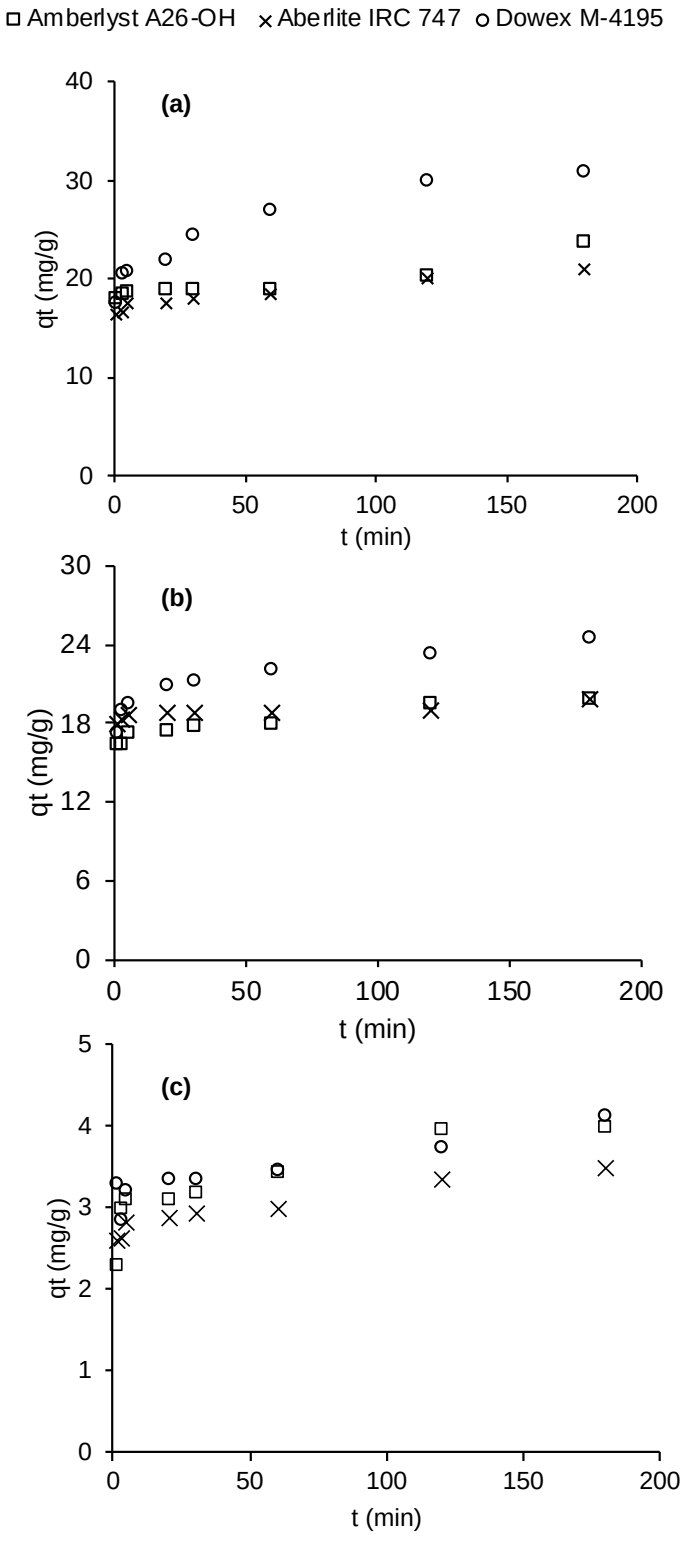

Figure 5.2 - Adsorption capacity along experimental time for (a) copper, (b) nickel and (c) cobalt for the different resins tested. Experimental conditions: contact time of 1 - 180 min, resin concentration of 8 g/L and temperature of 60 °C.

5.8 THERMODYNAMIC STUDIES

The results for the experiments at different temperature, along the thermodynamic parameters related to each resin and metal ion, are presented in Table 5.9. For comparison purposes, the adsorption capacities for nickel, copper and cobalt at different temperatures and resins were presented in Figure 5.3. It may be noticed that as the temperature decrease from 60 to 30ºC the ion exchange processes are disfavored regardless of the resin. The fact could be better observed in Figure 5.3, in which a visible trend for lower adsorption capacities is noticed at lower temperature conditions. For copper and nickel and the resin Dowex M4195, the one with a better performance for these ions' recovery, the adsorption capacity decreased form 30.8 – 30.1 mg/g and 16.5 – 11.3 mg/g when the temperature varied from 60 to 30 ºC, respectively. For cobalt and the resin Aberlite IRC 747, the adsorption capacity decreased from 1.6 – 0.5 mg/g for the same temperature range.

Another indicative to an unfavorable process at lower temperature conditions is the increase in Gibbs free energy change along the decrease in medium temperature (Table 5.9), as well as the positive enthalpy values that classified the exchange processes as endothermic. Meanwhile, the positive value of $\Delta S°$ indicated an increase in randomness at the aqueous-solid interface during the exchange of copper, nickel and cobalt ions onto the active sites of the resins.

The implications from these results are favorable to the use of ion exchange resins for by-products recovery from the DCMD concentrate considering the high temperature that it is generated (60 ºC). Otherwise, a cooling stage would be required, implying in a higher operating cost.

Table 5.9. Thermodynamic parameters for the adsorption of copper, nickel, and cobalt for the different resins. Experimental conditions: contact time of 24 h, resin concentration of 8 g/L and temperature of 30 – 60 ºC

Resin	Temperature	ΔGº (kJ/mol)			ΔHº (kJ/mol)			ΔSº (kJ/mol.k)			R^2		
	(ºC)	Copper	Nickel	Cobalt	Copper	Nickel	Cobalt	Copper	Nickel	Cobalt	Copper	Nickel	Cobalt
Amebrlyst A26-OH	30	-5.6	-5.6	-5.8	-7.49	-60.82	-53.18	0.208	0.165	0.142	0.999	0.987	0.999
	45	-8.8	-8.7	-7.9									
	60	-11.8	-10.6	-10.1									
Amberlite IRC 747	30	-9.0	-8.9	-6.3	-5.05	-34.61	-76.88	0.124	0.077	0.212	0.999	0.991	0.999
	45	-10.9	-10.3	-9.4									
	60	-12.7	-11.2	-12.6									
Dowex M4195	30	-1.3	-5.6	-9.2	-10.62	-18.37	-36.44	0.039	0.038	0.082	0.995	0.999	0.998
	45	-1.8	-6.2	-10.3									
	60	-2.4	-6.7	-11.6									

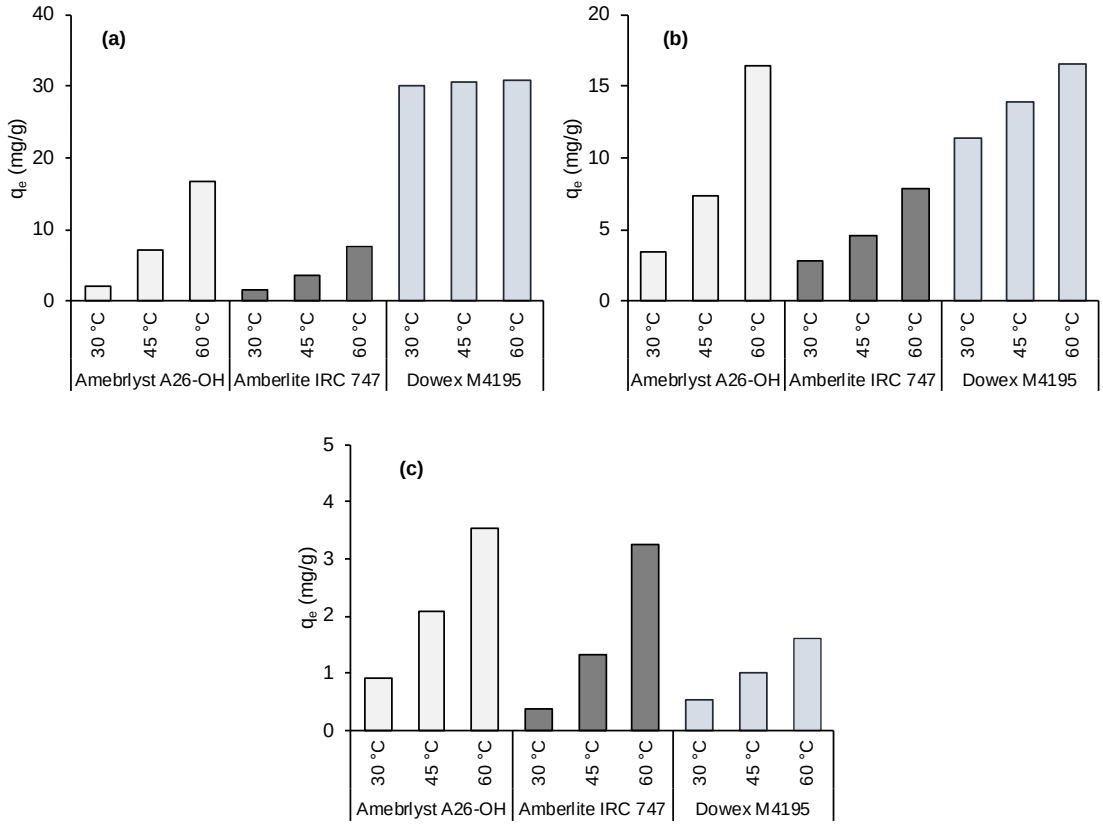

Figure 5.3 - Adsorption capacity for (a) copper , (b) nickel and (c) cobalt at different temperatures for the different resins. Experimental conditions: contact time of 24 h, resin concentration of 8 g/L and temperature of 30 – 60 °C.

When evaluating Figure 5.3, less temperature interference is perceived in the Dowex M4195 resin performance for copper removal. This low correlation was also noticed by Ajiboye et al. (2019), who reported that the increase in temperature from 25 ºC to 50 ºC has negligible effects on the copper adsorption.

5.9 METALS RECOVERY

The results regarding the recovery of the metals are presented in Table 5.10.

Table 5.10 - Recovery results for the three resins considering three different eluents. Experimental conditions: contact time of 3 h, resin concentration of 8 g/L, eluent concentration

of 1 mol/L (except for water) and temperature of 25 ºC (except for water, which experiments were conducted at 60 ºC)

Eluent	Metal	Recovery (%)		
		Amberlyst A26-OH (1)	**Aberlite IRC 747 (2)**	**Dowex M-4195 (3)**
H_2O at 60 ºC	Cu^{2+}	0.20	0.03	0.08
	Ni^{2+}	0.19	<0.01	0.20
	Co^{2+}	0.23	0.02	0.84
H_2SO_4	Cu^{2+}	0.19	<0.01	7.67
	Ni^{2+}	0.17	<0.01	14.68
	Co^{2+}	0.20	0.02	1.28
NH_4OH	Cu^{2+}	0.12	<0.01	<0.01
	Ni^{2+}	0.06	<0.01	11.24
	Co^{2+}	0.02	0.02	0.51

Considering the resin that was more efficient for the extraction of metals copper and nickel, the Dowex M-4195, the metal recovery was more efficient for the eluents H_2SO_4 (14.6%) and NH_4OH (11.24%), respectively.

It is noticed that the desorption was not efficient for the metals evaluated, resulting in low recovery grades. This may be associated with the fact that the eluent's contact time with the resin (180 min) was not sufficient. According to Kołodynska *et al*.(2014), in addition to the contact time, the pH and the presence of sulfate can interfere in the desorption process. They also reported that 1 M H_2SO_4 is not highly effective at eluting Cu^{2+} from Dowex M 4195.

For the cobalt, the resin that was most efficient in the extraction step, Amberlite IRC 747, exhibited low recoveries for this metal in all three eluting solutions used. It is evident then that the choice for the best resin should be guided not only by the extraction stage, but also in the elution stage. Considering this fact, it would be interesting to opt for the Dowex M-4195 resin to recovery cobalt, which, although did not exhibit the highest extraction efficiency, exhibits a good recovery efficiency.

When evaluating the adsorption (Table 5.6), it can be seen that, according to the isotherm model, which achieved the best fit, all metals showed greater affinity with the resin than with the solvent as can be observed considering the R_L between 0 and 1 for Languimiur and the n between 1 and 10 for the Freudlich isotherm. This fact interferes with the recovery of metals, since this characteristic can make desorption more difficult. In relation to the average adsorption energy, obtained by Dubinin-Radushke model, it can be seen that the adsorption processes are characterized as a chemical in nature, which are stronger, and therefore also contributed to the reduction of metal recovery. In addition, it is important to note that the adsorption kinetics was favorable to the connection between adsorbent and adsorbent, since the contact time to reach the equilibrium was short.

Because of its greater affinity with the solid phase, it is suggested for future studies that the chemical eluents concentrations, as well as the contact time with the adsorbent, be higher than those evaluated in the present work.

5.10 FINAL CONSIDERATIONS

The integration between DCMD and ion exchange by resins has shown promise in order to metals recovery, since the membrane separation process has allowed to increase these metals concentration and, consequently corroborates to the ion exchange efficiency. In addition, the effectiveness of the Cu^{2+}, Ni^{2+} and Co^{2+} sorption depends on concentration of the resins, since it was observed that the higher the resin quantity, the greater the adsorption capacity of these elements. Moreover, the interesting results of Cu^{2+} and Ni^{2+} adsorption by Dowex-4195M and the great Co^{2+} adsorption by Amberlite IRC 747 suggests the use of these resins mixtures, specially, in continuous column experiments. In that case, it would be possible to achieve great recoveries for all three elements. To increase the desorption efficiency, it is suggested to expand this process evaluation considering a longer contact time between resins and eluents, in addition to evaluating the combination of these eluents using, firstly, the sulfuric acid solution and, later, the solution of ammonium hydroxide in different concentrations.

6 CHAPTER 6

FINAL CONSIDERATIONS

6.1 FINAL CONSIDERATIONS

According to the results obtained in this study, it is clear that the integration of DCMD with ion exchange is promising in order to improve the effluent of POX through the recovery of two important by-products that make up this effluent: water and metals.

For the industrial reuse water generation, the direct contact membrane distillation proved to be promising. In this study, POX effluents with different characteristics were evaluated, which reinforced the robustness of the DCMD uses for several effluents that present similar characteristics to the POX effluent, which expands the possibility of this technique application. Although the recovery, that was achieved for the effluent that presented the highest contaminants concentrations, has not been elevated, the DCMD still interesting in economic terms, given that the residual heat from the POX effluent could be used as a driving force in the distillation. Therefore, it was unnecessary to include the feed's cooling step, which reduced the process energy demand, as well as making its operation simpler, also corroborating to this study first hypothesis. In addition, the permeate physical chemical quality was adequate for its application as an industrial reuse water, thus contributing to the reduction of the mining freshwater demand. However, in order to obtain DCMD's higher recovery grades, that is, to generate an even greater permeates volume without a decline in its quality, it is suggested to evaluate different membranes which are constitute by materials that are more resistant to this effluent characteristics (high acidity and temperature) thus delaying the membrane wetting.

It is also noteworthy that DCMD also results, inherently in the process, a stream whose contaminants concentration is higher than raw effluent, which makes it even more interesting to integrate this process with ionic exchange aiming the metals recovery, since this recovery is favored according to the adsorbate concentration. Furthermore, it was observed that the concentrate temperature (60 ºC) favored adsorption, confirming the initial hypothesis. Thus, it is also not necessary to adopt a cooling step in order to improve the interaction between adsorbent and adsorbate, which, consequently, contributes, economically, to this process integration.

The adsorption efficiency have had outstanding results for copper and nickel in Dowex resin and cobalt in Amberlite resin, which reinforces that the integration of membrane distillation followed by ion exchange is really promising. Although, being able to recover these metals and the resins

is essential for the adsorption process to be technically and economically viable and the operational conditions, that were proposed for the eluents in this study, were not enough efficient resulting in low percentage of metal recovery. In this sense, it is suggested to evaluate other conditions by increasing the chemical eluents concentration, as well as to evaluate a longer contact time between them and the resins to make the processes integration even more attractive.

It is essential to look for technologies that promote the circular economy to reduce environmental negative impacts and, consequently, improve our quality of life. The alternatives for more sustainable treatments must be increasingly studied and applied in order to achieve what the concept of sustainability advocates, guaranteeing economic development with less environmental degradation. These practices are motivated by stricter legislation and public awareness, that help to improve the adoption of these techniques by industries, which in addition to benefiting from environmental marketing, reduce their expenses through their processes by-products recovery.

7 CHAPTER 7

PRODUCTION

7.1 The published articles

FOUREAUX, A. F. S., LEBRON, Y. A. R., MOREIRA, V. R., GROSSI, L. B., SANTOS, L. V. S., & AMARAL, M. C. S. Technical and economic potential of high-temperature NF and DCMD for gold mining effluent reclamation. Chemical Engineering Research and Design, v. 162, p.149-161, 2020.

FOUREAUX, A. F. S., MOREIRA, V. R., LEBRON, Y. A. R., SANTOS, L. V. S., & AMARAL, M. C. S. Direct contact membrane distillation as an alternative to the conventional methods for value-added compounds recovery from acidic effluents: A review. Separation and Purification Technology, 236, 2020.

FOUREAUX, A. F. S., MOREIRA, V. R., LEBRON, Y. A. R., DE SOUZA SANTOS, L. V., & AMARAL, M. C. S. A sustainable solution for fresh-water demand in mining sectors: Process water reclamation from POX effluent by membrane distillation. Separation and Purification Technology, v. 256, 2021.

MOREIRA, V. R., LEBRON, Y. A. R., FOUREAUX, A. F. S., DE SOUZA SANTOS, L. V., & AMARAL, M. C. S. Acid and metal reclamation from mining effluents: current practices and future perspectives towards sustainability. Journal of Environmental Chemical Engineering, 2021.

Presententions

FOUREAUX, A. F. S.; LEBRON, Y. ; Moreira, V ; GROSSI, L. ; SANTOS, L. V. S. ; AMARAL, M. C. S. . Industrial reuse water generation from mining effluent applying reverse osmosis. 2019;

LEBRON, Y. ; MOREIRA, V. ; FOUREAUX, A. F. S. ; SANTOS, L. V. S. ; AMARAL, M. C. S. . Metals recovery from the pressure oxidation stage effluent via ion exchange resin. 2019;

MOREIRA, V. ; LEBRON, Y. ; FOUREAUX, A. F. S. ; SANTOS, L. V. S. ; AMARAL, M. C. S. . Metals Recovery From the Gold Pressure Oxidation Stage Effluent Using Solvent Extraction. 2019;

FOUREAUX, A. F. S.; Moreira, V ; ABNER, Y. ; SANTOS, L. V. S. ; AMARAL, M. C. S. . H2SO4 RECOVERY FROM THE GOLD MINING EFFLUENT BY DIRECT CONTACT MEMBRANE DISTILLATION. 2019;

ABNER, Y. ; FOUREAUX, A. F. S. ; Moreira, V ; SANTOS, L. V. S. ; AMARAL, M. C. S. . REUSE WATER GENERATION FROM THE POX EFFLUENT USING MEMBRANE DISTILLATION. 2019.

8 CHAPTER 8

REFERENCES

8.1 REFERENCES

ABBASI, P., MCKEVITT, B., DREISINGER, D.B. The kinetics of nickel recovery from ferrous containing solutions using an Iminodiacetic acid ion exchange resin, Hydrometallurgy, v. 175, p. 333–339, 2018.

AGRAWAL, A., KUMARI, S., RAY, B.C., SAHU, K.K. Extraction of acid and iron values from sulphate waste pickle liquor of a steel industry by solvent extraction route. *Hydrometallurgy*., v. 88, p. 58–66, 2007.

AGUIAR, A.O.; ANDRADE, L.H.; RICCI, B.C.; PIRES, W.L.; MIRANDA, G.A.; AMARAL, M.C.S. Gold acid mine drainage treatment by membrane separation processes: An evaluation of the main operational conditions. *Sep. Purif. Technol*, v. 170, 2016.

AJIBOYE, A. E.; OLASHINDE, F. E.; ADEBAYO, O. A.; AJAYI, O. Recovery of copper and nickel from polymetallic sulphate leach solution of printed circuit boards using Dowex M 4195. *Physicochemical Problems of Mineral Processing*,v. 55, 2019.

AKCIL, A.; KOLDAS, S. Acid Mine Drainage (AMD): causes, treatment and case studies. *Journal of Cleaner Production*, v.*14*, p. 1139-1145, 2006.

ALI, A., MACEDONIO, F., DRIOLI, E., ALJLIL, S., ALHARBI, O.A. Experimental and theoretical evaluation of temperature polarization phenomenon in direct contact membrane distillation. *Chem. Eng. Res*. Des., v. 91, p. 1966–1977, 2013.

ALKHUDHIRI, A.; DARWISH, N.; HILAL, N. Membrane distillation: A comprehensive review. *Desalination*, v. 287, p. 2–18, 2012.

ALKHUDHIRI, A.; HILAL, N. Membrane distillation—Principles, applications, configurations, design, and implementation. In: EMERGING TECHNOLOGIES FOR SUSTAINABLE DESALINATION HANDBOOK, 55-106., 2018, USA.

AL MAMUN, M.A.; BHATTACHARJEE, S.; PERNITSKY, D.; SADRZADEH, M. Colloidal fouling of nanofiltration membranes: Development of a standard operating procedure. *Membranes (Basel)*, v. 7, 2017.

ALKLAIBI, A.M.; LIOR, N. Membrane-distillation desalination: Status and potential. *Desalination*, v. 171, p. 111–131, 2005.

AL-OBAIDANI, S.; CURCIO, E.; MACEDONIO, F.; DI PROFIO, G.; AL-HINAI, H.; DRIOLI, E. Potential of membrane distillation in seawater desalination: Thermal efficiency, sensitivity study and cost estimation. *J. Memb. Sci.*, v. 323, p. 85–98, 2008.

ALWATBAN, A.M., ALSHWAIREKH, A.M., ALQSAIR, U.F., ALGHAFIS, A.A., OZTEKIN, A. Performance improvements by embedded spacer in direct contact membrane distillation – Computational study. Desalination, v. 470, p. 114103, 2019

AMARAL, M.C.S.; GROSSI, L.B.; RAMOS, R.L.; RICCI, B.C.; ANDRADE, L.H. Integrated UF–NF–RO route for gold mining effluent treatment: From bench-scale to pilot-scale. Desalination, v. 440, p. 111–121, 2018.

ANDRADE, L.H.; AGUIAR, A.O.; PIRES, W.L.; MIRANDA, G.A.; TEIXEIRA, L.P.T.; ALMEIDA, G.C.C.; AMARAL, M.C.S. NANOFILTRATION AND REVERSE OSMOSIS APPLIED TO GOLD MINING EFFLUENT TREATMENT AND REUSE. *Brazilian J. Chem. Eng*., v. 34, 2017.

ANM. Agência Nacional de Mineração. Anuário Mineral Brasileiro: Principais Substâncias Metálicas. Brasília, 2020. 35 p.

APHA, 2017. Standard methods for the examination of water and wastewater. 21. ed. Washington, D.C.

ARAHMAN N.; MULYATI, S.; LUBIS, M.R.; TAKAGI, R.; MATSUYAMA, H. Removal profile of sulfate ion from mix ion solution with different type and configuration of anion exchange membrane in elctrodialysis, *J. Water Process Eng*. v. 20, p.173–179, 2017.

ARSÈNE-PLOETZE, F.; CHIBOUB, O.; LIÈVREMONT, D.; FARASIN, J.; FREEL, K.C.; FOUTEAU, S.; BARBE, V. Adaptation in toxic environments: comparative genomics of loci carrying antibiotic resistance genes derived from acid mine drainage waters. *Environ. Sci. Pollut. Res*., v. 25, p. 1470–1483, 2018.

ASHOOR, B.B.; MANSOUR, S.; GIWA, A.; DUFOUR, V.; HASAN, S.W. Principles and applications of direct contact membrane distillation (DCMD): A comprehensive review. *Desalination*, v. 398, p. 222–246, 2016.

BAKER, J.S.; DUDLEY, L.Y. Biofouling in membrane systems — A review, *Desalination*. v. 118, p. 81–89, 1998.

BAKER, R.W. Membrane Technology. *Kirk-othmer encycl. chem. technol*. Hoboken, NJ, USA.: John Wiley & Sons, inc., 2000. v. 4.

BANAT, F.; JWAIED, N. Autonomous Membrane Distillation Pilot Plant Unit Driven Solar Energy: Experiences and Lessons Learned. *Int. J. Sustain. Water Environ. Syst.*, v. 1, p. 21–24, 2010.

BENÍTEZ, F.J.; ACERO, J.L.; LEAL, A.I. Application of microfiltration and ultrafiltration processes to cork processing wastewaters and assessment of the membrane fouling. *Sep. Purif. Technol.*, v. 50, p. 354–364, 2006.

BERGER, M., FINKBEINER, M. Water Footprinting: How to Address Water Use in Life Cycle Assessment?. Sustainability, v. 2, p. 919–944, 2010.

BINIAZ, P.; TORABI ARDEKANI, N.; MAKAREM, M.; RAHIMPOUR, M. Water and Wastewater Treatment Systems by Novel Integrated Membrane Distillation (MD). *ChemEngineering*, v. 3, p. 8, 2019.

BOGLER, A., LIN, S., BAR-ZEEV, E. Biofouling of membrane distillation, forward osmosis and pressure retarded osmosis: Principles, impacts and future directions. J. Memb. Sci., v. 542, p. 378–398, 2017.

BONDY, S.C. Low levels of aluminum can lead to behavioral and morphological changes associated with Alzheimer's disease and age-related neurodegeneration. *Neurotoxicology*, v. 52, p. 222–229, 2016.

BORMA, L. S.; SOARES, P.S.M. *Extração de ouro: princípios, tecnologia e meio ambiente.* Rio de Janeiro, Brazil: CETEM/MCT (Ed.), 2002. 344 p.

BUFFLE, J.; WILKINSON, K.J.; STOLL, S.; FILELLA, M.; ZHANG, J. A Generalized Description of Aquatic Colloidal Interactions: The Three-colloidal Component Approach. *Environ. Sci. Technol.*, v. 32, p. 2887–2899, 1998.

BUZZI, D.C.; VIEGAS, L.S.; SILVAS, F.P.C.; RODRIGUES, M.A.S.; ESPINOSA; D.C.R., SCHNEIDER; I.A.H., BERNARDES, TENÓRIO, A.M., J.A.S. Treatment of Acid Mine Drainage by Electrodialysis, in: Suppl. Proc., John Wiley & Sons, Inc., Hoboken, NJ, USA, 2011:

BUZZI, D.C.; VIEGAS, L.S.; RODRIGUES, M.A.S.; BERNARDES, A.M.; TENÓRIO, Water recovery from acid mine drainage by electrodialysis. *Miner. Eng.*, v. 40, p. 82–89, 2013.

CAMACHO, L. M.; DUMÉE, L.; ZHANG, J.; LI, J. D., DUKE, M.; GOMEZ, J.; GRAY, S. Advances in membrane distillation for water desalination and purification applications. *Water*, v. 5, n. 1, p. 94-196, 2013.

CARSON, B.L.; ELLIS, H. V.; MCCANN, J.L. Toxicology biological monitoring of metals in humans: Including feasibility and need. *CRC Press*, 2018.

CASTAÑO, A.; LUFIN, M.; ATIENZA, M. A structural path analysis of Chilean mining linkages between 1995 and 2011. What are the channels through which extractive activity affects the economy?, *Resources Policy*, v. 60, p. 106–117, 2019.

CHAMORRO, S.; BARATA, C.; PIÑA, B.; CASADO, M.; SCHWARZ, A.; SÁEZ, K.; VIDAL, G. Toxicological Analysis of Acid Mine Drainage by Water Quality and Land Use Bioassays. *Mine Water Environ*., v. 37, p. 88–97, 2018.

CHANG, E.-E.; YANG, S.-Y.; HUANG, C.-P.; LIANG, C.-H.; CHIANG, P.-C. Assessing the fouling mechanisms of high-pressure nanofiltration membrane using the modified Hermia model and the resistance-in-series model. *Sep. Purif. Technol.*, v. 79, p. 329–336, 2011.

CHEIRA, M. F.; ATIA, B. M.; KOURAIM, M. N. Uranium (VI) recovery from acidic leach liquor by Ambersep 920U SO4 resin: Kinetic, equilibrium and thermodynamic studies. Journal of radiation research and applied sciences, v. 10, n. 4, p. 307-319, 2017.

CHEN, T.; YAN, B.; LEI, C.; XIAO, X. Pollution control and metal resource recovery for acid mine drainage. *Hydrometallurgy*., v. 147–148, p. 112–119, 2014.

CHEN, Y.; ZHENG, R.; WANG, J.; LIU, Y.; WANG, Y.; LI, X.-M.; HE, T. Laminated PTFE membranes to enhance the performance in direct contact membrane distillation for high salinity solution. *Desalination*, v. 424, p. 140–148, 2017.

CIMINELLI, V.S.T.; DIAS, A.; BRAGA, H.C. Simultaneous production of impurity-free water and magnetite from steel pickling liquors by microwave-hydrothermal processing. *Hydrometallurgy.*, v. 84, p. 37–42, 2006.

CONAMA.Conselho Nacional do Meio Ambiente. *Conama 357*, Brazil, 2005.

COUTO, C.F.; MORAVIA, W.G.; AMARAL, M.C.S. Integration of microfiltration and nanofiltration to promote textile effluent reuse. *Clean Technol. Environ. Policy 19*, p. 2057–2073, 2017.

CSICSOVSZKI, G.; KÉKESI, T.; TÖRÖK, T.I. Selective recovery of Zn and Fe from spent pickling solutions by the combination of anion exchange and membrane electrowinning techniques. *Hydrometallurgy*., v. 77, p. 19–28, 2005.

CUI, R.-F., HU, M.-C., JIN, L.-H., LI, S.-N., JIANG, Y.-C., XIA, S.-P. Activity coefficients of rubidium chloride and cesium chloride in methanol–water mixtures and a comparative study of Pitzer and Pitzer–Simonson–Clegg models (298.15K). Fluid Phase Equilib., v. 251, p. 137–144, 2007.

CURCIO, E.; DRIOLI, E. Membrane Distillation and Related Operations—A Review. *Sep. Purif. Rev.,* v. 34, p. 35–86, 2005.

DENICOLA D.M.; STAPLETON, M.G. Impact of acid mine drainage on benthic communities in streams: the relative roles of substratum vs. aqueous effects. *Environ. Pollut*., v. 119, p. 303–315, 2002.

DENICOLA, D.M.; STAPLETON, M.G. Using macroinvertebrates to assess ecological integrity of streams remediated for acid mine drainage. *Restor. Ecol*., v. 24, p. 656–667, 2016.

DHAR, R.K., ZHENG, Y., RUBENSTONE, J., VAN GEEN, A. A rapid colorimetric method for measuring arsenic concentrations in groundwater. Anal. Chim. Acta, v. 526, p. 203–209, 2004.

DINIZ, C. V.; CIMINELLI, V. S.; DOYLE, F. M. The use of the chelating resin Dowex M-4195 in the adsorption of selected heavy metal ions from manganese solutions. Hydrometallurgy, v. 78, n. 3-4, p. 147-155, 2005.

DOW, N.; GRAY, S.; LI, J.; ZHANG, J.; OSTARCEVIC, E.; LIUBINAS, A.; ATHERTON, P.; ROESZLER, G.; GIBBS, A.; DUKE, M. Pilot trial of membrane distillation driven by low grade waste heat: Membrane fouling and energy assessment. *Desalination*, v. 391, p. 30–42, 2016.

DOW, N.; GRAY, S.; LI, J. D.; ZHANG, J.; OSTARCEVIC, E.; LIUBINAS, A.; DUKE, M. Power station water recycling using membrane distillation-A Plant trial. In: OZWATER'12. AUSTRALIAN WATER ASSOCIATION SYDNEY, 2012, Australia.

DOW, N.; VILLALOBOS GARCÍA, J.; NIADOO, L.; MILNE, L.; ZHANG, J.; GRAY, S.; DUKE, M. Demonstration of membrane distillation on textile waste water: assessment of long term performance, membrane cleaning and waste heat integration. *Environ. Sci. Water Res. Technol.*, v. 3, p. 433–449, 2017.

DOWEX-LENNTECH. Product information: Dowex® M4195, (2019). https://www.lenntech.com/Data-sheets/Dowex-M-4195-L.pdf (accessed January 9, 2019).

DRIOLI, E.; ALI, A.; MACEDONIO, F. Membrane distillation: Recent developments and perspectives. *Desalination*, v. 356, p. 56–84, 2015.

DUBININ, M. M. The Potential Theory of Adsorption of Gases and Vapors for Adsorbents with Energetically Nonuniform Surfaces. *Chemical Reviews*, v. 60, n. 2, p. 235–241, abr. 1960.

DUMÉE, L.F.; SEARS, K.; SCHÜTZ, J.; FINN, N.; HUYNH, C.; HAWKINS, S.; DUKE, M.; GRAY, S. Characterization and evaluation of carbon nanotube Bucky-Paper membranes for direct contact membrane distillation. *J. Memb. Sci.*, v. 351, p. 36–43, 2010.

DUMÉE, L.F.; SEARS, K.; SCHÜTZ, J.; FINN, N.; HUYNH, C.; HAWKINS, S.; DUKE, M.; GRAY, S. Characterization and evaluation of carbon nanotube Bucky-Paper membranes for direct contact membrane distillation. *J. Memb. Sci.*, v. 351, p. 36–43, 2010.

DUPONT, 2019a. NF90 Nanofiltration Elements for Commercial Systems.

DUPONT, 2019b. Specialty Membrane XUS290508 and XUS290504 Nanofiltration Elements.

ENVIRONMENTAL, L. Treatment of sulphate in mine effluents. In: INTERNATIONAL NETWORK FOR ACID PREVENTION, 2003, Utah.

ERAMET. Annual reference document 2019. Eramet Group, Abril 2020. França, Paris. Disponível em: < http://eramet.com/sites/default/files/2020-04/Eramet-2019-Universal-Registration-Document.pdf >. Accessed : jan. 2021.

ERDOĞAN, S.; ÖNAL, Y.; AKMIL-BAŞAR, C.; BILMEZ-ERDEMOĞLU, S.; SARICI-ÖZDEMIR, Ç.; KÖSEOĞLU, E.; İÇDUYGU, G. Optimization of nickel adsorption from aqueous solution by using activated carbon prepared from waste apricot by chemical activation. *Appl. Surf. Sci.*, v. 252, p. 1324–1331, 2005.

EYKENS, L.; REYNS, T.; DE SITTER, K.; DOTREMONT, C.; PINOY, L.; VAN DER BRUGGEN, B. How to select a membrane distillation configuration? Process conditions and membrane influence unraveled. *Desalination*, v. 399, p. 105–115, 2016.

FENG, X.; WU, P.; JIANG, L.Y. Titanium white waste acid concentration by DCMD: Wetting, crystallization, and fouling. *Desalination*, v. 440, p. 161–174, 2018.

FERNÁNDEZ, K.; ROECKEL, M.; ASPE, E. Heavy metals removal from influents to prevent mortality in salmon fry. Aquacultural engineering, v. 58, p.103-106, 2014.

FOUREAUX, A.F.S.; REIS, E.O.; LEBRON, Y.; MOREIRA,V.; SANTOS, L. V.; AMARAL, M.S.; LANGE, L.C. Rejection of pharmaceutical compounds from surface water by nanofiltration and reverse osmosis. *Sep. Purif. Technol*., v. 212, 2019.

FOUREAUX, A.F.S.; MOREIRA, V.R.; LEBRON, Y.A.R.; SANTOS, L.V.S.; AMARAL, M.C.S. Direct contact membrane distillation as an alternative to the conventional methods for value-added compounds recovery from acidic effluents: A review. Sep. Purif. Technol., v. 236, p. 116-251, 2020.

FOUREAUX, A. F. S.; MOREIRA, V. R.; LEBRON, Y. A. R.; DE SOUZA SANTOS, L. V.; AMARAL, M. C. S. A sustainable solution for fresh-water demand in mining sectors: Process water reclamation from POX effluent by membrane distillation. Separation and Purification, v.256, 2021.

FRASER, K. S., WALTON, R. H., WELLS, J. A. (1991). Processing of refractory gold ores. Minerals Engineering,v. 4, n. 4, p. 1029-1041, 1991.

FREUNDLICH, H. M. F. Over the Adsorption in Solution. *The Journal of Physical Chemistry*, 1906.

FU, X.; BEATTY, D. N.; GAUSTAD, G. G.; CEDER, G.; ROTH, R.; KIRCHAIN, R. E.; OLIVETTI, E. A. Perspectives on Cobalt Supply through 2030 in the Face of Changing Demand. Environmental Science & Technology, v. 54, n. 5, 2985-2993, 2020.

GALUCHI, T.P.D. Montagem e caracterização de unidade de eletrodiálise em escala de laboratório para tratamento de soluções salinas., Universidade de São Paulo, 2010.

GE, J., PENG, Y., LI, Z., CHEN, P., WANG, S. Membrane fouling and wetting in a DCMD process for RO brine concentration. Desalination, v. 344, p. 97–107, 2014.

GEISE, G.M.; PAUL, D.R.; FREEMAN, B.D. Fundamental water and salt transport properties of polymeric materials. *Prog. Polym. Sci*., v. 39, p. 1–24, 2014.

GHERNAOUT, D.; ELBOUGHDIRI, N.; AL ARNI, S. Water Reuse (WR): Dares, Restrictions, and Trends, Salah Al Arni. Water Reuse Dares, Restrict. Trends. Appl. Eng., v. 3, p. 159–170, 2019.

GONÇALVES, L.V., *Qualidade da água em lagos de mineração - estudos de caso: águas claras e riacho dos machados.* Dissertation (Master's degree in Sanitation, Environment and Water Resources) – School of Engineering, Federal University of Minas Gerais, Belo Horizonte, 2013.

GOYAL, S.; ROUTROY, S.; SHAH, H. Measuring the environmental sustainability of supply chain for Indian steel industry. *Business Process Management Journal*, 2018.

GRANDE, J.A.; SANTISTEBAN, M.; DE LA TORRE, M.L.; J.M. DÁVILA, M.L.; PÉREZ-OSTALÉ, E. Map of impact by acid mine drainage in the river network of The Iberian Pyrite

Belt (Sw Spain). *Chemosphere*, v. 19, p. 269–277, 2018.

GRAY, N.F. Environmental impact and remediation of acid mine drainage: a management problem, *Environ. Geol.*, v. 30, p. 62–71, 1997.

GRAY, S.; ZHANG, J.; DOW, N.; DUKE, M.; OSTARCEVIC, E.; LI, J. Identification of material and physical features of membrane distillation membranes for high performance desalination. *J. Memb. Sci.*, v. 349, p. 295–303, 2010.

GROMOV, P. B.; KASIKOV, A. G.; SHCHELOKOVA, E. A.; & PETROVA, A. M. Regeneration of sulfuric acid from electrolyte waste of the copper-smelting plant using solvent extraction. Hydrometallurgy, v. 175, p. 187-192, 2018.

GROSSI, L. de B. *Evaluation Of Membrane Distillation For The Treatment Of Surface Water During Emergency Situations*. 2018. 108 f. Dissertação (Master's degree in Samitation, Environment and Water Resources) – School of Engineering, Federal University of Minas Gerais, Belo Horizonte, 2018.

GROSSI, L.B., ALVIM, C.B., ALVARES, C.M.S., MARTINS, M.F., AMARAL, M.C.S. Purifying surface water contaminated with industrial failure using direct contact membrane distillation. Sep. Purif. Technol., v. 233, p. 116052, 2020.

GRYTA, M. Calcium sulphate scaling in membrane distillation process. *Chem. Pap*., v. 63, 2009.

GRYTA, M. Fouling in direct contact membrane distillation process. *J. Memb. Sci.*, v. 325, p. 383–394, 2008.

GRYTA, M. Influence of polypropylene membrane surface porosity on the performance of membrane distillation process. *J. Memb. Sci.*, v. 287, p. 67–78, 2007.

GRYTA, M. Long-term performance of membrane distillation process. *J. Memb. Sci.*, v. 265, p. 153–159, 2005.

GRYTA, M. The assessment of microorganism growth in the membrane distillation system. *Desalination*, v. 142, p. 79–88, 2002.

GRYTA, M.; KARAKULSKI, K.; MORAWSKI, A. Separation of effluents from regeneration of a cation exchanger by membrane distillation. *Desalination*, v. 197, p. 50-62, 2006.

GRYTA, M.; TOMASZEWSKA, M.; KARAKULSKI, K. Wastewater treatment by membrane distillation. *Desalination*, v. 198, p. 67–73, 2006.

GUILLEN-BURRIEZA, E.; MAVUKKANDY, M.O.; BILAD, M.R.; ARAFAT, H.A. Understanding wetting phenomena in membrane distillation and how operational parameters can affect it. *J. Memb. Sci.*, v. 515, p. 163–174, 2016.

GUIMARÃES, A.S. DA SILVA.; P.S. MANSUR.; M.B. Purification of nickel from multicomponent aqueous sulfuric solutions by synergistic solvent extraction using Cyanex 272

and Versatic 10, *Hydrometallurgy*, v. 150, p.173–177, 2014.

GUO, W.; NGO, H.-H.; LI, J. A mini-review on membrane fouling, *Bioresour. Technol.*, v. 122, p. 27–34, 2012.

GUO, J., FARID, M.U. LEE, E.-J., YAN, D.Y.-S., JEONG, S., KYOUNGJIN AN, A. Fouling behavior of negatively charged PVDF membrane in membrane distillation for removal of antibiotics from wastewater. J. Memb. Sci., v. 551, p. 12–19, 2018.

GUZMAN, I.; THORPE, S. J.; PAPANGELAKIS, V. G. Redox potential measurement during pressure oxidation (POX) of a refractory gold ore. Canadian Metallurgical Quarterly,v. 57, n.4, p. 382-389, 2018.

HAUSMANN, A.; SANCIOLO, P.; VASILJEVIC, T.; WEEKS, M.; DUKE, M. Integration of membrane distillation into heat paths of industrial processes. *Chem. Eng. J.*, v. 211–212, p. 378–387, 2012.

HE, F.; GILRON, J.; LEE, H.; SONG, L.; SIRKAR, K.K. Potential for scaling by sparingly soluble salts in crossflow DCMD. *J. Memb. Sci.*, v. 311, p. 68–80, 2008.

HER, S.; JAFFRAY, D.A.; ALLEN, C. Gold nanoparticles for applications in cancer radiotherapy: Mechanisms and recent advancements. *Adv. Drug Deliv.*, v. 109, p. 84–101, 2017.

I.B.D.E.M.- IBRAM, Informações Sobre a Economia Mineral Brasileira 2015, Brasília, 2015.

HERAS, F.; DUFOUR, J.; LÓPEZ-DELGADO, A.; NEGRO, C.; LÓPEZ-MATEOS, F. Feasibility Study of Metals Recycling from Nitric-Hydrofluoric Waste Pickle Baths. *Environ. Eng. Sci.*, v. 21, p. 583–590, 2004.

HERLIHY, A.; KAUFMANN, P.; MITCH, M.; BROWN, D. Regional estimates of acid mine drainage impact on streams in the mid-atlantic and Southeastern United States. *Water. Air. Soil Pollut.*, v. 50, 1990.

HEVIÁNKOVÁ, S.; BESTOVÁ, I.; KYNCL, M. The application of wood ash as a reagent in acid mine drainage treatment. *Miner. Eng.*, v. 56, p. 109–111, 2014.

HO, Y. .; MCKAY, G. Pseudo-second order model for sorption processes. *Process Biochemistry*, v. 34, n. 5, p. 451–465, jul. 1999.

HOEK, E.M.V.; ALLRED, J.; KNOELL, T.; JEONG, B.-H. Modeling the effects of fouling on full-scale reverse osmosis processes. *J. Memb. Sci.*, v. 314, p. 33–49, 2008.

HURTADO, C.; VIEDMA, P.; COTORAS, D. Design of a bioprocess for metal and sulfate removal from acid mine drainage, *Hydrometallurgy*, v. 180, p. 72–77, 2018.

HULL, E.J.; ZODROW, K.R. Acid Rock Drainage Treatment Using Membrane Distillation: Impacts of Chemical-Free Pretreatment on Scale Formation, Pore Wetting, and Product Water Quality. *Environ. Sci. Technol.*, v. 51, p. 11928–11934, 2017.

IBRAM, Mineração e Economia Verde. 2012.

IVANNIKOV, S.; AGEEV, O.; BRATSKAYA, S.; MEDKOV, M.; SHAMRAI, E.; YUDAKOV, A. Beneficiation and hydrometallurgical processing of gold-containing sludge. In: E3S WEB CONF, 56., 2018.

J.A.S. Water recovery from acid mine drainage by electrodialysis. *Miner. Eng.*, v. 40, p. 82–89, 2013.

JANDOVA, J.; MAIXNER, J.; GRYGAR, T. Reprocessing of zinc galvanic waste sludge by selective precipitation. *Ceram. - Silikaty*., v. 46, p. 52–55, 2002.

JIAO, B.; CASSANO, A.; DRIOLI, E. Recent advances on membrane processes for the concentration of fruit juices: a review. *J. Food Eng.*, v. 63, p. 303–324, 2004.

JOHN, W.; HUANMIN, L.; CHARLES, T.; SERGIO, S.; HERBERT, H. Solar and Waste Heat Desalination by Membrane Distillation. *El Paso*, 2004.

JOHNSON, D. Recent Developments in Microbiological Approaches for Securing Mine Wastes and for Recovering Metals from Mine Waters. *Minerals*., v. 4, 2014.

KABEEL, A.E.; ABDELGAIED, M.; EL-SAID, E.M.S. Study of a solar-driven membrane distillation system: Evaporative cooling effect on performance enhancement. *Renew. Energy.*, v. 106, p. 192–200, 2017.

KARIM, N. Copper and Human Health- A Review. *J. Bahria Univ. Med. Dent. Coll*., v. 8, p. 117–122, 2018.

KATSANDRI, A. A theoretical analysis of a spacer filled flat plate membrane distillation modules using CFD: Part I: velocity and shear stress analysis. Desalination, v. 408, p. 145–165, 2017.

KAUR, G.; COUPERTHWAITE, S.J.; HATTON-JONES, B.W.; MILLAR, G.J. Alternative neutralisation materials for acid mine drainage treatment. J. *Water Process Eng.*, v. 22, p. 46–58, 2018.

KAYA, Y.; GONDER, Z.B.; Vergili, I.; Barlas,H. The effect of transmembrane pressure and pH on treatment of paper machine process waters by using a two-step nanofiltration process: Flux decline analysis, *Desalination*, v. 250, p. 150–157, 2010.

KAYVANI FARD, A., MANAWI, Y.M., RHADFI, T., MAHMOUD, K.A., KHRAISHEH, M., BENYAHIA, F. Synoptic analysis of direct contact membrane distillation performance in Qatar: A case study. Desalination, v. 360, p. 97–107, 2015.

KEFENI, K. K.; MSAGATI, T. M.; & MAMBA, B. B. Synthesis and characterization of magnetic nanoparticles and study their removal capacity of metals from acid mine drainage. Chemical Engineering Journal, v. 276, p. 222-231, 2015.

KEFENI, K.K.; MAMBA, B.B.; MSAGATI, T.A.M. Magnetite and cobalt ferrite nanoparticles used as seeds for acid mine drainage treatment. *J. Hazard. Mater.*, v. 333, p. 308–318, 2017.

KEFENI, K.K.; MSAGATI, T.A.M.; MAMBA, B.B. Acid mine drainage: Prevention, treatment options, and resource recovery: A review. *J. Clean. Prod.*, v. 151, p. 475–493, 2017.

KEFENI, K.K.; MSAGATI, T.A.M.; NKAMBULE, T.T.I.; MAMBA, B.B. Synthesis and application of hematite nanoparticles for acid mine drainage treatment. *J. Environ. Chem. Eng.*, v. 6, p. 1865–1874, 2018.

KESIEME, U.K.; MILNE, N.; CHENG, C.Y.; ARAL, H.; DUKE, M. Recovery of water and acid from leach solutions using direct contact membrane distillation. *Water Sci. Technol.*, v. 69, p. 868–875, 2014.

KESIEME, U.K. *Mine waste water treatment and acid recovery using membrane distillation and solvent extraction*. 2015. Dissertation (PhD Thesis in management of Environment and Energy) – School of Engineering and Science, Victoria University, 2015.

KESIEME, U.K., ARAL, H. Application of membrane distillation and solvent extraction for water and acid recovery from acidic mining waste and process solutions. J. Environ. Chem. Eng., v. 3, p. 2050–2056, 2015.

KESIEME, U.K.; MILNE, N.; ARAL, H.; CHENG, C.Y.; DUKE, M. Economic analysis of desalination technologies in the context of carbon pricing, and opportunities for membrane distillation. *Desalination*, v. 323, p. 66–74, 2013.

KESIEME, U.K.; MILNE, N.; CHENG, C.Y.; ARAL, H.; DUKE, M. Recovery of water and acid from leach solutions using direct contact membrane distillation. *Water Sci. Technol.*, v. 69, p. 868–875, 2014.

KESTIN, J.; SOKOLOV, M.; WAKEHAM, W.A. Viscosity of liquid water in the range −8 °C to 150 °C. J. *Phys. Chem. Ref. Data*, v. 7, p. 941–948, 1978.

KHAYET, M.; MATSUURA, T. Membrane Distillation Principles and Applications. Elsevier, 2011.

KIM, Y.-D.; FRANCIS, L.; LEE, J.-G.; HAM, M.-G.; GHAFFOUR, N. Effect of non-woven net spacer on a direct contact membrane distillation performance: Experimental and theoretical studies. *J. Memb. Sci.*, v. 564, p. 193–203, 2018.

KIM, Y.-D.; THU, K.; GHAFFOUR, N.; CHOON NG, K. Performance investigation of a solar-assisted direct contact membrane distillation system. *J. Memb. Sci.*, v. 427, p. 345–364, 2013.

KIMBALL, B.A.; CALLENDER, E.; AXTMANN, E. V. Effects of colloids on metal transport in a river receiving acid mine drainage, upper Arkansas River, Colorado, U.S.A. *Appl. Geochemistry.*, v. 10, p. 285–306, 1995.

KOŁODYŃSKA, D.; SOFIŃSKA-CHMIEL, W.; MENDYK, E.; HUBICKI, Z. DOWEX M 4195 and LEWATIT®MonoPlus TP 220 in Heavy Metal Ions Removal from Acidic Streams. Separation Science and Technology, v. 49, n. 13, p. 2003–2015, 2014.

KOUSHA, M.; DANESHVAR, E.; DOPEIKAR, H.; TAGHAVI, D.; BHATNAGAR, A. Box–Behnken design optimization of Acid Black 1 dye biosorption by different brown macroalgae. *Chem. Eng. J.*, v. 179, p. 158–168, 2012.

KRIVOROT, M.; KUSHMARO, A.; OREN, Y.; GILRON, J. Factors affecting biofilm formation and biofouling in membrane distillation of seawater. *J. Memb. Sci*., v. 376, p. 15–24, 2011. . *Technol.*, v. 209, p. 815–825, 2019.

KUL, M.; OSKAY, K.O. Separation and recovery of valuable metals from real mix electroplating wastewater by solvent extraction, *Hydrometallurgy.* v. 155, p. 153–160, 2015.

LACKEY, K.; SHARKEY, S.; SHARVELLE, S.; KEHOE, P.; CHANG, P. Decentralized Water Reuse: Implementing and Regulating Onsite Nonpotable Water Systems. J. Sustain. Water Built Environ., v. 6, n. 1, 2020.

LAGERGREN, S. *Zur Theorie der sogenannten Adsorption geloster Stoffe*. [S.l: s.n.], 1898.

LAI, X.; LONG, R.; LIU, Z.; LIU, W. A hybrid system using direct contact membrane distillation for water production to harvest waste heat from the proton exchange membrane fuel cell. *Energy*, v. 147, p. 578–586, 2018.

LAN, W.; QIU, H.; ZHANG, J.; YU, Y.; YANG, K.; LIU, Z.; DING, G. Characteristic of a novel composite inorganic polymer coagulant–PFAC prepared by hydrochloric pickle liquor. *J. Hazard. Mater*., v. 162, 2009.

LANGMUIR, I. The adsorption of gases on plane surfaces of glass, mica and platinum. *Journal of the American Chemical Society*, 1918.

LAQBAQBI, M.; GARCÍA-PAYO, M.C.; KHAYET, M.; EL KHARRAZ, J.; CHAOUCH, M. Application of direct contact membrane distillation for textile wastewater treatment and fouling study. *Sep. Purif. Technol.*, v. 209, p. 815–825, 2019.

LEBRON, Y.A.R.; MOREIRA, V.R.; SANTOS, L.V.S.; JACOB, R.S. Remediation of methylene blue from aqueous solution by Chlorella pyrenoidosa and Spirulina maxima biosorption: Equilibrium, kinetics, thermodynamics and optimization studies. *J. Environ. Chem. Eng*., v 6, p. 6680–6690, 2018.

LEE, E.-J.; AN, A.K.; HE, T.; WOO, Y.C.; SHON, H.K. Electrospun nanofiber membranes incorporating fluorosilane-coated TiO2 nanocomposite for direct contact membrane distillation. *J. Memb. Sci.*, v. 520, p. 145–154, 2016.

LEE, J.-G.; LEE, E.-J.; JEONG, S.; GUO, J.; AN, A.K.; GUO, H.; KIM, J.; LEIKNES, T.; GHAFFOUR, N. Theoretical modeling and experimental validation of transport and separation properties of carbon nanotube electrospun membrane distillation. *J. Memb. Sci.*, v. 526, p. 395–

408, 2017.

LE GOUELLEC, Y. Calcium sulfate (gypsum) scaling in nanofiltration of agricultural drainage water. *J. Memb. Sci*., v. 205, p. 279–291, 2002.

LENNTECH. Product information: Amberlite IRC747, (2019). https://www.lenntech.com/Data-sheets/Amberlite-IRC-747-L.pdf (accessed January 9, 2019).

LI, Q.; BEIER, L.-J.; TAN, J.; BROWN, C.; LIAN, B.; ZHONG, W.; WANG, Y.; JI, C.; DAI, P.; LI, T.; LE CLECH, P.; TYAGI, H.; LIU, XG.; LESLIE, G.; TAYLOR, R.A. An integrated, solar-driven membrane distillation system for water purification and energy generation. *Appl. Energy*, v. 237, p. 534–548, 2019.

LIAO, J.; WEN, Z.; RU, X.; CHEN, J.; WU, H.; WEI, C. Distribution and migration of heavy metals in soil and crops affected by acid mine drainage: Public health implications in Guangdong Province, China. *Ecotoxicol. Environ. Saf*., v. 124, p. 460–469, 2016.

LONDON METAL EXCHANGE, Quotation LME, 2021.

LONG, R.; LAI, X.; LIU, Z.; LIU, W. Direct contact membrane distillation system for waste heat recovery: Modelling and multi-objective optimization. *Energy*, v. 148, p. 1060–1068, 2018.

LÓPEZ, J.; REIG, M.; GIBERT, O.; TORRES, E.; AYORA, C.; CORTINA, J.L. Application of nanofiltration for acidic waters containing rare earth elements: Influence of transition elements, acidity and membrane stability. *Desalination,* v. 430, p. 33–44, 2018.

LUZ, A.B.; SAMPAIO, J.; ALMEIDA, S.L.M. *Tratamento de Minérios*, 4 ed. Rio de Janeiro: CEFET/MCT., 2004.

LV, Y.; ZONG, L.; LIU, Z.; DU, J.; WANG, F.; ZHANG, Y.; LIU, F. Sequential separation of Cu (II)/Ni (II)/Fe (II) from strong-acidic pickling wastewater with a two-stage process based on a bi-pyridine chelating resin. Chinese Chemical Letters, 2021.

MALAEB, L.; AYOUB, G.M. Reverse osmosis technology for water treatment: State of the art review. *Desalination,* v. 267, p. 1–8, 2011.

MANNA, A.K.; PAL, P. Solar-driven flash vaporization membrane distillation for arsenic removal from groundwater: Experimental investigation and analysis of performance parameters. *Chem. Eng. Process. Process Intensif.*, v. 99, p. 51–57, 2016.

MCCARTHY, T.S. The impact of acid mine drainage in South Africa. *S. Afr. J. Sci*., v. 107, 2011.

MENDES, F.D.; MARTINS, A.H. Selective sorption of nickel and cobalt from sulphate solutions using chelating resins. Int. *J. Miner. Process*., v. 74, p. 359–371, 2004.

MIGASZEWSKI, Z.M.; GAŁUSZKA, A.; DOŁĘGOWSKA, S. Arsenic in the Wiśniówka acid mine drainage area (south-central Poland) – Mineralogy, hydrogeochemistry, remediation. *Chem. Geol.*, v. 493, p. 491–503, 2018.

MILLER, S.; SHEMER, H.; SEMIAT, R. Energy and environmental issues in desalination, Desalination. v. 366, p. 2–8, 2014.

MITROGIANNIS, D.; MARKOU, G.; ÇELEKLI, A; BOZKURT, H. Biosorption of methylene blue onto Arthrospira platensis biomass: Kinetic, equilibrium and thermodynamic studies. *J. Environ. Chem. Eng*., v. 3, p. 670–680, 2015.

MOCQ, J.; HARE, L. Influence of Acid Mine Drainage, and Its Remediation, on Lakewater Quality and Benthic Invertebrate Communities. *Water, Air, Soil Pollut*., v. 229, p. 28, 2018.

MOHAMMADI, T.; ESMAEELIFAR, A. Wastewater treatment of a vegetable oil factory by a hybrid ultrafiltration-activated carbon process, *J. Memb. Sci.*, v. 254, p. 129, 137, 2005.

MOHAMMED ABDUL, K.S.; JAYASINGHE, S.S.; CHANDANA, E.P.S.; JAYASUMANA, C.; DE SILVA, P.M.C.S. Arsenic and human health effects: A review. *Environ. Toxicol. Pharmacol.*, v. 40, p. 828–846, 2015.

MONDAL, P., BHOWMICK, S., CHATTERJEE, D., FIGOLI, A., VAN DER BRUGGEN, B. Remediation of inorganic arsenic in groundwater for safe water supply: A critical assessment of technological solutions. Chemosphere, v. 92, 157–170, 2013.

MORADI, R.; MONFARED, S.M.; AMINI, Y.; DASTBAZ, A. Vacuum enhanced membrane distillation for trace contaminant removal of heavy metals from water by electrospun PVDF/TiO2 hybrid membranes. *Korean J. Chem. Eng.*, v. 33, p. 2160–2168, 2016.

MOREIRA, V.R.; LEBRON, Y.A.R.; FOUREAUX, A.F.S.; DE S. SANTOS, L.V.; AMARAL, M.C.S. Acid and metal reclamation from mining effluents: Current practices and future perspectives towards sustainability. *J. Environ. Chem. Eng*., v. 9, p. 105169, 2021.

NAGIB, S.; INOUE, K.; YAMAGUCHI, T.; TAMARU, T. Recovery of Ni from a large excess of Al generated from spent hydrodesulfurization catalyst using picolylamine type chelating resin and complexane types of chemically modified chitosan. Hydrometallurgy, v. 51, n. 1, p. 73-85, 1999.

NAIDU, G.; RYU, S.; THIRUVENKATACHARI, R.; CHOI, Y.; JEONG, S.; VIGNESWARAN, S. A critical review on remediation, reuse, and resource recovery from acid mine drainage.Environ. Pollut., v. 247, p. 1110–1124, 2019.

NASCIMENTO, R. F. *et al. Adsorção: Aspectos teóricos e aplicações ambientais*. [S.l: s.n.], 2014.

NG, H.Y.; ELIMELECH, M. Influence of colloidal fouling on rejection of trace organic contaminants by reverse osmosis. *J. Memb. Sci*., v. 244, p. 215–226, 2004.

NASCIMENTO, R. F. *et al. Adsorção: Aspectos teóricos e aplicações ambientais*. [S.l: s.n.], 2014.

NILSSON, M.; TRÄGÅRDH, G.; ÖSTERGREN, K. The influence of pH, salt and temperature on nanofiltration performance. *J. Memb. Sci*., v. 312, p. 97–106, 2008.

NIYOGI, D.K.; MCKNIGHT, D.M.; LEWIS, W.M. Influences of water and substrate quality for periphyton in a montane stream affected by acid mine drainage. *Limnol. Oceanogr*., v. 44, p. 804–809, 1999.

J. Soil Sci., v. 66, p. 257–276, 2015.

PABBY, A.K.; RIZVI, S.H. *Handbook of Membrane Separations*: Chemical, Pharmaceutical. CRC Press, 2009.

PANG, S. K.; YUNG, K. C. Chelating resin for removal of nickel impurities from gold electroplating solutions. Industrial & Engineering Chemistry Research, v. 52, p. 2418-2424, 2013.

PAQUAY, E.; CLARINVAL, A.-M., DELVAUX, A., DEGREZ, M., HURWITZ, H. Applications of electrodialysis for acid pickling wastewater treatment. *Chem. Eng. J.*, v. 79, p. 197–201, 2000.

PARK, S.-M.; SHIN, S.-Y.; YANG, J.-S.; JI, S.-W.; BAEK, K. Selective Recovery of Dissolved Metals from Mine Drainage Using Electrochemical Reactions. *Electrochim. Acta*., v. 181, p. 248–254, 2015.

PARKHURST, D.L., APPELO, C.A.J. Description of Input and Examples for PHREEQC Version 3 — A Computer Program for Speciation , Batch-Reaction , One-Dimensional Transport, and Inverse Geochemical Calculations. U.S. Geol. Surv. Tech. Methods, B. 6, Chapter A43., 6-43A., 2013.

PEHLIVAN, E.; ALTUN, T. The study of various parameters affecting the ion exchange of Cu2+, Zn2+, Ni2+, Cd2+, and Pb2+ from aqueous solution on Dowex 50W synthetic resin. Journal of hazardous materials, v. 134, n. 1-3, p.149-156, 2006.

PEIRAVI, M.; MOTE, S.R.; MOHANTY, M.K.; LIU, J. Bioelectrochemical treatment of acid mine drainage (AMD) from an abandoned coal mine under aerobic condition. *J. Hazard. Mater*., v. 333, p. 329–338, 2017.

PÉREZ-VILLASEÑOR, F., IGLESIAS-SILVA, G.A., HALL, K.R. Osmotic and Activity Coefficients Using a Modified Pitzer Equation for Strong Electrolytes 1:1 and 1:2 at 298.15 K. Ind. Eng. Chem. Res., v. 41, p. 1031–1037, 2002.

PHATTARANAWIK, J., JIRARATANANON, R., FANE, A.G. Heat transport and membrane distillation coefficients in direct contact membrane distillation. J. Memb. Sci., v. 212, p. 177–193, 2003.

PINO, L.; VARGAS, C.; SCHWARZ, A.; BORQUEZ, R. Influence of operating conditions on the removal of metals and sulfate from copper acid mine drainage by nanofiltration. *Chem. Eng. J*., v. 345, 2018.

PLUMLEE, G.S.; MORMAN, S.A.; ZIEGLER, T.L. 2. The Toxicological Geochemistry of Earth Materials: An Overview of Processes and the Interdisciplinary Methods Used to Understand Them. Boston: Reviews in Mineralogy and Geochemistry, 2006. p. 5-57.

POZO, G.; PONGY, S.; KELLER, J.; LEDEZMA, P.; FREGUIA, S. A novel bioelectrochemical system for chemical-free permanent treatment of acid mine drainage. *Water Res.*, v. 126, p. 411–420, 2017.

PRISCIANDARO, M., CAPOCELLI, M., PIEMONTE, V., BARBA, D. Process analysis applied to water reuse for a "closed water cycle" approach. Chem. Eng. J., v. 304, p. 602–608, 2016.

QIN, L.; ZENG, G.; LAI, C.; HUANG, D.; XU, P.; ZHANG, C.; CHENG, M.; LIU, X.; LIU, S.; LI, B.; YI, H. "Gold rush" in modern science: Fabrication strategies and typical advanced applications of gold nanoparticles in sensing. *Coord. Chem.*, v. 359, p. 1–31, 2018.

QTAISHAT, M., MATSUURA, T., KRUCZEK, B., KHAYET, M. Heat and mass transfer analysis in direct contact membrane distillation. Desalination, v. 219, p. 272–292, 2018.

QU, D.; WANG, J.; HOU, D.; LUAN, Z.; FAN, B.; ZHAO, C. Experimental study of arsenic removal by direct contact membrane distillation. *J. Hazard. Mater*., v. 163, p. 874–879, 2009.

QUIST-JENSEN, C.A., ALI, A., MONDAL, S., MACEDONIO, F., DRIOLI, E. A study of membrane distillation and crystallization for lithium recovery from high-concentrated aqueous solutions. J. Memb. Sci, v. 505, p. 167–173, 2016.

RAHIMPOUR, M.R.; KAZEROONI, N.M.; PARHOUDEH, M. Water Treatment by Renewable Energy-Driven Membrane Distillation. Curr. Trends Futur. Dev. Membr., Elsevier, p. 179–211, 2019.

RAMBABU, K.; BANAT, F.; PHAM, Q.M.; HO, S.-H.; REN, N.-Q.; SHOW, P.L. Biological remediation of acid mine drainage: Review of past trends and current outlook. Environ. Sci. Ecotechnology, v. 2, p. 100024, 2020.

RAVINDRA BABU, B.; RASTOGI, N.K.; RAGHAVARAO, K.S.M.S. Concentration and temperature polarization effects during osmotic membrane distillation. *J. Memb. Sci.*, v. 322, p. 146–153, 2008.

REHMAN, W. U.; MUHAMMAD, A.; YOUNAS, M.; WU, C.; HU,Y.; LI, J. Effect of membrane wetting on the performance of PVDF and PTFE membranes in the concentration of pomegranate juice through osmotic distillation. J. Memb. Sci, v 584, p. 66–78, 2019.

REIS, B. G.; ARAÚJO, A. L. B.; AMARAL, M. C. S.; & FERRAZ, H. C. Comparison of Nanofiltration and Direct Contact Membrane Distillation as an alternative for gold mining effluent reclamation. Chemical Engineering and Processing-Process Intensification, v. 133, p. 24-33, 2018.

REIS, B.G., ARAÚJO, A.L.B., VIEIRA, C.C., AMARAL, M.C.S., FERRAZ, H.C. Assessing potential of nanofiltration for sulfuric acid plant effluent reclamation: Operational and economic aspects. Sep. Purif. Technol., v. 222, p. 369–380, 2019.

RENGARAJ, S.; YEON, J.-W.; KIM, Y.; JUNG, Y.; HA, Y.-K.; KIM, W.-H. Adsorption characteristics of Cu(II) onto ion exchange resins 252H and 1500H: Kinetics, isotherms and error analysis. *J. Hazard. Mater*., v. 143, p. 469–477, 2007.

REZAEI, M.; WARSINGER, D. M.; DUKE, M. C., MATSUURA, T.; SAMHABER, W. M. Wetting phenomena in membrane distillation: Mechanisms, reversal, and prevention. Water research, v.139, p. 329-352, 2018.

RICCI, B.C.; FERREIRA, C.D.; AGUIAR, A.O.; AMARAL, M.C.S. Integration of nanofiltration and reverse osmosis for metal separation and sulfuric acid recovery from gold mining effluent. Sep. Purif. Technol., v. 154, p. 11–21, 2015.

RICCI, B.C.; FERREIRA, C.D.; MARQUES, L.S.; MARTINS, S.S.; AMARAL, M.C.S. Assessment of nanofiltration and reverse osmosis potentialities to recover metals, sulfuric acid, and recycled water from acid gold mining effluent. Water Sci. Technol., v. 74, n. 2, p. 367–374, 2016.

RICCI, B.C.; FERREIRA, C.D.; MARQUES, L.S.; MARTINS, S.S.; REIS, B. G.; AMARAL, M.C.S. Assessment of the chemical stability of nanofiltration and reverse osmosis membranes employed in treatment of acid gold mining effluent. Separation and Purification Technology., v. 174, p. 301-311, 2017.

RICCI, B.C., SKIBINSKI, B., KOCH, K., MANCEL, C., CELESTINO, C.Q., CUNHA, I.L.C., SILVA, M.R., ALVIM, C.B., FARIA, C.V., ANDRADE L.H., LANGE, L.C., AMARAL, M.C.S. Critical performance assessment of a submerged hybrid forward osmosis - membrane distillation system. Desalination, v. 468, p. 114082, 2019.

RODRUIGUES, M.A.; SILVA, P.P.; GUERRA, W. Cobre. *Química Nov. Na Esc.*, v. 34, p. 161–162, 2012.

ROYCHOWDHURY, A.; SARKAR, D.; DATTA, R. Remediation of Acid Mine Drainage-Impacted Water. *Curr. Pollut. Reports*, v. 1, p. 131–141, 2015.

RYAN, M.J.; KNEY, A.D.; CARLEY, T.L. A study of selective precipitation techniques used to recover refined iron oxide pigments for the production of paint from a synthetic acid mine drainage solution, *Appl. Geochemistry*, v. 79, p.27–35, 2017.

RYU, S.; NAIDU, G.; HASAN JOHIR, M.A.; CHOI, Y.; JEONG, S.; VIGNESWARAN, S. Acid mine drainage treatment by integrated submerged membrane distillation–sorption system, *Chemosphere*, v. 218, p. 955–965, 2019.

SALLS, K.A.; WON, D.; KOLODZIEJ, E.P.; CHILDRESS, A.E.; HIIBEL, S.R. Evaluation of semi-volatile contaminant transport in a novel, gas-tight direct contact membrane distillation system. Desalination, v. 427, p. 35–41, 2018.

SCARAZZATO, T. Tratamento de efluente contendo HEDP por eletrodiálise., Universidade de São Paulo, 2013.

SCHAEP, J.; VANDECASTEELE, C. Evaluating the charge of nanofiltration membranes. *J. Memb. Sci*., v. 188, p. 129–136, 2001.

SCHÄFER, A.I.; SCHWICKER, U.; FISCHER, M.M.; FANE, A.G.; WAITE, T.D. Microfiltration of colloids and natural organic matter. *J. Memb. Sci.*, v. 171, p. 151–172, 2000.

SCHNEIDER, K.; HÖLZ, W.; WOLLBECK, R.; RIPPERGER, S. Membranes and modules for transmembrane distillation. *J. Memb. Sci.*, v. 39, p. 25–42, 1998.

SCHWANTES, R,; CIPOLLINA, A.; GROSS, F.; KOSCHIKOWSKI, J.; PFEIFLE, D.; ROLLETSCHEK, M,; SUBIELA, V. Membrane distillation: Solar and waste heat driven demonstration plants for desalination. *Desalination*, v. 323, p. 93–106, 2013.

SEO, E.Y.; CHEONG, Y.W.; YIM, G.J.; MIN, K.W.; GERONI, J.N. Recovery of Fe, Al and Mn in acid coal mine drainage by sequential selective precipitation with control of pH. *CATENA*., v. 148, p. 11–16, 2017.

SETHI, S.; WIESNER, M.R. Cost modeling and estimation of crossflow membrane filtration processes. *Environ. Eng. Sci*., v. 17, p. 61–79, 2000.

SHAO, M.; ZHU, Y.; HAO, R.; YU, Z., SONG, M. The health hazards of potentially toxic metals in the daily diets of adults and children from a mining and smelting region (Hezhang County) in southwestern China. *Environ. Monit. Assess*., v. 190, p. 432, 2018.

SHENVI, S.S.; ISLOOR, A.M.; ISMAIL, A.F.; SHILTON, S.J.; AL AHMED, A. Humic Acid Based Biopolymeric Membrane for Effective Removal of Methylene Blue and Rhodamine B. *Ind. Eng. Chem. Res*., v. 54, p. 4965–4975, 2015.

SHETH, B.; NATH, K. Analysis of molar flux and current density in the electrodialytic separation of sulfuric acid from spent liquor using an anion exchange membrane, *Korean J. Chem. Eng*. v. 35, p.1878–1888, 2018.

SHIRAZI, M.M.A.; KARGARI, A.; ISMAIL, A.F.; MATSUURA, T. Computational Fluid Dynamic (CFD) opportunities applied to the membrane distillation process: State-of-the-art and perspectives. *Desalination.,* v. 377, p. 73–90, 2016.

SILVA, M.R.; REIS,B.G.;GROSSI L.B.; M.C.S. Improving the energetic efficiency of direct-contact membrane distillation in mining effluent by using the waste-heat-and-water process as the cooling fluid, J. Clean. Prod. v.260. 2020.

SILVA, R. A.; ZHANG, Y.; HAWBOLDT, K.; JAMES, L. A. Study on iron-nickel separation using ion exchange resins with different functional groups for potential iron sub-production. Mineral Processing and Extractive Metallurgy Review, p. 1-15, 2019.

SIROLA, K.; LAATIKAINEN, M.; PAATER.; E. Effect of temperature on sorption of metals by silica-supported 2-(aminomethyl) pyridine. Part I: Binding equilibria. *Reactive and functional polymers*, v.70, p. 48-55, 2010.

SKOUSEN, J.; ZIPPER, C.E.; ROSE, A., ZIEMKIEWICZ, P.F., NAIRN, R., MCDONALD, L.M., KLEINMANN, R.L. Review of Passive Systems for Acid Mine Drainage Treatment. *Mine Water Environ*., v. 36, p. 133–153, 2017.

SOFIA, A.; MONTEIRO, C. Recursos Geológicos e Saúde Humana : O uso do Cobalto na Radioterapia. *Universidade do Porto.*, 2016.

SOUHAIMI, M.K.; MATSUURA, T. Membrane Distillation. *Elsevier*, 2011.

SRISURICHAN, S.; JIRARATANANON, R.; FANE, A.G. Humic acid fouling in the membrane distillation process. *Desalination*, v. 174, p. 63–72, 2005.

SRISURICHAN, S.; JIRARATANANON, R.; FANE, A.G. Mass transfer mechanisms and transport resistances in direct contact membrane distillation process. *J. Memb. Sci.,* v. 277, p. 186–194, 2006.

SUK, D.E.; MATSUURA, T.; PARK, H.B.; LEE, Y.M. Development of novel surface modified phase inversion membranes having hydrophobic surface-modifying macromolecule (nSMM) for vacuum membrane distillation. *Desalination,* v. 261, p. 300–312, 2010.

SWADDIWUDHIPONG, W.; NGUNTRA, P.; KAEWNATE, Y.; MAHASAKPAN, P.; LIMPATANACHOTE, P.; AUNJAI, T.; JEEKEEREE, W.; PUNTA, B.; FUNKHIEW, T.; PHOPUENG, I. Human health effects from cadmium exposure: Comparison between persons living in cadmium-contaminated and non-contaminated areas in northwestern Thailand. *Southeast Asian J. Trop. Med. Public Health,* v. 46, p. 133–142, 2015.

TAI, Z.S.; AZIZ, M.H.A.; OTHMAN, M.H.D.; ISMAIL, A.F.; RAHMAN, M.A.; JAAFAR, J. An Overview of Membrane Distillation. Membr. Sep. Princ. Appl., Elsevier, p. 251–281, 2019.

TANG, B.; YUAN, L.; SHI, T.; YU, L.; ZHU, Y. Preparation of nano-sized magnetic particles from spent pickling liquors by ultrasonic-assisted chemical co-precipitation. *J. Hazard. Mater*., v. 163, p. 1173–1178, 2009.

TANG, C.Y.; CHONG, T.H.; FANE, A.G. Colloidal interactions and fouling of NF and RO membranes: A review. *Adv. Colloid Interface Sci.*, v. 164, p. 126–143, 2011.

TARNACKI, K.; MENESES, M.; MELIN, T.; VAN MEDEVOORT, J.; JANSEN, A. Environmental assessment of desalination processes: Reverse osmosis and Memstill®. *Desalination*, v. 296, p. 69–80, 2012.

TARNACKI, K.M.; MELIN, T.; JANSEN, A.E.; VAN MEDEVOORT, J. Comparison of environmental impact and energy efficiency of desalination processes by LCA. *Water Sci. Technol. Water Supply.*, v. 11, p. 246–251, 2011.

TEMKIN, I., M. Kinetics of ammonia synthesis on promoted iron catalysts. *Acta Physiochim.*

URSS, v. 12, p. 327–356, 1940.

TIAN, M.; YIN, Y.; YANG, C.; ZHAO, B.; SONG, J.; LIU, J.; LI, X.-M.; HE, T. CF4 plasma modified highly interconnective porous polysulfone membranes for direct contact membrane distillation (DCMD). *Desalination*, v. 369, p. 105–114, 2015.

TIJING, L.D.; WOO, Y.C.; CHOI, J.-S.; LEE, S.; KIM, S.-H.; SHON, H.K. Fouling and its control in membrane distillation—A review. *J. Memb. Sci.*, v. 475, p. 215–244, 2015.

TOLONEN, E.-T.; SARPOLA, A.; HU, T.; RÄMÖ, J.; LASSI, U. Acid mine drainage treatment using by-products from quicklime manufacturing as neutralization chemicals. *Chemosphere*., v. 117, p. 419–424, 2014.

TOMASZEWSKA, M. Preparation and properties of flat-sheet membranes from poly(vinylidene fluoride) for membrane distillation. *Desalination*, v. 104, p. 1–11, 1996.

TOMASZEWSKA, M. Recovery of hydrochloric acid from metal pickling solutions by membrane distillation. *Sep. Purif. Technol*., v. 22–23, p. 591–600, 2001.

TOMASZEWSKA, M.; GRYTA, M.; MORAWSKI, A.W. Mass transfer of HCl and H2O across the hydrophobic membrane during membrane distillation. *J. Memb. Sci.*, v. 166, p. 149–157, 2000.

TOMASZEWSKA, M.; GRYTA, M.; MORAWSKI, A.W. Study on the concentration of acids by membrane distillation. *J. Memb. Sci.*, v. 102, p. 113–122, 1995.

TOMASZEWSKA, M.; GRYTA, M.; MORAWSKI, A.W. The influence of salt in solutions on hydrochloric acid recovery by membrane distillation. *Sep. Purif. Technol*., v. 14, p. 183–188, 1998.

TOST, M.; HITCH, M.; CHANDURKAR, V.; MOSER, P.; FEIEL, S. The state of environmental sustainability considerations in mining. *Journal of cleaner production*, v. 182, p. 969-977, 2018.

TZOTZI, C.; PAHIADAKI, T.; YIANTSIOS, S.G.; KARABELAS, A.J.; ANDRITSOS, N. 2007. A study of CaCO3scale formation and inhibition in RO and NF membrane processes. *J. Memb. Sci*., v. 296, p. 171–184, 2007.

ULLAH, R.; KHRAISHEH, M.; ESTEVES, R.J.; MCLESKEY, J.T.; ALGHOUTI, M.; GAD-EL-HAK, M.; VAHEDI TAFRESHI, H. Energy efficiency of direct contact membrane distillation. Desalination, v. 433, p. 56–67, 2018.

ULLOA, L.; BRINGAS, E.; SAN-ROMÁN, M. F. Simultaneous separation of nickel and copper from sulfuric acid using chelating weak base resins. Journal of Chemical Technology & Biotechnology, v. 95, p. 1906-1914, n. 7, 2020.

URAGAMI, T. Science and Technology of Separation Membranes. Chichester, UK: Wiley, 2017.

URANO, K.; ASE, T.; NAITO, Y. Recovery of acid from wastewater by electrodialysis. *Desalination*., v. 51, p. 213–226, 1984

URTIAGA, A.M.; PÉREZ, G.; IBÁÑEZ, R.; ORTIZ, I. Removal of pharmaceuticals from a WWTP secondary effluent by ultrafiltration/reverse osmosis followed by electrochemical oxidation of the RO concentrate. *Desalination*, v. 331, p. 26–34, 2013.

USEPA. Drinking Water Standards and Health Advisories, 2002.

VAN DER BRUGGEN, B.; SCHAEP, J.; WILMS, D.; VANDECASTEELE, C. Influence of molecular size, polarity and charge on the retention of organic molecules by nanofiltration. *J. Memb. Sci*., v. 156, p. 29–41, 1999.

VECINO, X.; REIG, M.; LÓPEZ, J.; VALDERRAMA, C.; CORTINA, J. L. Valorisation options for Zn and Cu recovery from metal influenced acid mine waters through selective precipitation and ion-exchange processes: promotion of on-site/off-site management options. Journal of Environmental Management, v. 283, p. 112004, 2021.

VIERS, J.; GRANDE, J.A.; ZOUITEN, C.; FREYDIER, R.; MASBOU, J.; VALENTE, T.; DE LA TORRE, M.-L.; DESTRIGNEVILLE, C.; POKROVSKY, O.S. Are Cu isotopes a useful tool to trace metal sources and processes in acid mine drainage (AMD) context?. *Chemosphere*, p. 193, 2018.

VIVODA, V.; KEMP, D. How do national mining industry associations compare on sustainable development?. *The Extractive Industries and Society*, v. 6, n. 1, p. 22-28, 2019.

VOULVOULIS. N. Water reuse from a circular economy perspective and potential risks from an unregulated approach. Curr. Opin. Environ. Sci. Heal., v. 2, p. 32–45, 2018.

VROUWENVELDER, J.S.; VAN DER KOOIJ, D. Diagnosis, prediction and prevention of biofouling of NF and RO membranes. *Desalination*, v. 139, p. 65–71, 2001.

W.G. Council, Global gold demand - Global gold demand, (2018).

WAITE, T.; FANE, A.; SCHÄFER, A. Nanofiltration: Principles and Applications. *Elsevier*, 2005.

WANG, S. Cobalt—Its recovery, recycling, and application. Jom, v. 58, n. 10, p. 47-50, 2006.

WANG, P.; CHUNG, T.-S. Recent advances in membrane distillation processes: Membrane development, configuration design and application exploring. *J. Memb. Sci.*, v. 474, p. 39–56, 2015.

WANG, J.; HE, H.; WANG, M.; XIAO, Z.; CHEN, Y.; WANG, Y.; SONG, J.; LI, X.-M.; ZHANG, Y.; HE, T. 3-[[3-(Triethoxysilyl)-propyl] amino] propane-1-sulfonic acid zwitterion grafted polyvinylidene fluoride antifouling membranes for concentrating greywater in direct contact membrane distillation. *Desalination*, v. 455, p. 71–78, 2019.

WANG, C.; HUANG, X.; LIM, M. K.; TSENG, M. L.; GHADIMI, P. Mapping the structural evolution in the global scrap copper trade network. Journal of Cleaner Production, v. 275, p. 122934, 2020.

WARSINGER, D.E.M.; SWAMINATHAN, J.; MASWADEH, L.A.; LIENHARD V, J.H. Superhydrophobic condenser surfaces for air gap membrane distillation. *J. Memb. Sci.*, v. 492, p. 578–587, 2015.

WARSINGER, D.M.; SWAMINATHAN, J.; GUILLEN-BURRIEZA, E.; ARAFAT, H.A.; LIENHARD V, J.H. Scaling and fouling in membrane distillation for desalination applications: A review. *Desalination*, v. 356, p. 294–313, 2015.

WEI, X.; ZHAO, B.; LI, X.-M.; WANG, Z.; HE, B.-Q.; HE, T.; JIANG, B. CF4 plasma surface modification of asymmetric hydrophilic polyethersulfone membranes for direct contact membrane distillation. *J. Memb. Sci.*, v. 407–408, p. 164–175, 2012.

WIŚNIEWSKI, J.; WIŚNIEWSKA, G. Water and acid recovery from the rinse after metal etching operations. *Hydrometallurgy*, v. 53, n. 2, p. 105-119, 1999.

WOŁOWICZ, A.; HUBICKI, Z. Comparison of strongly basic anion exchange resins applicability for the removal of palladium (II) ions from acidic solutions. Chemical engineering journal, v. 171, n. 1, p. 206-215, 2011.

XIAO, Z.; LI, Z.; GUO, H.; LIU, Y.; WANG, Y.; YIN, H.; LI, X.; SONG, J.; NGHIEM, L.D.; HE, T. Scaling mitigation in membrane distillation: From superhydrophobic to slippery. *Desalination*, v. 466, p. 36–43, 2019.

XIAO, Z.; ZHENG, R.; LIU, Y.; HE, H.; YUAN, X.; JI, Y.; LI, D.; YIN, H.; ZHANG, Y.; LI, X.-M.; HE, T. Slippery for scaling resistance in membrane distillation: A novel porous micropillared superhydrophobic surface. *Water Res.*, v. 155, p. 152–161, 2019.

YANG, C.; LI, X.-M.; GILRON, J.; KONG, D.; YIN, Y.; OREN, Y.; LINDER, C.; HE, T.CF4 plasma-modified superhydrophobic PVDF membranes for direct contact membrane distillation. *J. Memb. Sci*., v. 456, 2014.

YANG, C.; TIAN, M.; XIE, Y.; LI, X.-M.; ZHAO, B.; HE, T.; LIU, J. Effective evaporation of CF4 plasma modified PVDF membranes in direct contact membrane distillation. *J. Memb. Sci.*, v. 482, p. 25–32, 2015.

YING ZHAO, Y.; XIN KONG, F.; WANG, Z.; WEI YANG, H.; MAO WANG, X.; XIE, Y.F.; WAITE, T.D. Role of membrane and compound properties in affecting the rejection of pharmaceuticals by different RO/NF membranes. *Front. Environ. Sci. Eng*., v. 11, p. 20, 2017.

YU, L.; LI, S.; LIU, Q.; DENG, J.; LUO, B.; LIANG, Y.; LAI, H. Gold recovery from refractory gold concentrates by pressure oxidation pre-treatment and thiosulfate leaching. Physicochemical Problems of Mineral Processing, v.55, 2019.

ZADNIPRYANY, I.; TRETIAKOVA, O.; SATAIEVA, T.; ZUKOW, W. Experimental review

of cobalt induced cardiomyopathy. *Russ. Open Med. J.*, v. 6, p. 1-4, 2017.

ZARE, S.; KARGARI, A. Membrane properties in membrane distillation. In: V.G. GUDE (ED.), EMERG. TECHNOL. SUSTAIN. DESALIN. HANDB., ELSEVIER, 107–156., 2018.

ZHANG, X.; TANG, S.; WANG, M.; SUN, W.; XIE, Y.; PENG, H.; ZHONG, A.; LIU, H.; ZHANG, X.; YU, H.; GIESY, P.; HECKER, M. Acid mine drainage affects the diversity and metal resistance gene profile of sediment bacterial community along a river. *Chemosphere*, v. 217, p. 790–799, 2019.

ZHANG, Y.; ROTTIERS, T.; MEESSCHAERT, B.; PINOY, L.; VAN DER BRUGGEN, B. Wastewater Treatment by Renewable Energy Driven Membrane Processes. Curr. Trends Futur. Dev. Membr., Elsevier, p. 1–19, 2019.ZHAO, D.; YU, S. A review of recent advance in fouling mitigation of NF/RO membranes in water treatment: pretreatment, membrane modification, and chemical cleaning. *Desalin. Water Treat.*, v. 55, p. 870–891, 2015.